CO_2-MEDIATED FORMATION OF POLYMER/CLAY NANOCOMPOSITES

Qian Zhao

A dissertation submitted to the faculty of the University of North Carolina at Chapel Hill in partial fulfillment of the requirements for the degree of Doctor of Philosophy in the Curriculum in Applied and Materials Sciences.

Chapel Hill
2006

Approved by

Advisor: Edward T. Samulski

Reader: Dr. Valerie Sheares Ashby

Reader: Joseph M. DeSimone

Reader: Dr. Yue Wu

Reader: Dr. Otto Zhou

ABSTRACT

QIAN ZHAO: CO_2-mediated formation of polymer/clay nanocomposites (Under the direction of Edward T. Samulski)

In this thesis, the feasibility of $scCO_2$ as both a processing medium and a polymerization medium for preparation of polymer/clay nanocomposites has been explored, with the first part discussing a CO_2-mediated intercalation of poly(ethylene oxide) (PEO) in clay. It has been shown that CO_2 can act as a plasticizer to promote intercalation similar to that achieved in polymer melts. Intercalation kinetics in both melt intercalation and CO_2-mediated intercalation were studied by Differential Scanning Calorimetry (DSC). Data and results towards both intercalation kinetic and thermal behavior of PEO were discussed.

In the second part, we explored the feasibility of $scCO_2$ as a polymerization medium for in-situ polymerization of vinyl monomers and exfoliation of clay. By using a CO_2-philic fluorinated surfactant (10F-clay) to modify clay, partially exfoliated poly(methyl methacrylate) (PMMA)/clay nanocomposites were synthesized in high yields via a pseudo-dispersion polymerization of MMA in $scCO_2$. It was found that 10F-clay was an effective stabilizer (as compared to conventional hydrocarbon surfactant modified clay) for PMMA polymerization in CO_2. A stabilization mechanism was proposed, wherein FT-IR studies indicated hydrogen bond formation between MMA and clay. Thermal and mechanical properties of the PMMA nanocomposites were also studied.

Pseudo-dispersion polymerization was also conducted on polystyrene to study the effect of clay on non-hydrogen-bonding polymers. By using a poly(dimethylsiloxane) (PDMS) surfactant to modify clay, PMMA and polystyrene/clay nanocomposites were synthesized and compared in this study. The effects of the PDMS-clay concentration on polymer conversion, molecular weight, and morphology were investigated. The distributions of clay in both polymers were compared, and two different interaction mechanisms were proposed. The effects of clay distribution on both thermal properties and mechanical properties of the polymers have also been discussed.

TO MY PARENTS

ACKNOWLEDGMENTS

First of all, I would like to thank my advisor, Prof. Edward T. Samulski for giving me the opportunity and independence to work on things that interest me most and work my own way on them. I am in debt to him not only for his support and the many invaluable discussions that made this dissertation possible, but also for his immeasurable influence in the various aspects of my personal development. In him I found not only a source of knowledge but also a friend.

Other thanks go to all the group members (present and past): Lei Zhang, Wensheng Shi, Lou Madsen, Joette Russell Tanner, E-Joon Choi, Jinrong Liu, Nick Zafiropoulousand and Walter Schenck for all your help and care during our time together. I would like to especially thank Bin Cheng, who has helped me to get started when I first joined the group, and who has always been there when I was looking for help in experiments. Appreciation also to Jane in Otto's lab: thank you for being my friend, talking God to me and helping me with the instrument I want to use in your lab.

I would also like to express my thanks to Prof. Otto Zhou for allowing me to use the instruments in his lab, Dr. Wallace Ambrose for training me on SEM and TEM and his assistance in TEM sample sectioning. Especially I am grateful to Prof. Joe DeSimone, whose pioneer work in supercritical carbon dioxide has opened the door of

research for me. Being in the NSF-STC center has been a fruitful experience for me.

Finally, I thank my family for your unending love, support and encouragement. Special thanks is owed to Lilong: without your love and support, I could not have made this far, in life and in work. Thank you for everything!

CONTENTS

LIST OF FIGURES

LIST OF TABLES

LIST OF ABBREVIATIONS

Å	angstrom
AIBN	2,2-azobis(isobutyronitrile)
AP-PDMS	aminopropyl-terminated poly(dimethylsiloxane)
^{o}C	degrees Celsius
CEC	cation exchange capacity
cm^{-1}	wavenumber
CO_2	carbon dioxide
C12-clay	dodecylpyridinium modified clay
2C18-clay	dimethyldistearylammonium modified clay
C18FH	octadecylammonium modified fluorohectorite
DMA	dynamic mechanical analysis
DSC	differential scanning calorimetry
E'	storage modulus
E"	loss modulus
10F-clay	1H,1H,1H,2H-perfluorododecylpyridinium modified clay
FT-IR	fourier-transform infared
g	gram
GPC	gel permeation chromatography
h	hour

J	joule
KDa	kiloDalton
μm	micrometer
meq	milliequivalent
min	minute
ml	milliliter
MMA	methyl methacrylate
M_w	weight average molecular weight
MMT	montmorrillonite
N_2	nitrogen
Na-MMT	sodium-montmorrillonite
nm	nanometer
NMR	nuclear magnetic resonance
Pa	pascal
P_c	critical pressure
PDMS	poly(dimethylsiloxane)
PDMS-clay	aminopropyl-terminated poly(dimethylsiloxane) modified clay
PEO	poly(ethylene oxide)
PFOA	poly(1,1-dihydroperfluorooctylacrylate)
PMMA	poly(methyl methacrylate)
ppm	parts per million
PS	polystyrene

psi	pounds per square inch
PVDF	poly(vinylidene fluoride)
SEM	scanning electron microscopy
sc	supercritical
tanδ	loss tangent
TEM	transmission electron microscopy
$\mathbf{T}_c$	critical temperature
$\mathbf{T}_g$	glass transition temperature
$\mathbf{T}_m$	melting temperature
TGA	thermogravimetric analysis
wt	weight
XRD	X-ray diffraction

CHAPTER 1

INTRODUCTION

1.1 Polymer/clay Nanocomposites

Filling of polymer matrices by inorganic compounds has been studied over many decades to improve their performance, such as greater mechanical strength or impact resistance, reduced permeability to gases and moisture, etc. In these conventional materials, there is usually a distinct macroscopic separation between the organic and inorganic phase without any significant interactions between them. In this case, the inactive fillers represent the lowest level of reinforcing and simply stretch the polymers to reduce the costs of these materials. By treating the surface of the inorganic material and make it compatible with the hydrophobic polymer, microscopic dispersion is the most that can be achieved and can provide certain degree of reinforcement for the polymer.

In contrast to these conventionally scaled composites, nanocomposites constitute a new class of materials with a least one dimension of the dispersed particles in the nanometer range which endows them with unique properties not shared by conventional materials and offers new technological and economic opportunities. Depending on how

many dimensions of the dispersed particles is in the nanometer range, three types of nanocomposites can be classified. Isodimensional nanoparticles, such as spherical silica nanoparticles [1, 2, 3] and semiconductor nanoclusters [4] have all three dimensions in the order of nanometers whereas nanotubes or whiskers have elongated structure with two dimensions in the nanometer scale. Finally, in the third type of nanocomposites, the filler is present in the form of sheets of one to a few nanometer thick to hundreds to thousands nanometers long. Such layered host crystals include graphite [5], metal chalcogenides such as MoS_2 [6], graphite oxide [7, 8], metal phosphates such as $Zr(HPO_4)$ [9], clays and layered silicates such as montmorrillonite and kaolinite, and layered double hydroxides [10, 11], etc.

Partly because of the availability and low cost, as well as the well studied intercalation chemistry of clays, nanocomposites based on clay and layered silicates have been widely investigated [12]. Owing to the nanometer-size particles obtained by dispersion, these nanocomposites exhibit markedly improved properties such as increased moduli, strength and heat resistance, decreased gas permeability and flammability when compared with the pure polymer or conventional (microscale) composites. The first industrial application was demonstrated by Kojima and coworkers for nylon-6 nanocomposites [13]. This material was then marketed by UBE industries and Bayer. It is currently used to make the timing belt cover of Toyota's car engines and for the production of packaging films.

1.1.1 Structure of Layered Silicates

The layered silicates used in nanocomposites belong to the structural family known as the 2:1 phyllosilicates, same as the better known minerals talc and mica [14]. Their crystal lattice consists of two-dimensional, 1 nm thick layers formed by fusing two silica tetrahedral sheets with an edge-shared octahedral sheet of alumina or magnesium. The lateral dimensions of these layers vary from 20 nm to tens of micron depending on the particular type of silicate. Stacking of the layers generates a regular van der Walls gap known as the interlayer or gallery. The galleries are typically occupied by cations (i.e. Na^+ or Ca^{2+}) which balance the charge deficiency generated by isomorphous substitution within the layers (for example, Al^{3+} replaced by Mg^{2+} or Mg^{2+} replaced by Li^+. Because of the relatively weak forces between the layers, intercalation of small molecules, even polymers, between the layers is easy [12].

Because pristine mica-type layered silicates usually contain hydrated Na^+ or Ca^{2+} ions, they are hydrophilic in nature and have poor miscibility with most hydrophobic polymers. In order to render the hydrophilic phyllosilicates more organophilic, the hydrated cations of the interlayer can be exchanged with cationic surfactants such as primary, tertiary and quaternary ammonium or phosphonium ions. The alkyl ammonium cations in the modified clay (or organoclay) can lower the surface energy of the inorganic host and improve the compatibility with the polymer matrix.

The most commonly used layered silicates are montmorillonite, hectorite and saponite. Their structure and chemical formula are shown in Figure 1.1 and Table 1.1 respectively. The ability of a clay mineral to exchange ions is measured by its cation exchange capac-

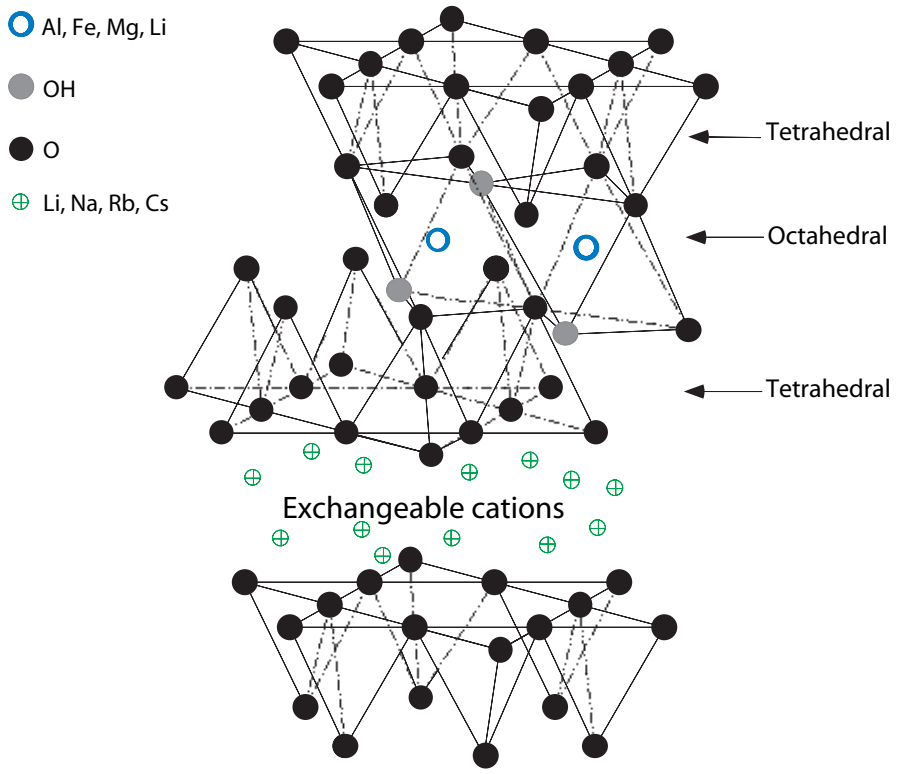

Figure 1.1: Structure of 2:1 layered silicates [15].

ity, which is known as CEC and expressed in meq/100 g. As the layer charge varies from layer to layer, the CEC must be considered as an average value over the whole crystal rather than being locally constant. Since the majority of the exchangeable cations is located inside the galleries, an ion-exchange during which the hydrated metal cations are exchanged with more bulky organic cations such as alkylammoniums typically results in a larger interlayer spacing.

Table 1.1: Chemical Structure of commonly used 2:1 phyllosilicates [a]

2:1 Phyllosilicate	Formula
Montmorillonite	$M_x(Al_{4-x}Mg_x)Si_8O_{20}(OH)_4$
Hectorite	$M_x(Al_{6-x}Li_x)Si_8O_{20}(OH)_4$
Saponite	$M_xMg_6(Si_{8-x}Al_x)O_{20}(OH)_4$

[a] M=monovalent cation; x=degree of isomorphous substitution (between 0.5 and 1.3)

1.1.2 Nanocomposite Structures

In general, depending on the interaction between layered silicates and polymers, three main types of composites may be obtained when a layered silicate is associated with a polymer (Figure 1.2).

When the polymer is unable to intercalate between the silicate sheets, a phase separated composite (Figure 1.2a) results, whose properties lie in the same range as conventional microcomposites. On the other hand, intercalated structure(Figure 1.2b) is obtained when a single (and sometimes more than one) extended polymer chain is intercalated between the silicate layers thereby the silicate galleries are expanded whereas the registry is still retained as a well ordered multilayer morphology. When the silicate layers are completely disordered and uniformly dispersed in the continuous polymer matrix, an exfoliated structure is formed (Figure 1.2c).

X-ray diffraction (XRD) and transmission electron microscopy (TEM) are the two complementary techniques to characterize those structures. XRD is most commonly

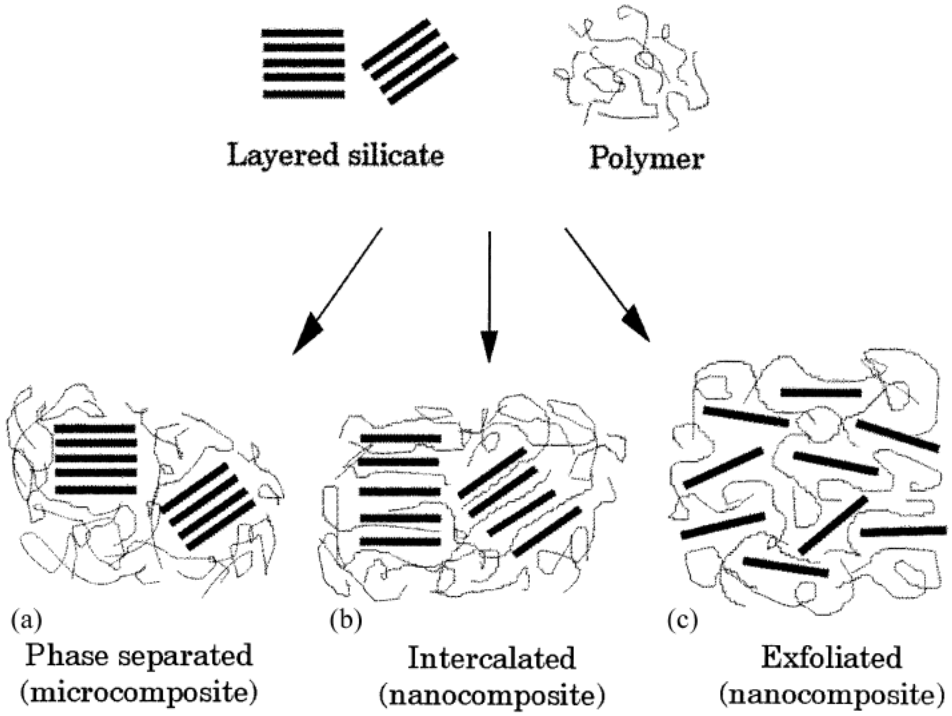

Figure 1.2: Scheme of different types of composites of polymers and layered silicates: (a) phase-separated microcomposite; (b) intercalated nanocomposite and (c) exfoliated nanocomposites.

used to identify intercalated structures due to periodic arrangement of the silicate layers in both the pristine and intercalated states. The interlayer spacing can be calculated by the characteristic diffraction peak shown in XRD pattern, according to Bragg equation:

$$2d \sin\theta = n\lambda \tag{1.1}$$

where λ is the wave length of the X-ray radiation, n is the order of diffraction, d is the interlayer spacing and θ is the diffraction angle. When interlayer expands as a result of polymer intercalation, the position of the diffraction peak will shift to a lower angle. However, when the interlayer spacing increases beyond a certain distance (i.e. exceeding 8 nm in the case of ordered exfoliated structure) or the ordering of the layers diminishes (i.e. in the case of disordered exfoliated structure), no more diffraction peaks are visible in the XRD pattern. In these cases where XRD is not sufficient to discern ordered exfoliated structure versus disordered exfoliated structure, TEM is extremely useful in providing more details in the spacial arrangement of silicate layers. Due to the higher electron density of silicates than most polymers, the fringes of the silicate layers appear dark lines under electron microscope, providing direct observations of the spacial correlations of the silicate layers as well as of the homogeneity of clay dispersion in the polymer matrix. However, as the TEM observation is highly localized and qualitative in nature compared to XRD, these two techniques are best to be used together to complement each other in determining nanocomposite structures.

Differential scanning calorimetry (DSC) provides more information concerning intercalation. The many interactions the intercalated chains of the polymer form with the

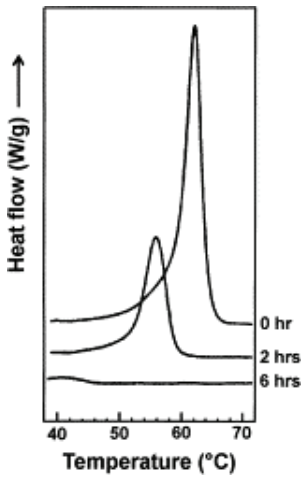

Figure 1.3: DSC traces for PEO/Na-montmorillonite mixtures heated to 80 °C for 0, 2 and 6 hours [16].

silicate hosts greatly reduce its rotational and translational mobility, which can be readily detected by DSC. For example, DSC measurements (Figure 1.3) on an intercalated PEO/montmorillonite nanocomposite (20 wt% PEO) showed a decreased endotherm corresponding to the melting transition of PEO with the intercalation time [16]. As the intercalation reaction progressed, more PEO chains were intercalated and lost its bulk crystallinity. DSC studies of polystyrene intercalated organically modified layered silicate also indicated that the intercalated nanocomposite does not show a thermal transition in the range corresponding to the glass transition of pure polystyrene [17]. In fact, the glass transition occurs at temperatures higher than those shown in Figure 1.4 due to elevation of the energy shreshold needed for the intercalated polymer.

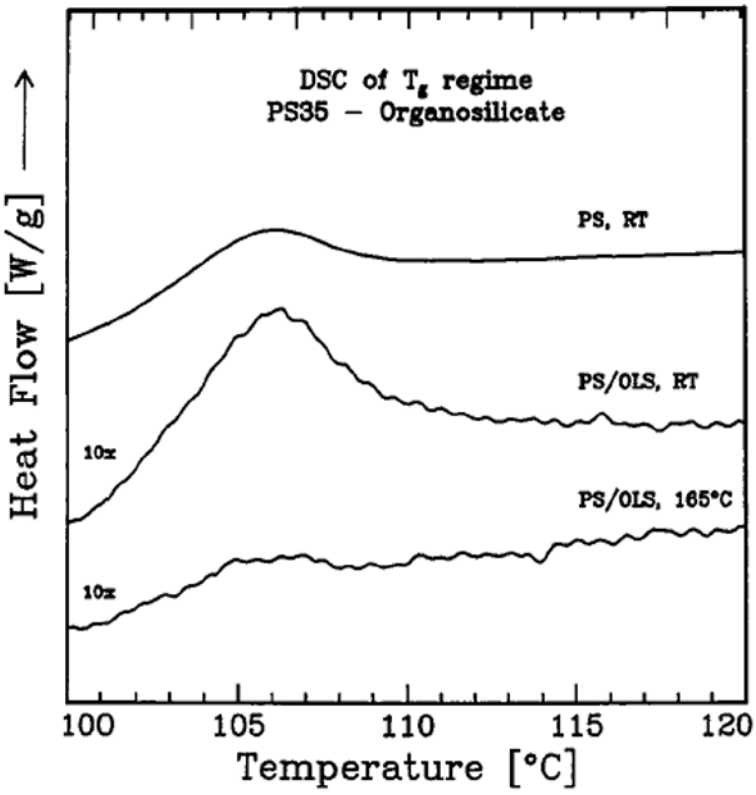

Figure 1.4: DSC traces of pure polystyrene (PS, RT), a physical mixture of PS/organosilicate (PS/OLS, RT), and polystyrene intercalated organosilicate (PS/OLS, 165 °C) [17].

1.1.3 Nanocomposite Preparation

Three approaches have been used to fabricate polymer/clay nanocomposites, according to the type of starting materials and processing methods.

1.1.3.1 Solution Intercalation

Solution intercalation is based on a solvent system in which the polymer is soluble and the silicate layers are swellable. The layered silicate is first swollen or delaminated in a solvent, depending on the interaction of the solvent and the layered silicate. When the polymer and silicate solutions are mixed, the dissolved polymer chains either adsorb on to the delaminated silicate layers or intercalate and displace the solvent within the silicate interlayer. In both cases, however, upon solvent removal, the layers usually reassemble to reform the ordered structures with polymer chains sandwiched in between silicate layers, resulting in intercalated nanocomposites. Water soluble polymers, such as poly(ethylene oxide) [18, 19], poly(vinyl alcohol) [18, 20], poly(vinylpyrrolidone) [21] and poly(acrylic acid) [22] have been intercalated into clay galleries via this method. Organic solvents have also been used to produce nanocomposites based on high-density polyethylene [23], poly(lactide) [24] and polyimide [25]. However, one of the disadvantages of this method is that intercalation only occurs for certain polymer/solvent pair. In addition, solution intercalation typically involves use of large quantities of aqueous or organic solvent, which is both environmentally unfriendly and economically prohibitive for an industrial-scale application.

1.1.3.2 In-situ Polymerization

The most promising reaction to create polymer/clay nanocomposites is the intercalation of monomers into the clay gallery followed by polymerization (in-situ polymerization). Because of the low viscosity of the monomer, it is much easier for the monomer to migrate into the clay gallery and break up particle agglomerates after polymerization. Although in-situ polymerization has been studied since the 1960s, the first systematic study on polymer/clay nanocomposites was pioneered by researchers from Toyota Motor Company, who synthesized the first exfoliated nylon-6/clay nanocompoiste for automotive applications in the 1990s [13, 26]. Since then, this technique has been applied to various thermoplastics such as polystyrene [27], polypropylene [28] as well as thermosets such as epoxy [29], unsaturated polyester [30] and elastomers [31].

1.1.3.3 Melt Intercalation

Instead of using solvent as the medium, the layered silicate can be mixed directly with molten polymer either statically or under shear. Under optimal conditions and if the layer surfaces are sufficiently compatible with the polymer, the polymer chains can crawl into the interlayer space and form either an intercalated or an exfoliated nanocomposite. Because it eliminates the use of aqueous/organic solvents and is more compatible with conventional polymer processing techniques such as extrusion, compounding and injection molding, melt intercalation has become increasingly attractive since it came to prominence in 1990s [17]. A wide range of polymers, such as PEO [16], polystyrene [17], polypropylene and polyamide 6 have been intercalated into organoclays using this

method.

1.1.4 Dynamics of Confined Polymers

The fact that polymer melts can intercalate into layered silicates unassisted by shear or solvents implies that polymer chains can undergo large center of mass displacement in almost two dimensional interstices as the distances between the confining surfaces are substantially smaller than the unperturbed radius of gyration of the polymer and are comparable to the monomer size. The thermodynamics that drives the polymer melt intercalation has been addressed by a lattice-based mean field theory by Vaia and Giannelis [32]. In general, the outcome of polymer intercalation is determined by an interplay of entropic and enthalpic factors. Confinement of the polymer inside the interlayers results in a decrease in the overall entropy of the polymer chains. However, the entropic penalty of polymer confinement may be compensated by the increased conformational freedom of the tethered surfactant chains in a less confined environment, as the layers separate. Since for small increases in gallery height the total entropy change is small, the possibility of intercalation will rather be driven by an "enthalpic force", namely, the establishment of favorable polymer-surface interactions to overcome the entropic penalty of polymer confinement.

Vaia et al. [33] have studied the kinetics of melt intercalation by following the time evolution of XRD diffraction patterns for statically annealed polystyrene/octadecylammonium modified fluorohectorite. Figure 1.5 shows a typical temporal series of XRD patterns for a polystyrene PS30 (M_w= 30 KDa)/octadecylammonium modified

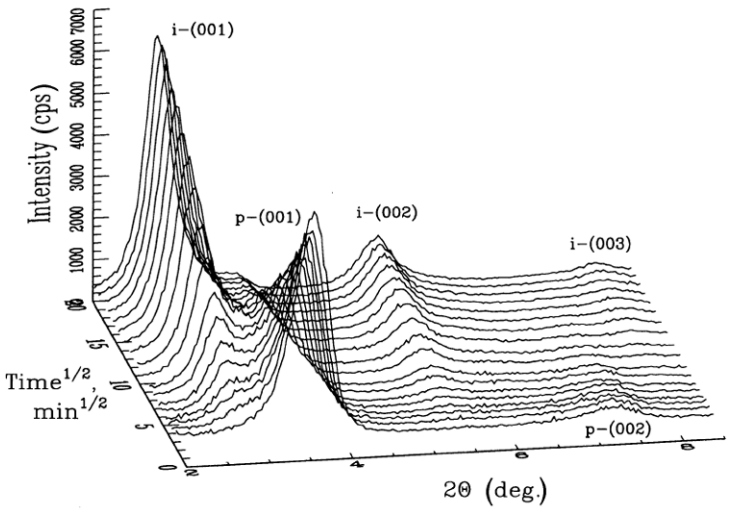

Figure 1.5: Typical temporal series of XRD patterns for a polystyrene (M_w=30 KDa)/C18FH mixture annealed in-situ at 160 °C in vacuum [33].

fluorohectorite (C18FH) mixture annealed in-situ at 160 °C in vacuum. The two initial peaks p(001) and p(002) at 2θ= 4.15 and 8.03 respectively are due to the spacing between the silicate layers in C18FH, corresponding a interlayer distance d(001)= 2.13 nm. Their intensities decrease as the annealing proceeds and new peaks representing the intercalated nanocomposite appear. The intercalated nanocomposite has a larger interlayer distance caused by insertion of the polymer. The basal reflections of the intercalate, i(001), i(002) and i(003) are observed at 2θ= 2.82, 5.66 and 8.07 and correspond to d(001)= 3.13 nm. By integrating the intensity of both non-intercalated and intercalated peaks, the authors were able to estimate the fraction of intercalated silicates as a function of the annealing time, which is shown in Figure 1.6. It was found that high annealing temperature as well as lower molecular weights increase the rate of PS intercalation.

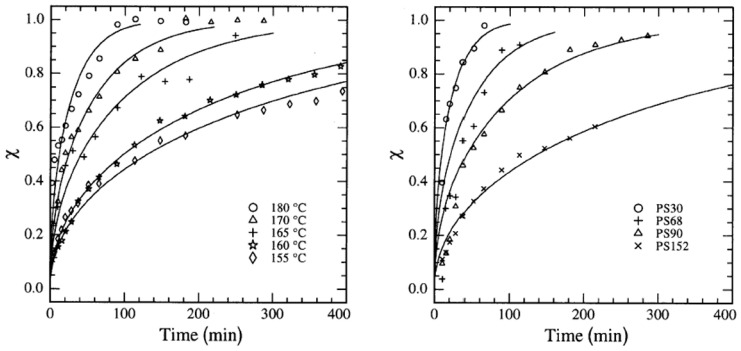

Figure 1.6: The fraction of polystyrene intercalated in C18FH at various annealing temperatures (PS30, M=30 KDa) (left) and for various polymer molecular weights at 180 °C (right). The molecular weights of polystyrene used were 30 KDa for PS30, 68KDa for PS68, 90KDa for PS90 and 152KDa for PS152 [33].

1.1.5 Properties

Layered silicates have proved to provide tremendous property improvements of the polymer in which they are dispersed. The enhancements include increased modulus and strength, enhanced thermal stability and fire retardancy as well as reduced gas and solvent permeability, etc.

The Young's modulus (or tensile modulus), which expresses the stiffness of a material at the start of a tensile test, has shown to be strongly improved when exfoliated nanocompoistes are formed. Table 1.2 compares the properties of Nylon-6 and those of the Nylon-6 nanocomposites at 4.7 wt% of clay loading [13, 26]. It is interesting to note that the Nylon-6 nanocomposite has a remarkable enhancement of tensile modulus, tensile strength which is not accompanied by a sacrifice of its impact strength usually displayed by conventional microcomposites.

The storage modulus of a material is often measured by dynamic mechanical analysis (DMA), which records the response of a material to a cyclic deformation (i.e. tensile

Table 1.2: Properties of Nylon-6 and Nylon-6/clay nanocomposites

Property	Nylon-6	Nano-composite
Tensile modulus (GPa)	1.11	1.87
Tensile strength (MPa)	68.6	97.2
Heat distortion temperature (°C)	65	152
Impact strength (kJ/m^2)	6.21	6.06
Water adsorption	0.87	0.51

deformation) as a function of the temperature. DMA results are usually expressed by three main parameters: (1) the storage modulus (E'), corresponding to the elastic response to the deformation; (2) the loss modulus (E"), corresponding to the elastic response to the deformation and (3) tanδ, ratio of E'/E", useful for determining the occurrence of molecular mobility transitions such as the glass transition temperature.

No significant difference in E' can be seen for an intercalated PMMA [34] or polystyrene [35] nanocomposite, indicating the inefficiency of intercalated structures in improving the elastic properties of the polymer matrix. On the other hand, the shift and broadening of the tan δ peak towards higher temperatures for the nanocomposite indicate an increase in the glass transition temperature together with some broadening of this transition. This behavior has been ascribed to the restricted segmental motions at the organic-inorganic interfaces.

Another interesting property exhibited by polymer/clay nanocomposites is their increased thermal stability as well as the ability to retard flame at low filler loadings. The thermal stability of a material is usually assessed by thermogravimetric analysis (TGA), which measures the sample mass loss due to volatilization of degraded by-products as a function of a temperature ramp. Higher onset decomposition temperatures have been observed for many polymer/clay nanocomposites, in both exfoliated and intercalated states [14, 34]. The increase of thermal stability is usually attributed to the hindered out-diffusion of the volatile decomposition products, as a direct result of the decrease in permeability [14], while other researchers consider char formation as the main reason for the enhanced thermal stability [36].

1.2 Polymer Processing and Synthesis in Supercritical Carbon Dioxide

1.2.1 Supercritical Carbon Dioxide ($scCO_2$) as a Reaction Medium and Processing Aid

Carbon dioxide (CO_2) is an abundant, inexpensive, nontoxic and nonflammable solvent that has attracted extensive interest as a polymerization and processing medium in recent years, primarily driven by the need to replace conventional solvents with more environmentally benign and economically viable procedures [37]. With a relatively low and accessible critical temperature (T_c) of 31.1 °C and critical pressure (P_c) of 73.8

Table 1.3: Physical properties of supercritical fluids compared to liquids and gases. [39]

Phase	Density ($g\ cm^{-3}$)	Viscosity ($g\ cm^{-1}s^{-1}$)	Diffusion Coefficient (cm^2s^{-1})
Gas (STP)	10^{-3}	10^{-4}	10^{-1}
Supercritical Fluid	0.3 – 0.8	10^{-4}– 10^{-3}	10^{-3}– 10^{-4}
Liquid	1	10^{-2}	$<10^{-5}$

bar [38], CO_2 can be readily employed as a supercritical fluid, which has many unique advantages such as gas-like transport properties, liquid-like densities (Table 1.3) and near-to-zero surface tension, etc. Due to the high compressibility of CO_2, its physiochemical properties (density, viscosity, diffusivity, solubility parameter, etc) can be adjusted from gas-like to liquid-like values by simply varying the temperature or pressure of the system. Furthermore, the fact that CO_2 is a gas under ambient conditions makes its separation from the polymeric products facile, circumventing the costly drying process associated with conventional organic solvents, which is very important in polymer processing and synthesis.

Another important property of CO_2 is its ability to plasticize many polymers, which is due to its substantial solubility in these polymers and often leads to a dramatic decrease in the glass transition temperature (T_g) of these materials. For example, the T_g of polystyrene was found to be reduced by up to 50 °C under CO_2 pressures of only 25 bar [40]. It has been shown by various methods [41] that CO_2 is a good plasti-

cizer for a range of polymers, including polystyrene [42, 43, 44, 45, 46], polyethylene [47, 48], poly(ethylene terphthalate) [40, 47, 49], polyisoprene [43], polypropylene [47], poly(vinyl chloride) [40, 49], nylon [47] and poly(2,6-dimethylphenylene oxide) [49]. CO_2 has also been shown to plasticize polymethacrylate [40, 43, 44, 45, 49, 50, 51, 52, 53, 54, 55, 56, 57], polycarbonates [40, 45, 49, 56, 58], polyurethanes [49, 59], polyimides [49], crosslinked elastomers [60] and networks [61], and a number of block copolymers [43] and polymer blends [40, 62, 63, 64].

While the plasticization effect of CO_2 in depressing T_g in a variety of polymers has been investigated extensively in the literature, the effect of CO_2 on the melting temperatures has only been analyzed for a few systems [65]. Handa et al. have shown that CO_2 has a direct effect on the melting behavior of semicrystalline polymers. A significant depression in the melting temperature was observed in $scCO_2$, due to its high solubility in syndiotactic polystyrene (s-PS), whereas there was no change in T_m when CO_2 was replaced with N_2. This behavior has been observed in PET as well, showing that the depression in melting temperature is dictated by both the polymer-gas interactions and the intrinsic crystal characteristics.

1.2.2 Processing of Polymer in Carbon Dioxide

$ScCO_2$-assisted polymer processing generally takes advantage of the unique ability of CO_2 to swell and plasticize many polymers, which leads to significant increases in free volume and mobility of polymer chain and often manifests as a depression of T_g. The increased chain mobility and reduced T_g of polymers swollen in CO_2 have been

employed by several groups to enhance conventional polymer processing.

1.2.2.1 CO_2-induced Crystallization

The increase of chain mobility induced by $scCO_2$ has important implications especially for semicrystalline polymers. This happens in some polymers when CO_2 induced plasticization allows polymer chains to rearrange into more energetically favored ordered configurations, thus forming crystallites. This effect has been applied in drawing fibers, in which the presence of CO_2 can impart a significant amount of molecular orientation and under certain conditions can induce cystallization [66]. Hobbs and Lesser [67, 68] have investigated the drawing of flexible chain polymers in presence of $scCO_2$. They have shown that the draw ratio of the PET fibers drawn in $scCO_2$ was 30% higher compared to fibers that were cold-drawn. Also, due to the significantly higher crystallinity and enhanced orientation in these $scCO_2$-drawn fibers, they exhibit improved moduli and ultimate strength.

$ScCO_2$ has also been found to change the degree of crystallinity in various other polymers such as poly(phenylene sulfide) [69, 70], poly(bisphenol A carbonate) [71], poly(aryl ether ketone) [72], syndiotactic PS [73, 74], though no change in degree of crystallinity was observed for PVDF under dense CO_2 [75].

1.2.2.2 Foaming of Polymers and Polymer/clay Nanocomposites

Microcellular foams are generally defined as foams with cell size less than 10 um and a cell density of ca. 10^8 cell/cm^3, which can be turnable over a wide range. These

microcellular polymeric foams may have properties superior to those of unfoamed polymers, e.g., higher impact strength, higher toughness, higher stiffness to weight ratio, higher fatigue life, higher thermal stability, lower dielectric constant and lower thermal conductivity [62]. In general, a reduced cell size and an increase in the cell density promote improved properties.

$ScCO_2$ can be used as a foaming agent in polymer melt processing since, as pressure of a polymer plasticized with CO_2 is rapidly released, a plastic foam may be produced. A vast amount of research has used CO_2 as a foaming agent to produce microcellular polymeric foams, including polycarbonate [76], PET [77], polystyrene [78], polypropylene [79, 80], PMMA [81] and biodegradable polymers such as poly(lactide-co-glycolide) (PLGA) copolymer [82]. Due to its relatively high solubility in polymers, CO_2 has proven a better foaming agent (in terms of higher cell densities) than other non-expensive atmospheric gases like nitrogen [83, 84]. An example of commercially available process to produce foams of thermoplastics (including polystyrene, polyolefines and polyesters) is the NuCell® process developed by Trexel Inc., who claims production of foams with superior properties than hydrocarbon-blown foams of similar densities.

Compared to conventional micron-sized filler particles used in the foaming process, the extremely fine dimensions, large surface area and intimate contact between clay particles and polymer matrix may greatly alter cell nucleation and growth. Zeng et al. [85] have developed a new strategy of improving nucleation efficiency in CO_2 foaming by introducing clay as a nucleation agent to produce PMMA and PS/clay nanocomposite

foams. They have found that clay serves as a very efficient nucleation agent which greatly reduces the cell size and increases the cell density of the foams. The nucleation effect is also found to be closely related to the dispersion state of clay, i.e., intercalated vs. exfoliated, wherein the exfoliated nanocomposite foam provides the highest density and smallest cell size.

With a different emphasis on producing polymer/clay nanocomposites, Garcia-Leiner et al. applied the similar procedure in extrusion foaming to make high-density polyethylene (HDPE) and poly(trimethyleneterephthalate) (PTT)/clay nanocomposites using $scCO_2$ [86]. Intercalated structures were produced in the presence of $scCO_2$ even when favorable interactions between the polymer and the clay are not present: e.g. a 33% increase in the typical clay d-spacing was realized for HDPE/clay nanocomposites with the assistance of $scCO_2$, while a 10% increase was observed for PTT/clay nanocomposites.

1.2.2.3 CO_2-assisted Melt Processing

High viscosity has been a major obstacle to the processing of high-molecular-weight polymers or particles filled composites with conventional processing technique such as injection molding and extrusion. Consequently, the plasticization effect of CO_2 in polymers may be applied in injection molding and extrusion processes where lower temperatures with respect of conventional processes may be used, thus preventing degradation of thermal sensitive polymers. Early work on the effect of $scCO_2$ in viscosity reduction involved studies on viscosity reduction for polydimethylsiloxane (PDMS) with dissolved

CO_2. Gerhardt et al. [87] demonstrated a reduction up to 60% in viscosity at 50 °C and low shear rates. Lee et al. performed CO_2-assisted PE/PS blending using single and twin-screw extruders with different arrangements, claiming a decrease of size and a more even distribution of the dispersed PS domains in the blend by increasing the CO_2 dose rate [62]. Other studied polymer systems include poly(ethylene glycol) [88, 89, 90, 91, 92], polystyrene [42, 93, 94, 95, 96], blend of polystyrene and PMMA [97], etc.

1.2.2.4 Reactive Blending of Polymer/Polymer and Polymer/Inorganic Composites

McCarthy and colleagues have extended the idea of polymerization being facilitated by plasticization of the polymer phase to develop a new route to polymer/polymer blends [98, 99, 100]. The general procedure has been to use $scCO_2$ as a swelling agent in order to infuse or "impregnate" a CO_2-insoluble polymeric host with a mixture of monomer(s) and an initiator. Polymerization is then initiated thermally within the host polymer to form a blend, either in the presence of $scCO_2$ or after venting the CO_2 solution. In these experiments, the solid CO_2-swollen polymer matrices explored include poly(chlorotrifluoroethylene) (PCTFE), poly(4-methyl-1-pentene) (PMP), low-density polyethylene (LDPE), bisphenol A polycarbonate, poly(oxymethylene), and nylon-6,6. Since this work, McCarthy and others have extended this method to prepare several different polymer/polymer blends, such as polystyrene/polyethylene composites [101], poly(vinyl chloride) (PVC)/poly(methacrylic acid) (PMAA) composites [102],

and poly(tetrofluoroethylene-co-hexafluoropropene) (FEP)/polystyrene blends [103]. It has been shown that, by a proper selection of operative conditions, it is possible to vary the penetration depth, thus achieving surface modification leaving unaltered the bulk of the polymer matrix [104].

Since polymer/clay nanocomposites have been found to have interesting physical and mechanical properties, Lesser and coworkers have developed a synthetic route to polymer/clay nanocomposites with high concentrations of clay and a high degree of order [105]. $ScCO_2$ was primarily used as the reaction medium allowing homogeneous dispersion of monomer, initiator and subsequent polymerization under low viscosity. This overcomes the challenges of high viscosity usually encountered in the processing of these materials at clays concentration above 20 wt%. The resultant nanocomposites were found to have intercalated structures and exhibit a significantly higher storage modulus compared to neat polymer. By inducing a nematic order to the silicates, a 220% increase in tensile modulus was achieved for the glassy polymer.

1.2.3 Synthesis of Polymer in Carbon Dioxide

Although CO_2 has been demonstrated to be a good solvent for many small molecules including many common vinyl monomers [106], it is an exceedingly poor solvent for most high molar mass polymers except for certain amorphous or low-melting flcomparisonuoropolymers and silicones [107, 108, 109, 110]. Consequently, the relative insolubility of many hydrocarbon polymers in CO_2 necessitates the use of heterogeneous polymerization for most industrially important polymers.

Table 1.4: Comparison of common heterogeneous polymerization processes.

Characteristic	Emulsion	Suspension	Dispersion	Precipitation
Monomer Solubility in Continuous Phase	Insoluble	Insoluble	Soluble	Soluble
Polymer Solubility in Continuous Phase	Insoluble	Insoluble	Insoluble	Insoluble
Initiator Location	Continuous Phase	Monomer Phase	Continuous Phase	Continuous Phase
Particle Stabilized?	Yes	Yes	Yes	No
Particle Size Range	50 – 500 nm	20 – 1000 μm	0.1 – 10 μm	N/A

1.2.3.1 Heterogeneous Polymerization in Carbon Dioxide

There are four types of common heterogeneous polymerization processes, namely emulsion, suspension, dispersion and precipitation polymerization, based on the initial state of the polymerization mixture, the kinetics of polymerization, the mechanism of particle formation and the shape of size of the final polymer particles [111]. A comparison of some of the characteristic and parameters of these heterogeneous processes is shown in Table 1.4. In both emulsion and suspension polymerizations, the monomer and polymer are insoluble in the continuous phase. Due to the high solubility of most vinyl monomers in $scCO_2$, suspension and emulsion polymerizations are relatively rare in $scCO_2$ and probably will not be a very useful process for commercially important monomers.

In emulsion polymerization, the initiator is soluble in $scCO_2$ so the monomer and initiator are initially segregated due to the poor solubility of the monomer in $scCO_2$. A surfactant is typically added to the system at concentrations above its critical micelle concentration so that micelles form which can disperse the monomer within them. As the polymerization takes place by thermal or ultraviolet radiation, the polymer particles form almost exclusively in the micelles, reach their critical molecular weight, precipitate and then become stabilized by the surfactant. As a result, emulsion polymerization typically leads to small, uniform particles with diameter ranging from 50 to 500 nm [112, 113].

In suspension polymerization, both the monomer and initiator are insoluble in the continuous phase whereas the polymer and initiator are soluble in the dispersed monomer droplets. High loadings of polymeric stabilizers are typically added into the system to stabilize the initiator-containing monomer droplets. As the polymerization proceeds, the monomer-rich phase is polymerized, with each initial monomer droplet becoming a polymer particle, ranging from 5 to 1000 μm in diameter.

With precipitation polymerization, the monomer and initiator are initially soluble in the reaction medium, but as the polymer grows in size, it becomes insoluble and precipitates out of the medium. Since nothing is added to control the polymer precipitation, it finally forms aggregates in various undefined morphologies.

In contrast to precipitation polymerization, a dispersion polymerization is identical in its starting composition with the exception of the addition of a solvent-soluble stabilizer. Once the polymer chains reach a critical molecular weight, the polymer is

stabilized as a colloid, and coagulation or agglomeration of the particles is prevented by the presence of the surface active stabilizer, leading to production of spherical polymer particles typically in the range of 0.1– 10 μm in diameter [114]. Due to the good solubility of many small molecules in CO_2, dispersion polymerization constitutes the most useful method thus far for producing high molecular weight, insoluble, industrially important hydrocarbon polymers in CO_2-based system.

1.2.3.2 Dispersion Polymerization in Carbon Dioxide

In 1994, DeSimone et al. reported the first dispersion polymerization of methyl methacrylate (MMA) in $scCO_2$ [115]. In the presence of 2-4% w/v of a CO_2-soluble fluorinated homopolymer (poly(dihydroperfluorooctyl acrylate) PFOA), a stable, opaque-white colloidal dispersion was formed in the reaction vessel. Upon venting CO_2, PMMA could be recovered as a dry, free flowing powder with high molecular weights ((190-325) KDa) and yields (>90%). Scanning electron micrographs (Figure 1.7) showed that the product consisted of uniform spherical particles with average diameters in the range of 1.2-2.5 um. In contrast, in the absence of any stabilizers, the precipitation polymerization of MMA in $scCO_2$ led to nondescript PMMA morphologies (Figure 1.8) with relatively low molecular weights ((77-149) KDa) and low yields (10-40%). They postulated that PFOA was an effective amphiphilic stabilizer because it contained a lipophilic backbone that could anchor onto the acrylic surface of the growing polymer particles. The CO_2-philic nature of the fluoroalkyl side chains on the stabilizer caused extension of the PFOA chain into the continuous phase, thus giving rise to steric stabilization

and preventing particle flocculation (Figure 1.9).

These initial findings have prompted a large number of subsequent investigations by the DeSimone group and others. Successful dispersion polymerizations in $scCO_2$ have been reported for a wide range of vinyl monomers, including methyl methacrylate [116, 117, 118, 119, 120, 121], styrene [122, 123, 124, 125], 2-hydroxyethyl methacrylate [126], vinyl acetate [127], acrylonitrile [128], N-vinyl pyrrolidinone [129, 130], glycidyl methacrylate [131, 132], and copolymer of methyl methacrylate and ethyl methacrylate [133]. Since most hydrocarbon polymers are insoluble in $scCO_2$, the key to making high molecular weight polymer in $scCO_2$ is to use a surfactant (or stabilizer), which ensures that the growing polymer chains remain dispersed in CO_2 and the polymerization continues to higher degree of polymerization than the analogous precipitation reaction in the absence of stabilizer. The effectiveness of a surfactant is governed by two factors: 1) the stabilizer needs an anchoring segment which attaches to the monomer/polymer particle either through physical adsorption or chemical grafting; 2) a CO_2-philic (fluorinated- or siloxane-based) segment which projects into the continuous CO_2 phase and provides steric stabilization for the growing polymer particles. Building on the success of fluorinated homopolymers (Figure 1.10(a)) such as PFOA, a range of other stabilizers has been developed for dispersion polymerization in $scCO_2$, including diblock copolymers (Figure 1.10(b)) [123, 134, 135, 121, 127, 136, 137, 138, 139, 126, 131], graft copolymers (Figure 1.10(c)) [118, 140, 141] and random copolymers (Figure 1.10(d)) [134, 125, 142, 143].

Silicone polymers are attractive as stabilizers, primarily because they are consider-

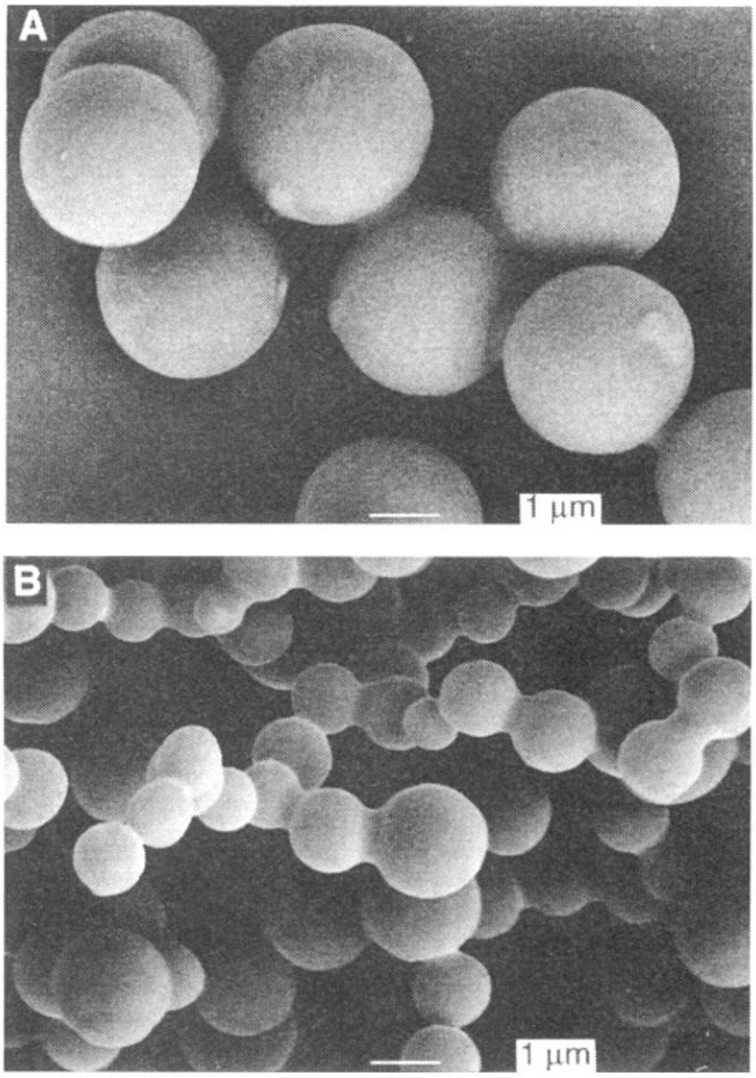

Figure 1.7: SEM images of PMMA particles synthesized in CO_2 with AIBN used as the initiator and with (A) 2% (w/v) HMW poly(FOA) or (B) 2% (w/v) LMW poly(FOA) [115].

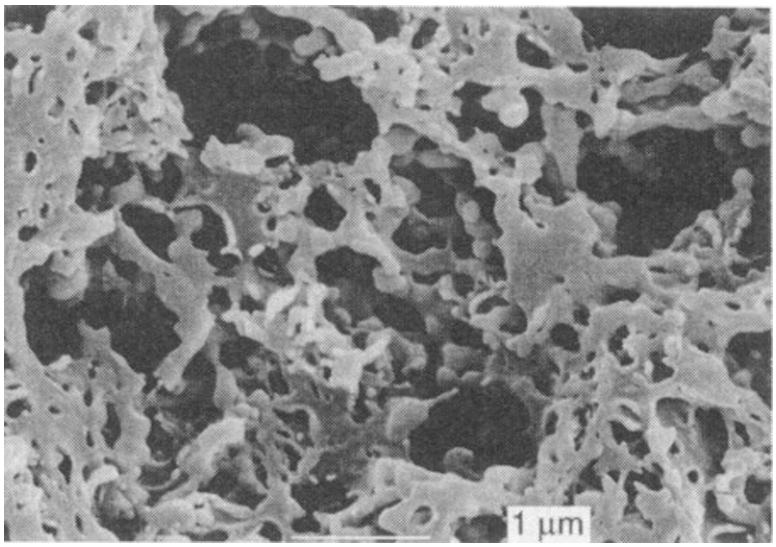

Figure 1.8: SEM image of PMMA synthesized in CO_2 without stabilizer [115].

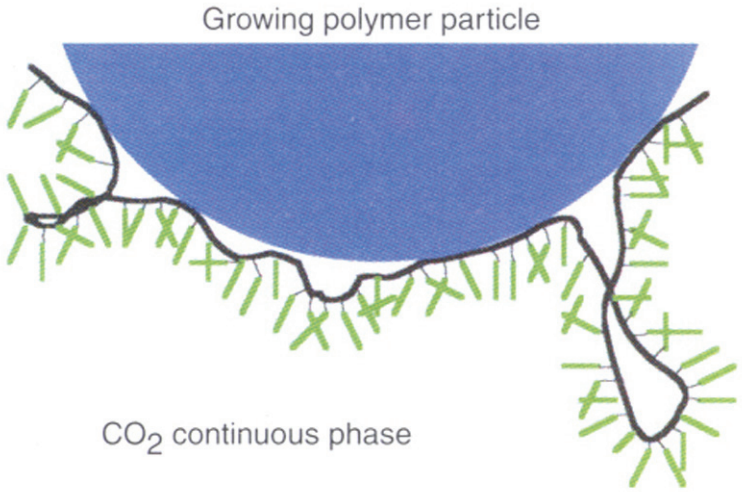

Figure 1.9: Schematic illustration of a PMMA particle (shown in blue) stabilized by poly(FOA) in which the lipophilic backbone (shown in black) acts as an anchor for the fluorocarbon steric stabilizing moieties (shown in green) [115].

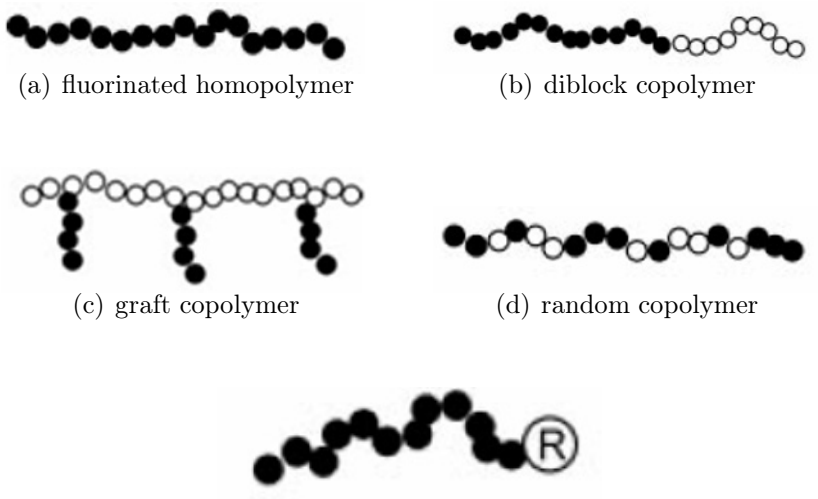

(a) fluorinated homopolymer (b) diblock copolymer

(c) graft copolymer (d) random copolymer

(e) reactive macromonomer

Figure 1.10: Stabilizer morphologies used for dispersion polymerization in CO_2. Filled circules = CO_2-philic monomer units, open circles = CO_2-phobic monomer units, R = reactive polymerizable end-group [144].

ably less expensive than fluorinated materials and demonstrate reasonable solubility in CO_2. Silicones are also soluble in many conventional organic solvents, which makes the characterization of these materials somewhat easier than in the case of high molecular weight fluoropolymers. Another alternative approach to the stabilization of polymer colloids is to use a macromonomer which has a reactive end-group that can graft into the growing polymer particles (Figure 1.10(e)). The first successful dispersion polymerizations of styrene and MMA using PDMS-containing macromonomers were reported in 1996 [120]. More recent examples of dispersion polymerization via a commercially available methacrylate terminated poly(dimethyl siloxane) (PDMS-MMA) macromonomer stabilization have been investigated by other research groups [145, 146, 133, 147].

The drawback to the use of this type of stabilizer, however, is that it is ultimately incorporated in the final polymer product so that the polymer is contaminated with the

stabilizer. In order to remedy this situation, a commercially available, acid-terminated perfluoropolyether (PFPE) stabilizer that anchors to PMMA chains by a reversible hydrogen bonding interaction has also been reported [148, 149]. FTIR evidence confirmed the existence of a hydrogen bond between the terminal acid functionality of the stabilizer and the ester group of MMA. More recently, the same stabilization effect has been observed for an ester terminated PFPE material, which is thought to interact with the PMMA particles through a weak van der Waals interaction [150].

CHAPTER 2

SUPERCRITICAL CO_2-MEDIATED INTERCALATION OF PEO IN CLAY AND INTERCALATION KINETICS

2.1 Supercritical CO_2-Mediated Intercalation of PEO in Clay

2.1.1 Introduction

Among the typical methods to prepare polymer/clay nanocomposites, solution intercalation has been known for over a century and has proved to be one of the most successful methods of incorporating delaminated clay into polymers [151]. Many poly-

mers have been intercalated into clay via this method: Examples include water soluble polymers such as poly(ethylene oxide) and poly(vinyl alcohol) [18, 152], and organic solvent soluble polymers such as high density polyethylene [23], poly (1-lactide) [24], etc. Despite many laboratory successes with solution intercalation, its application on an industrial scale is still hindered by two major problems: 1) involvement of large quantities of aqueous/organic solvent; 2) a limited number of solvent/polymer pairs available for polymer dissolution and subsequent intercalation.

As mentioned in Chapter 1, supercritical carbon dioxide ($scCO_2$) has attracted a great deal of attention as an environmentally benign, inexpensive, and nonflammable alternative solvent for polymer synthesis and processing [37, 153]. The low viscosity, near-zero surface tension, relative chemical inertness, and high diffusivity of $scCO_2$ results in negligible competitive adsorption with guest molecules on the host substrate and therefore facilitates solute transfer relative to normal solvents. Furthermore, since CO_2 is a gas at ambient conditions, the tedious drying procedure associated with conventional liquid solvents is circumvented and the product is free of residual solvent upon depressurization.

These unique properties of $scCO_2$ have been exploited to prepare polymer blends [154, 155, 98, 101]. The usual method employs $scCO_2$ as a swelling agent to facilitate the diffusion of a guest monomer into a CO_2-swollen polymer matrix. Subsequent polymerization develops a blend of submicron phase-separated polymers.

Intercalation of un-reactive small molecules into layered clay in the presence of $scCO_2$ has also been described [156, 157, 158]. In a recent report, Isii et al. compared

$scCO_2$ with other organic solvents for the intercalation of the dye 4-Phenylazoaniline into a pillared clay [159]. They found $scCO_2$ was a superior adsorption medium for both the equilibrium absorptivity and the adsorption kinetics of the dye intercalation. They attributed the superiority of CO_2 to the lower dye solubility, the solvents higher diffusivity, and its much lower viscosity relative to normal liquids. Although most technologically important polymers are relatively insoluble in CO_2, Garcia-Leiner and Lesser [86] recently reported that $scCO_2$ stimulates intercalation during the foaming of melt-extruded polyethylene and polyesters.

In this chapter, we present unambiguous evidence for $scCO_2$-mediated intercalation of a polymer into silicate nano-layers. We chose PEO/ Na-Montmorillonite as a model system since it is a well-studied system for both solution intercalation and melt intercalation [152, 160, 16]. Conventional solution intercalation is limited to certain polymer/solvent pairs, in which the polymer is soluble and the silicate layers are swellable [20]. Here, $scCO_2$ intercalation is qualitatively different from conventional solution interaction as PEO is not soluble in $scCO_2$. Rather, PEO is reversibly plasticized by $scCO_2$ depressing its melting point and effectively facilitating a melt-like intercalation.

2.1.2 Experimental

2.1.2.1 Materials

Sodium Montmorrillonite (MMT) was obtained from Gelest, Inc and used as received. Poly(ethylene oxide) of average molecular weight M_w=1×10^5 Da was supplied by Aldrich

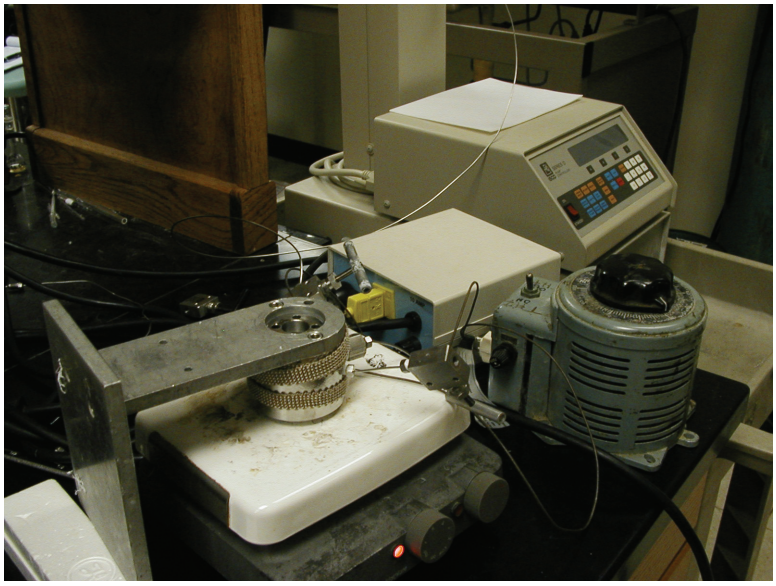

Figure 2.1: High pressure experimental set-up

Chemical Company, Inc.

2.1.2.2 Methods

Composites were fabricated in CO_2 in a 2.5 ml, high-pressure cell equipped with sapphire windows that allow visual observation of the mixture (Figure 2.1). PEO and MMT power mixtures were weighed into the cell according to designated ratios. An Isco automatic syringe pump (Model 260D) was used to pressurize the cell with CO_2 to 193 ± 7 bar, and the mixture was heated to 48 °C with a heating tape wrapped around the cell. After the desired pressure and temperature were reached, the intercalation was allowed to proceed with stirring for 1 day. At the end of the intercalation period, the cell was cooled and CO_2 was slowly vented from the cell. The final product was taken out and dried at room temperature in a vacuum oven overnight, and the resultant materials stored in a desiccator.

2.1.2.3 Characterization

Powder X-ray diffraction (XRD) data between $2\theta = 2°$ and $2\theta = 10°$ were collected on a Rigaku multiflex diffractometer using Cu Kα radiation (40 kV, 40 mA) at 0.5°/min. Thermogravimetric analysis (TGA) and differential scanning calorimetry (DSC) were performed using a Perkin-Elmer Pyris 1 TGA and DSC system. For the DSC measurement, samples weighing 5-10 mg were loaded into an aluminum pan and the sample chamber was purged with argon prior to heating at 10 °C/min. For TGA measurement, approximately 10 mg of samples were loaded in an open ceramic crucible and heated in an argon atmosphere at a heating rate of 10 °C/min.

2.1.3 Results and Discussion

2.1.3.1 XRD Analysis

The efficacy of CO_2-mediated intercalation is shown by the expansion of (001) d-spacing of the PEO/MMT composites. An increase in the gallery spacing is displayed in Figure 2.2. The (001) peak of the PEO/MMT composite shifts from 1.20 nm in the pristine MMT (the gallery contains a monolayer of water) to 1.71 nm at a PEO content of 16.7%. This change in the d-spacing corresponds to a gallery expansion of 0.75 nm, since anhydrous MMT is known to have a 0.96 nm basal plane spacing [152]. At a PEO content of 9.1%, a lower d-spacing is observed (d= 1.38 nm), corresponding to a gallery expansion of 0.42 nm. These results are similar to aqueous solution intercalation results by Shen and coworkers using PEO in water [160]. They reported a smaller gallery

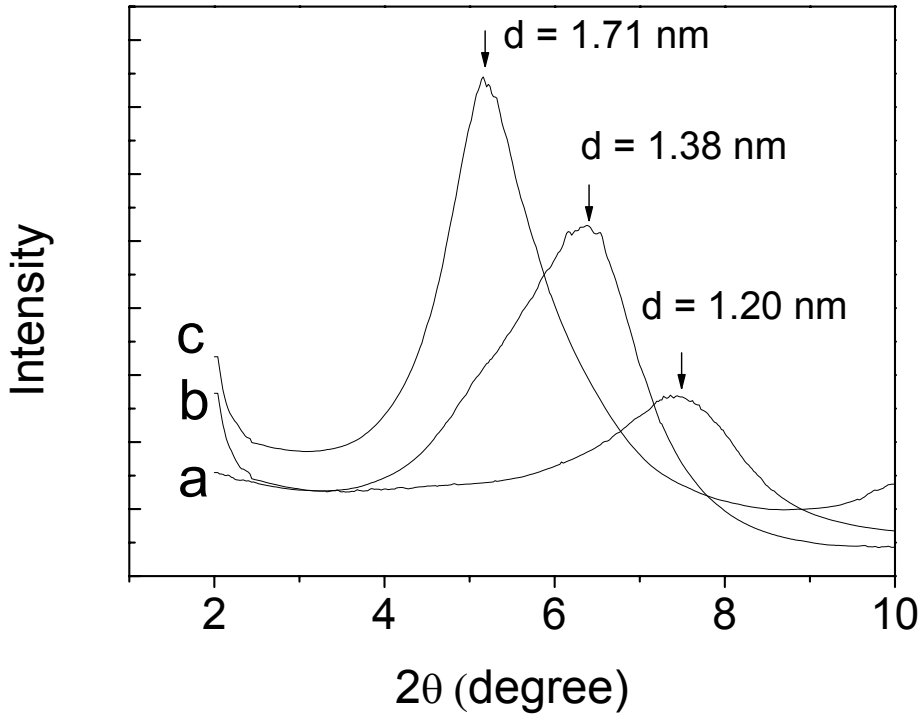

Figure 2.2: XRD patterns of PEO/MMT nanocomposites prepared by $scCO_2$-mediated intercalation.

expansion (from 0.47 to 0.53 nm) when PEO was less than 15%, and a larger gallery expansion (0.83 nm) for PEO contents $\geq$ 15%.

2.1.3.2 TGA Analysis

Figure 3.10 shows the TGA curves of pristine MMT, PEO/MMT nanocomposites (PEO content is 9.1% and 16.7% respectively) and pure PEO obtained under argon atmosphere at 10 °C/min. The TGA profile of pristine MMT (Curve a) shows two typical weight loss transitions. The one below 100 °C is due to dehydration of physisorbed water molecules in the gallery interlayer, and the other around 630 °C is due to dehydroxylation of the aluminosilicate structure. As shown in Curves b and c, the intercalated

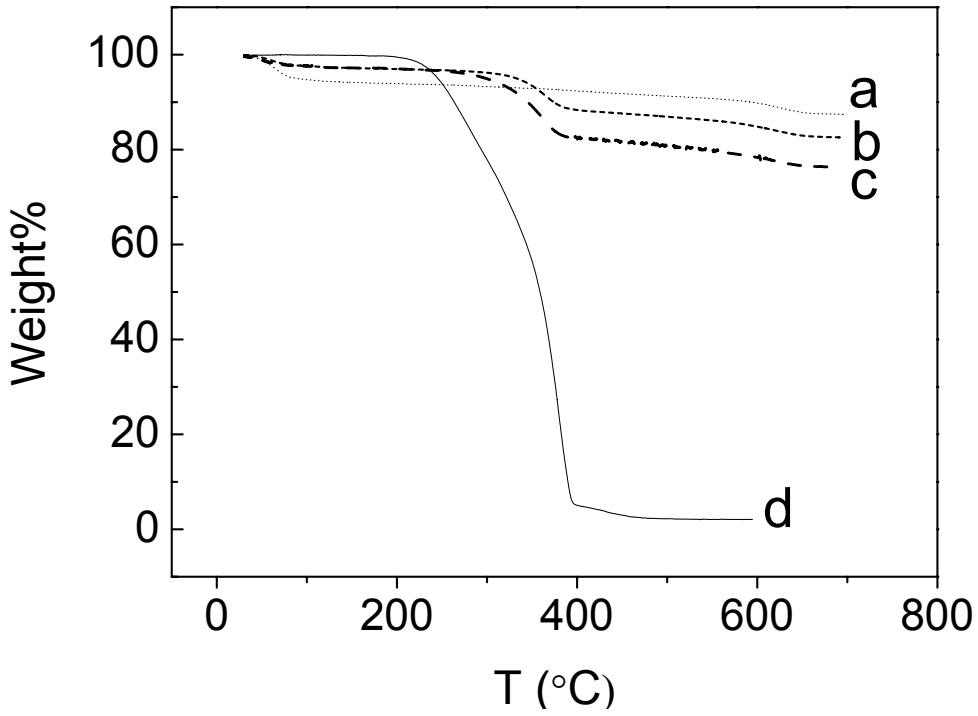

Figure 2.3: TGA curves of PEO and PEO/MMT nanocomposites under argon atmosphere. (a) pristine MMT; (b) PEO content 9.1%; (c) PEO content 16.7%; (d) pure PEO.

PEO in the MMT composites begins to decompose around 300 °C, a temperature much higher than the decomposition temperature of pure PEO (around 200 °C, Curve d). The higher decomposition temperature is frequently attributed to the barrier characteristics of clay nano-layers which mandate a tortuous pathway for volatile degradation products [14], but there may be specific clay-PEO interactions that also increase the thermal stability. The major weight loss for the two composites occurs around 400 °C and corresponds to complete elimination of PEO, in agreement with the initial targeted organic contents (PEO% = 9.1% and 16.7%).

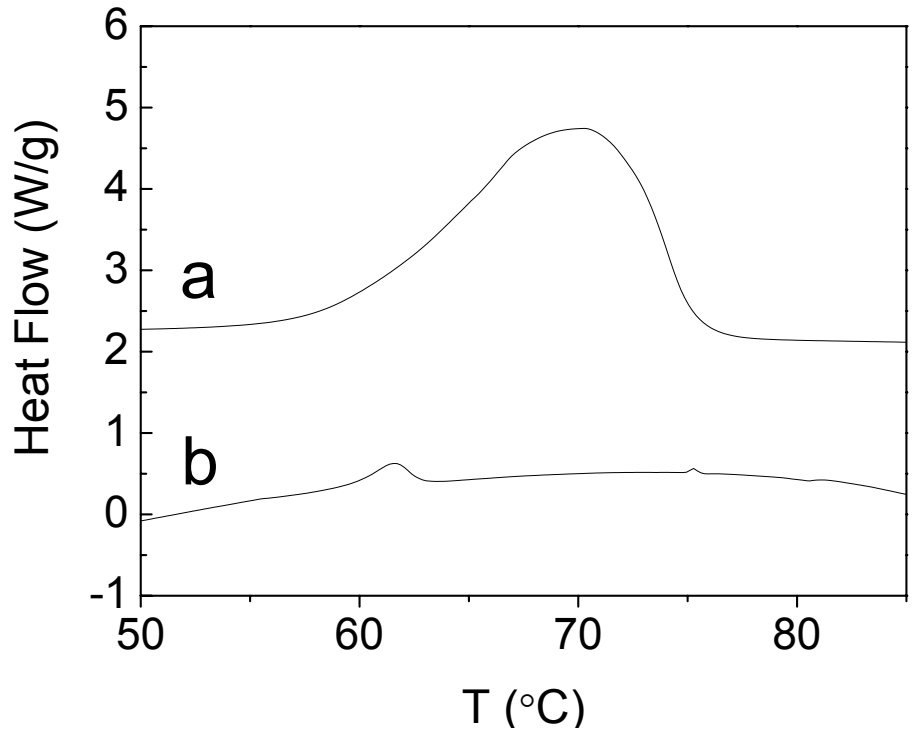

Figure 2.4: DSC traces of PEO and PEO/MMT nanocomposites: (a) pure PEO; (b) PEO content 16.7%.

2.1.3.3 DSC Analysis

Further evidence for intercalation is obtained from differential scanning calorimetry (DSC) analysis of the melting peak of PEO. As shown in Figure 2.4, the endotherm-peak area of the PEO melting in the MMT/PEO composite is significantly reduced after CO_2-mediated intercalation and suggests that most of the PEO resides in the MMT galleries. The apparent shift in the melting transition has been attributed to water incorporation into the PEO crystals [16] and/or imperfect crystals in the constraining environment of the interlamellar gallery [161].

2.1.3.4 Comparison Study of Intercalation with XRD

Solution intercalation with water, methanol and n-hexane under the same conditions (PEO content 16.7%, reacting for 1 day at 48 °C) was also investigated for comparison with the CO_2-mediated intercalation. In Figure 2.5 the XRD patterns of both water and methanol intercalation are similar; the dominant peak (∼1.7 nm) indicates successful intercalations using these solvents. This is not surprising since water and methanol are both good solvents for PEO, and both have proved to be effective intercalation solvents according to previous reports [152, 160]. By contrast, n-hexane is a non-polar solvent and does not dissolve PEO and PEO cannot intercalate into MMT; the (001) peak is unchanged from that of pristine clay, as is shown in curve d, Figure 2.5. $ScCO_2$ is also a non-polar solvent, yet it shows intercalation comparable to that of the polar solvents water and methanol.

2.1.3.5 Optical Microscopy Study

In order to gain a better appreciation on the effect of CO_2 in PEO intercalation, we studied the swelling behavior of PEO using a custom-made, high pressure mini-cell in conjunction with optical microscopy. Preliminary qualitative observations show that, even at room temperature, exposure to CO_2 at 103 bar causes the initial sharply-defined semi-crystalline PEO thin film (Figure 2.6a) melt and all of its edges become rounded (Figure 2.6b). Upon depressurization, the rounded swollen film foams and bubbles are visible (Figure 2.6c). It is known that CO_2 can swell and assist melting of certain polymers [162], and low molecular weight (M_w =1500 Da) PEG was recently reported

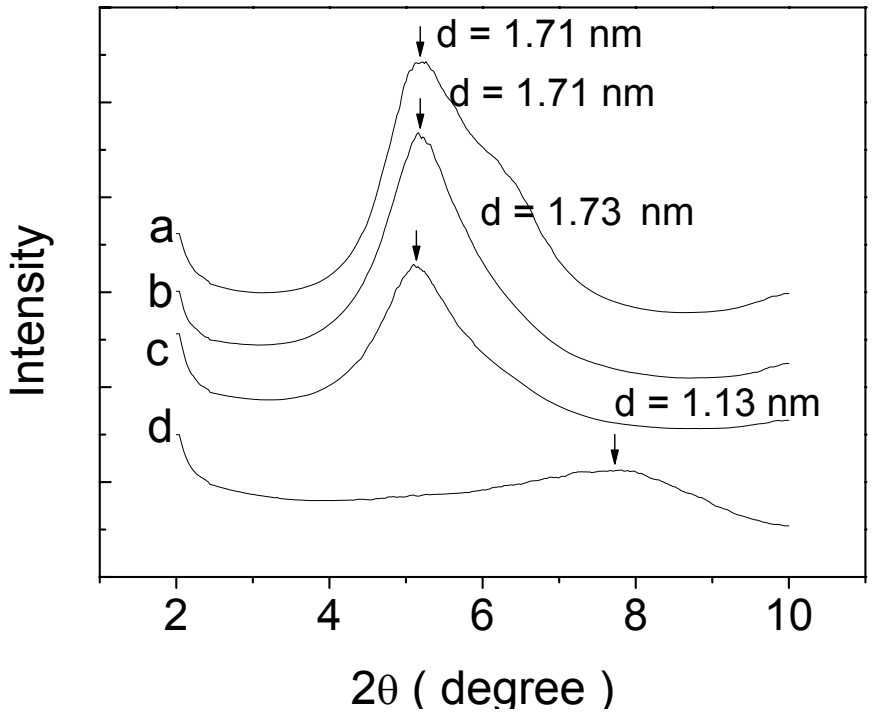

Figure 2.5: XRD patterns of PEO/MMT (PEO content 16.7%) nanocomposites from different solvents: (a) water; (b) $scCO_2$; (c) methanol; (d) n-hexane.

to be in the molten state at 40 °C under CO_2 pressure [163].

2.1.4 Conclusions

Polymer intercalation in solution has been long thought to be an entropy driven process, in which the translational entropy gained by desorption of solvent molecules from the gallery interlayer compensates the entropy decrease of the confined polymer chains [151]. However, this mechanism is probably not applicable to scCO_2-mediated intercalation. As anticipated, thermogravimetric analysis (TGA) shows that after MMT is incubated in CO_2 under the same conditions (24 hours, 48 °C), the MMT has about the same weight loss in the range between 50 °C and 100 °C as the original untreated MMT. There appears to be no release of water from the host gallery by the CO_2 treatment. Further evidence from the PEO swelling experiment corroborates the strong plasticizing effect of CO_2 on PEO and suggests that the intercalation mechanism is similar to that in polymer melts. Therefore, the CO_2-mediated intercalation must be an enthalpically driven process, deriving from a favorable interaction between MMT and PEO, one that is sufficient to overcome the entropy penalty for the confinement of PEO. That is, polar interactions between clay and polymer drive intercalation [164].

In summary, we have successfully intercalated PEO into clay via a CO_2-mediated process. The resultant nanocomposites have been characterized by XRD, TGA and DSC, and showed results comparable to those achieved with conventional solution intercalation. While conventional solution intercalation is based on a solvent system in which the polymer is soluble and driven primarily by the entropy gained by desorption

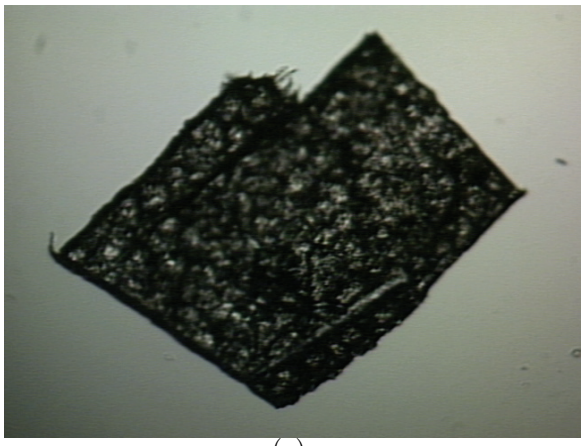

(a)

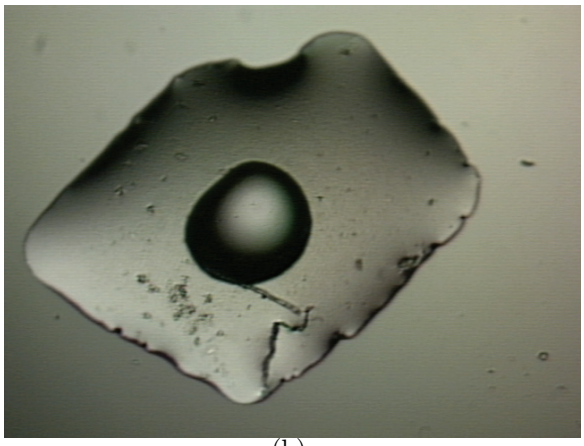

(b)

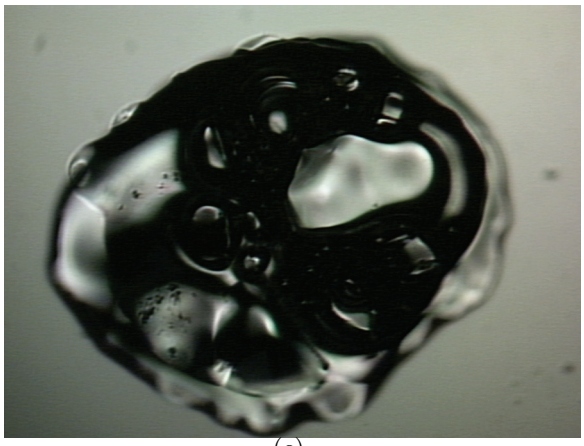

(c)

Figure 2.6: Optical microscope images of a PEO thin film ($M_w = 10^5$) treated with CO_2 at room temperature and 1500 psi (a) 1 min exposure time; (b) 19 hours exposure time; (c) after CO_2 vented.

of solvent molecules within the clay gallery, the CO_2-mediated intercalation appears to be an enthalpically driven process, one which is facilitated by a reversible CO_2 plasticizing effect. Hence CO_2-mediated intercalation mainly depends on the nature of the polymer-clay interactions rather than the solubility of the polymer. This suggests that, by judiciously choosing plasticizable polymers that have propensity for interacting with clay, the CO_2-mediated process may expand the range of polymer/clay nanocomposites.

2.2 Intercalation Kinetics of PEO in Clay

2.2.1 Introduction

As discussed in the previous section, we have found that CO_2 can mediate intercalation of PEO in clay by promoting intercalation similar to that achieved in polymer melts. Herein, in order to better understand the role of CO_2 on PEO melt intercalation, we compare the intercalation kinetics of PEO/clay by conventional melt intercalation and by CO_2-mediated melt intercalation at two different temperatures: 80 °C and 50 °C. Previous studies on the kinetics of polymer melt intercalation in layered silicates were conducted by time resolved XRD, wherein the changes in the integrated intensity of the basal reflection of the silicates at different intercalation times were monitored either in-situ [33] or ex-situ [165]. In this work, we employed another method, DSC to monitor the intercalation kinetics of PEO in clay. The advantage of DSC compared to XRD is that it can not only provide quantitative profile on the intercalation kinetic, but also simultaneously probe the thermal behaviours of the polymer, such as

melting temperature (T_m). Herein, we determine the fraction of intercalated layered silicates by monitoring the change of PEO melting enthalpy with intercalation time. Our calculations are based on the following assumptions: 1) PEO completely loses its crystallinity after it is intercalated in the silicate galleries. 2) Un-intercalated PEO retains its bulk (unfilled) enthalpy of melting. 3) The layered silicates are completely intercalated (saturated) with PEO after sufficiently long time (14 hours in this work). Consequently, χ_t, the fraction of layered silicates that have been intercalated with PEO at intercalation time t can be derived from the following equation:

$$\chi_t = \frac{\text{loss of PEO melting enthalpy at time } t}{\text{total loss of PEO melting enthalpy}} \tag{2.1}$$

where loss of PEO melting enthalpy at time t = beginning PEO melting enthalpy − PEO melting enthalpy at time t; total loss of PEO melting enthalpy = beginning PEO melting enthalpy − ending PEO melting enthalpy (PEO melting enthalpy at 14 hours).

2.2.2 Experimental

Sodium Montmorrillonite (MMT) was obtained from Gelest, Inc and used as received. Poly(ethylene oxide) of average molecular weight M_w=1×10^5 Da was supplied by Aldrich Chemical Company, Inc. Powers of MMT and PEO were sieved into a narrow size distribution (175±25 μm) using a Cu mesh sieves. A 29:71 (wt) mixture of PEO:MMT was mechanically mixed and pressed into a pellet. Excess PEO (saturation ratio is 21:79 [161]) was used to avoid depletion during intercalation. The static melt interca-

lation process was accomplished by annealing the pellet in the air or in CO_2 (1400 psi) for a given time at given temperatures. The annealed sample was taken out for DSC measurements (Pyris 1 DSC, heating rate 10°/min), and the second heating cycle was recorded for analysis.

2.2.3 Results and Discussion

As expected, the DSC results (Figure 2.7) show that the melting enthalpies of PEO in both CO_2-mediated intercalation and conventional melt intercalation at 80 °C decrease with increase of intercalation (annealing) time, because confinement of the polymer chains between the silicate layers effectively prohibits bulk-like crystallization. Since we use an excessive amount of PEO, a small fraction of PEO is eventually left out of the sillicate galleries and remains un-intercalated, which contributes to the small melting peak at the end of intercalation. Comparing Figure 2.7 (a) and (b), an interesting observation is that, in CO_2-mediated intercalation, the melting temperature of PEO remains about 65 °C regardless of intercalation time; whereas for conventional melt intercalation in air, the melting temperature shifts to lower temperature as the intercalation proceeds. Such significantly depressed melting temperature in conventional melt intercalation has also been observed by other authors, and was attributed to thin, defective crystals resulting from crystallization of excess un-intercalated polymer within the moderately confining defect regions between montmorillonite crystallites [166, 161]. In contrast, the constant melting temperature of PEO in CO_2-mediated intercalation may indicate that the crystal structure of un-intercalated PEO are better preserved in

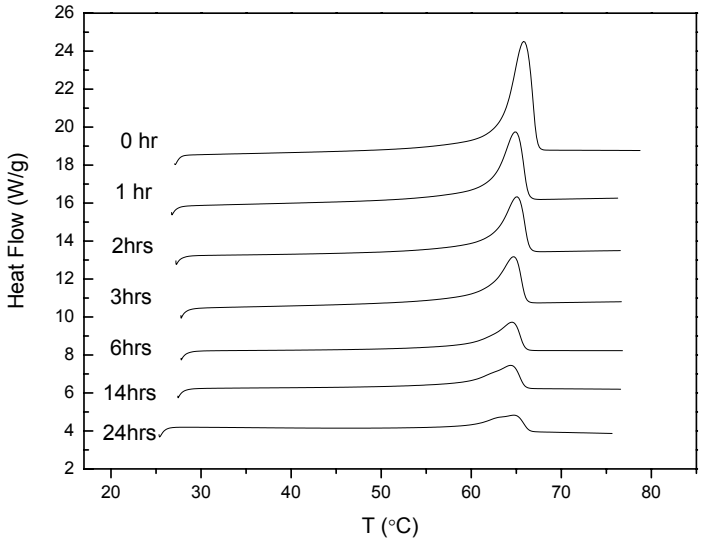

(a)

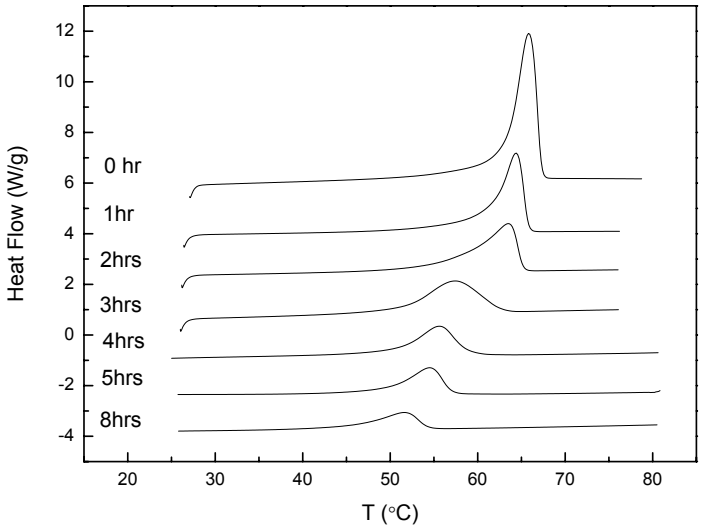

(b)

Figure 2.7: DSC curves of PEO in clay at 80 °C in: (a) CO_2-mediated intercalation; (b) conventional melt intercalation (in air).

the CO_2-mediated condition.

In order to calculate the intercalation kinetics, quantitative DSC data is listed in Table 2.1. As measured by DSC, the beginning PEO melting enthalpy is 136.0 J/g, which is in agreement with literature value for pure semicrystalline PEO [167]. As we assume that intercalation is complete after 14 hours in both CO_2-mediated intercalation and conventional melt intercalation, we take the melting enthalpy of PEO at 14 hours (i.e. 49.9 J/g for CO_2-mediated intercalation; 26.0 J/g for conventional melt intercalation) as the ending PEO melting enthalpy in each process, respectively. Thus, the total loss of PEO enthalpy in CO_2-mediated intercalation and conventional melt intercalation is 86.1 J/g and 110.0 J/g, respectively. Using Equation 2.1, we then obtain the loss of PEO melting enthalpy and fraction of intercalated silicates at different intercalation time (Table 2.1) and plot them in Figure 2.8.

Comparing the slope of the two series of kinetic data in Figure 2.8(b), it is clear that the intercalation kinetic in CO_2-mediated process at 80 °C is slightly higher than that in conventional melt intercalation at 80 °C. The faster kinetic in CO_2-mediated intercalation can actually be due to the plasticization effect of CO_2 on polymers. As discussed in section 2.1, since CO_2 can depress the melting temperature of PEO under our experimental conditions, the effective temperature in the CO_2-mediated intercalation is actually higher than that employed in the conventional melt intercalation. Interestingly, it appears that the total enthalpy loss (86.1 J/g) in CO_2-mediated intercalation is lower than that (110.0 J/g) in the conventional melt intercalation. In conjunction of the previous study on the melting temperatures being constant, it is possible that

Table 2.1: DSC data for CO_2-mediated intercalation and conventional melt intercalation at 80 °C

CO_2-mediated intercalation at 80°C

Intercalation time (hrs)	Melting Enthalpy (J/g)	Loss of Melting Enthalpy (J/g)	Fraction of Intercalated silicates (χ_t)
0	136.0	0	0
1	94.1	41.9	0.487
2	75.6	60.4	0.702
3	71.9	64.1	0.744
4	65.7	70.3	0.816
6	51.0	85.0	0.987
8	50.0	86.0	0.999
14	49.9	86.1	1

Conventional melt intercalation at 80 °C

Intercalation time (hrs)	Melting Enthalpy (J/g)	Loss of Melting Enthalpy (J/g)	Fraction of Intercalated silicates (χ_t)
0	136.0	0	0
1	89.0	47.0	0.427
2.2	75.9	60.1	0.546
3	65.9	70.1	0.637
4.2	53.2	82.8	0.753
6	37.2	98.8	0.898
7	33.6	102.4	0.931
8	27.4	108.6	0.987
9.2	26.9	109.1	0.992
14	26.0	110.0	1

the well preserved un-intercalated PEO crystals in CO_2-mediated intercalation have a larger melting enthalpy than the defective un-intercalated PEO crystals in conventional melt intercalation. Or another possibility is that CO_2 can induce crystallization of un-intercalated PEO, as reviewed in section 1.2.2.1. Either possibility can result in a higher remaining PEO melting enthalpy in CO_2-mediated intercalation than that in conventional melt intercalation.

For comparison, the intercalation kinetics at 50 °C are also examined and shown in Figure 2.9. Since 50 °C is well below the melting temperature of PEO (65 °C), the conventional melt intercalation proceeds at an extraordinarily low speed with only 10% layered silicates intercalated after 18 hours annealing. In contrast, the intercalation kinetics is must faster in the CO_2-mediated intercalation, and the intercalation is almost complete after 19 hours, as shown in Figure 2.9(b). This must faster kinetics in the CO_2-mediated intercalation suggests that, in our experimental condition (1400 psi), CO_2 can effectively depress the melting temperature of PEO to lower than 50 °C. This further corroborates our previous finding that CO_2 promotes a melt-like PEO intercalation in clay at the temperature (48 °C) lower than PEO melting temperature.

2.2.4 Future Directions

In this research, we have used DSC to measure the intercalation kinetics of PEO in clay by conventional melt intercalation and by CO_2-mediated melt intercalation. Although comparison has been done at two temperatures (80 °C and 50 °C), more kinetic data at temperatures between 80 °C and 50 °C is needed in order to get a better picture of

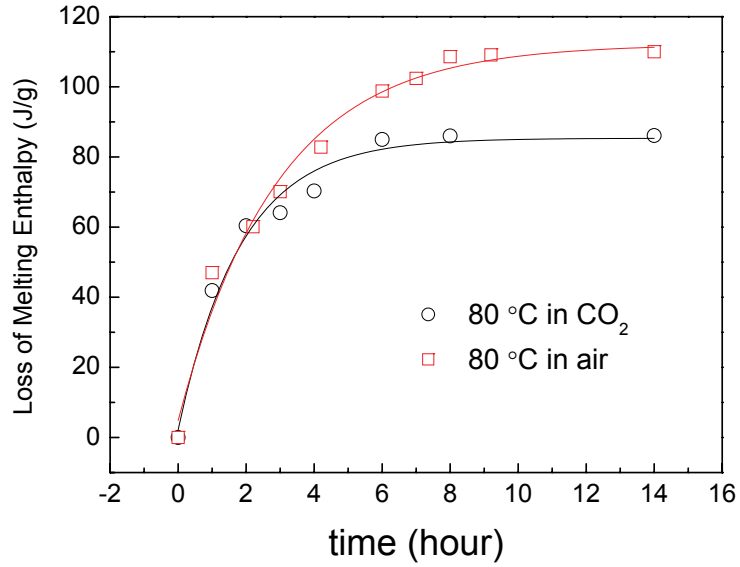

(a)

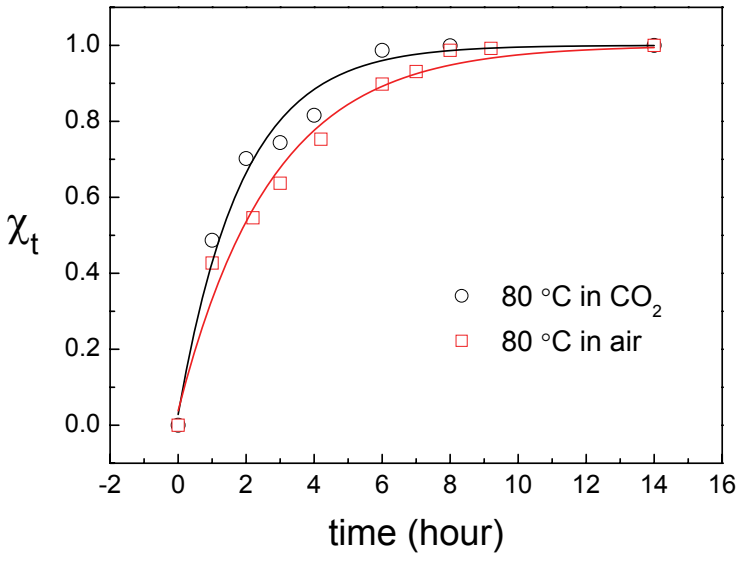

(b)

Figure 2.8: Intercalation kinetics of PEO in clay annealed at 80 °C: (a) Loss of PEO melting enthalpy as a function of intercalation time; (b) Fraction of intercalated silicates as a function of intercalation time.

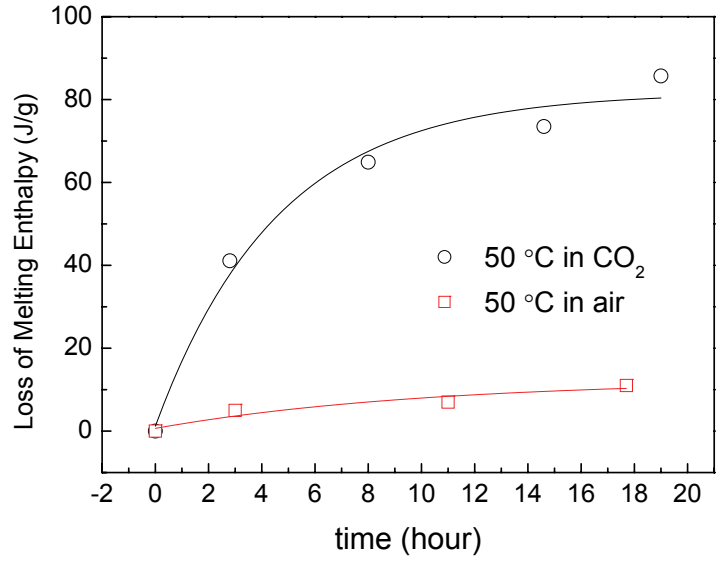

(a)

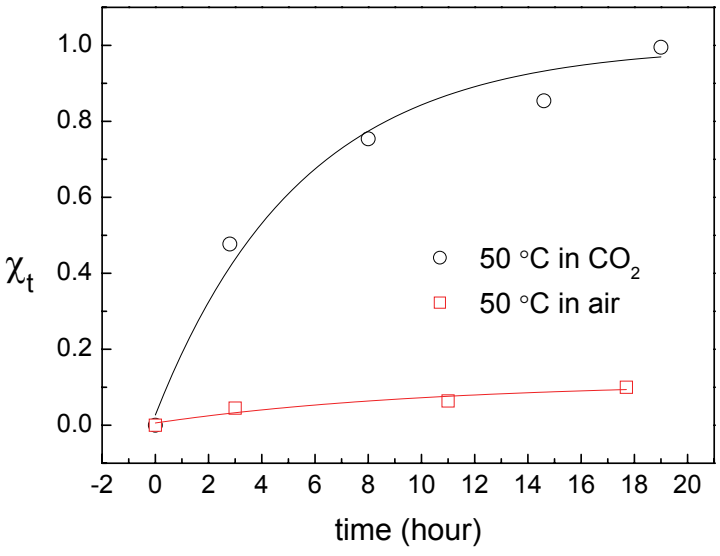

(b)

Figure 2.9: Intercalation kinetics of PEO in clay annealed at 50 °C: (a) Loss of PEO melting enthalpy as a function of intercalation time; (b) Fraction of intercalated silicates as a function of intercalation time.

the kinetic profile. This could be made easier by employing another technique, high pressure NMR to probe the intercalation kinetic of PEO in clay. Traditionally, NMR studies on polymer/clay nanocomposites have been hampered by paramagnetic Fe^{3+} in the common montmorillonite clay, but this problem has been largely circumvented by using the related, non-paramagnetic hectorite clay in several studies [6, 168]. Recently, Schmidt-Rohr et al. has been able to detect PEO near the silicate surfaces with high sensitivity by ^{1}H, ^{29}Si, and ^{13}C NMR experiments [169]. Thus, the ability to differentiate intercalated PEO from un-intercalated PEO both qualitatively and quantitatively would enable us to obtain the intercalation kinetic of PEO in-situ by using high temperature, high pressure NMR technique developed here at UNC. In this way, efficiency can also be greatly improved by circumventing the tedious periodic sampling used in DSC measurements.

CHAPTER 3

PREPARATION OF PMMA/CLAY NANOCOMPOSITES WITH A FLUORINATED SURFACTANT-MODIFIED CLAY IN SUPERCRITICAL CO_2

3.1 Introduction

As mentioned in Chapter 1.1.2, there are two idealized nanocomposites morphologies possible depending on the degree of polymer penetration into the clay framework: intercalated (silicate layers retain coplanar order but with their gallery distance expanded) and exfoliated (silicate layers are completely separated and disordered). While the

exfoliated structures are usually claimed to have the most significant property improvements, there are in reality very few unequivocal examples because the strong electrostatic force between clay layers tends to hold them together and underlies the preferred face-to-face stacking geometry in agglomerated clay tactoids. On the other hand, partially exfoliated nanocomposites are more readily produced having silicate layers exfoliated into secondary particles which contain several stacked, coplanar layers. Moreover, such mixtures of partially exfoliated/intercalated structures exhibit enhanced properties, i.e., high modulus and impact strength, etc [170], especially when these secondary particles are uniformly dispersed in the polymer matrix. Among the typical methods to prepare nanocomposites, in-situ polymerization appears to be the most promising one, pioneered by researchers from Toyota Motor Company [13, 26] who synthesized the first exfoliated nylon-6/clay hybrid for automotive applications. However, a drawback of this method is that it usually involves large quantities of aqueous/organic solvents as the polymerization medium, which is both environmentally unfriendly and economically prohibitive for an industrial-scale application.

On the other hand, as discussed in Chapter 1.2.1, supercritical carbon dioxide ($scCO_2$) has attracted extensive interest as a polymerization and processing medium, primarily driven by the need to replace conventional solvents with more environmentally benign and economically viable procedures [37]. One area of interest has been the dispersion polymerization of vinyl monomers, which has been pioneered by DeSimone et al., who reported the first dispersion polymerization of methyl methacrylate in $scCO_2$ [115]. Because the product, poly(methyl methacrylate) is insoluble in $scCO_2$, they used

a CO_2-soluble fluorinated homopolymer (poly(dihydroperfluorooctyl acrylate) PFOA) as the stabilizer for the polymerization system. Consequently, the successful dispersion polymerization led to a significant improvement in the yield, molecular weight and morphology of the resultant polymer. Typically, an effective stabilizer for CO_2 polymerizations should have two prerequisites: 1) an anchoring segment which attaches to the monomer/polymer particle either through physical adsorption or chemical grafting; 2) a CO_2-philic (fluorinated- or siloxane-based) segment which projects into the continuous CO_2 phase and provides steric stabilization for the growing polymer particles. By employing an amphiphilic surfactant to stabilize the polymer, dispersion polymerizations of many industrially important vinyl monomers have been successfully demonstrated in $scCO_2$, as mentioned in Chapter 1.2.3.2.

In this chapter, we describe a route to incorporate clays into polymer via in-situ polymerization in $scCO_2$. Previous work by Zerda et al. used $scCO_2$ as a reaction medium to prepare highly filled polymer/clay nanocomposites [105]. In their work, CO_2 is primarily used to lower the viscosity resulting from high loadings (up to 40%) of clay; the clay was modified by conventional hydrocarbon surfactants and resulted in intercalated nanocomposites. By contrast, our work employed much lower loadings (6 wt%) of clay, which is a typical concentration for nanocomposites. Furthermore, the clay was modified by a fluorinated surfactant in which the fluorinated tail is CO_2-philic and thus can help provide steric stabilization in $scCO_2$. We found that the fluorinated surfactant-modified clay can itself serve as an effective stabilizer and help produce polymer in high yields in $scCO_2$. Although the clay is not soluble in CO_2, the

stabilization mechanism is similar to that in a conventional dispersion polymerization. We will refer to this technique as a pseudo-dispersion polymerization.

3.2 Experimental

3.2.1 Materials

Sodium Montmorrillonite (Na-MMT) was obtained from Gelest, Inc and used as received. 1H,1H,1H,2H-perfluorododecyl iodide was obtained from Oakwood Products, Inc. Dodecylpyridinium chloride and dimethyldistearylammonium bromide were supplied by TCI America and used as received. Methyl methacrylate (MMA) was purchased from Aldrich Chemical Company and purified by distillation before use. The free radical initiator, 2,2-azobis(isobutyronitrile) (AIBN) was supplied by Polysciences, Inc. A very high molecular weight (M_w= 996 kDa) PMMA, used as an control, was obtained from Aldrich Chemical Company.

3.2.2 Synthesis of 1H,1H,1H,2H-perfluorododecylpyridinium iodide

Cationic fluorocarbon surfactant 1H,1H,1H,2H-perfluorododecylpyridinium iodide was synthesized from 1H,1H,1H,2H-perfluorododecyl iodide and pyridine according to reported methods [171] (Figure 3.1). Briefly, 5 g 1H,1H,1H,2H-perfluorododecyl iodide and 2.5 g dry pyridine were refluxed for 30 min. After cooling the reaction mixture, yellow precipitates were obtained. The precipitates were washed with diethyl ether

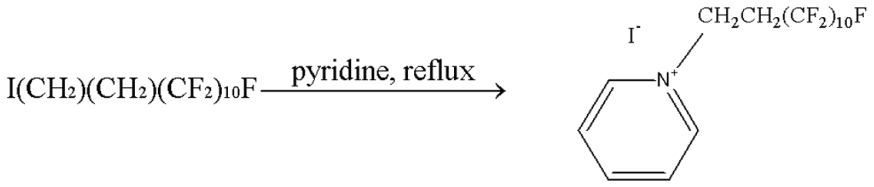

Figure 3.1: Reaction scheme for synthesis of 1H,1H,1H,2H-perfluorododecylpyridinium iodide.

and were recrystallized twice from acetone. The ^{1}H NMR spectra (Varian 300 MHz) of 1H,1H,1H,2H-perfluorododecyl iodide and 1H,1H,1H,2H-perfluorododecylpyridinium iodide dissolved in d-acetone are shown in Figure 3.2. The two methylene resonates at ∼3.4 ppm and 2.9 ppm in the starting material shift to 5.4 ppm and 3.4 ppm in the product, indicating that the reaction is complete and 1H,1H,1H,2H-perfluorododecylpyridinium iodide is formed.

3.2.3 Modification of Clay

1 g Na-MMT (1.19 meq/g) was dispersed in 50 ml distilled water under vigorous stirring to form a suspension. The fluorinated surfactant (1 fold cation exchange capacity of the MMT) was dissolved in 50 ml ethanol and added to the aqueous suspension. The mixture was then stirred for 6 hours between 50-70 °C before it was collected by filtration. The solid was subsequently washed with hot water/ethanol mixture several times until there was no white precipitate observed by an $AgNO_3$ test, indicating an absence of halide anions. The product was then vacuum-dried at 50 °C overnight, ground into powder and stored in a desiccator. The modified clay was denoted 10F-clay. For controls, we also modified clay with two other hydrocarbon surfactants using

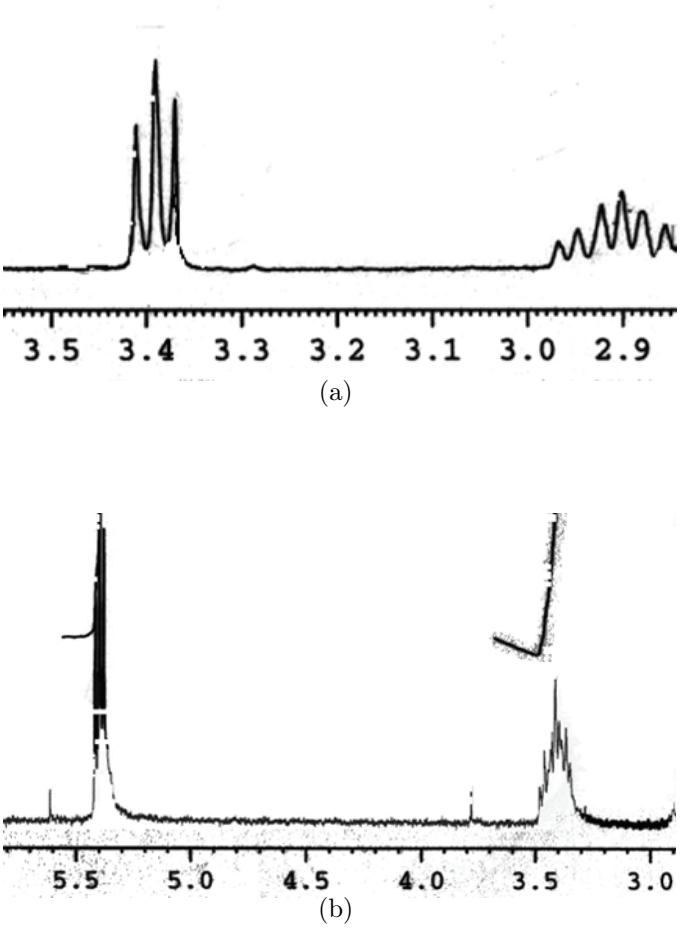

Figure 3.2: ^{1}H NMR spectra of (a) 1H,1H,1H,2H-perfluorododecyl iodide; (b) 1H,1H,1H,2H-perfluorododecylpyridinium iodide.

Table 3.1: Physical Data for Modified Clays[a]

Clays	Modifying cations[1)]	d spacing[2)] (nm)	Surfactant intercalated[3)] (wt%)
Na-MMT	None	1.2	N/A
10F-clay	$CF_3(CF_2)_9(CH_2)_2Py^+$	1.4	35
12C-clay	$CH_3(CH_2)_{11}Py^+$	1.6	8
2C18-clay	$[CH_3(CH_2)_{17}]_2(CH_3)_2N^+$	3.9	40

[a]1) Py = pyridine 2) determined by XRD 3) determined by TGA

the same method. One is dodecylpyridinium chloride, which is the hydrocarbon analog of the fluorinated surfactant we have synthesized; the modified clay was denoted C12-clay. The second surfactant is dimethyldistearylammonium bromide, with which the modified clay is comparable to a commercially used clay (Cloisite 20A from Southern Clay), and it was denoted 2C18-clay. The physical data of these modified clays is summarized in Table 3.1.

3.2.4 Polymerization

Polymerizations were conducted in CO_2 in a 2.5 ml, high-pressure cell equipped with sapphire windows that allow visual observation of the mixture. In a typical polymerization, the initiator (AIBN 0.003 g) and clay (0.03 g) were weighed into the cell containing a magnetic stir bar. The cell was purged with CO_2 via an Isco automatic syringe pump (Model 260D) for a few minutes; then the monomer (0.5 ml MMA) was injected into

the cell. The cell was then filled with CO_2 to ∼70 bar, and heated to 65 °C. After the desired temperature was reached, the desired pressure (241 bar) was achieved by the addition of more CO_2. The reaction was allowed to proceed with stirring for 4 hours, and then the cell was cooled and the CO_2 was slowly vented. Unless specified, the final product was taken out and dried at room temperature in a vacuum oven overnight, and the resultant materials stored in a desiccator for characterization. Yields of PMMA were determined gravimetrically. For dynamical mechanical analysis, the composite was heated in a vacuum oven at 150 °C overnight to remove residual CO_2 trapped within the polymer. The sample was then pulverized and compression molded (180 °C, 54 MPa) into a thin plaque.

3.2.5 Characterization

Powder X-ray diffraction (XRD) data (2θ = 2° and 2θ =10°) were collected on a Rigaku multiflex diffractometer using Cu Kα radiation (40 kV, 40 mA) at a scan rate of 0.5°/min. Scanning electron microscopy (JEM6300 microscope) and transmission electron microscopy (Phillips CM12) were used to investigate the microstructure of the PMMA nancomposites. Samples for SEM were mounted on aluminum stubs using an adhesive carbon tab then gold coated. Samples for TEM were cut from both the powdery sample and the compression molded sample, embedded and cured in epoxy resin and thin-sectioned using a ultramicrotome (Reichert Supernova) equipped with a diamond knife. Thermogravimetric analysis (TGA) was performed using a Perkin-Elmer Pyris 1 TGA system in an argon atmosphere at a heating rate of 20 °C/min. The

storage modulus and glass transition temperature of the composites were measured by a dynamic mechanical analyzer (Perkin Elmer DMA 7e) using a extension measuring system operating at a frequency of 1 Hz; measurements were conducted in the air from room temperature to 140 °C at a scan rate of 5 °C/min. The FTIR spectra were recorded on a Fourier-transform infrared spectrometer (BIO-RAD FTS 6000). Molecular weights of filtered PMMA were obtained by gel permeation chromatography (GPC) using Waters microstyragel columns (pore size 10^5, 10^4, and 10^3 Å) and a differential refractometry (Waters model 410) detector. Polystyrene standards were used for calibration.

3.3 Results and Discussion

3.3.1 Synthesis

Data for PMMA resulting from polymerizations of MMA in supercritical CO_2 with different clays are summarized in Table 3.2. Unlike typical dispersion polymerizations in which reactions start out homogeneously with a stabilizer soluble in the CO_2 phase, the pseudo-dispersion polymerizations were heterogeneous throughout the reaction due to the insolubility of clay in CO_2. The mixture formed a suspension under magnetic stirring. When 10F-clay was used, it was observed that the suspension appeared to thicken as the reaction proceeded, and precipitated powder accumulated on the cell windows during the 4 hour reaction. Upon venting CO_2 at the end of the reaction, a dry powder was recovered in the form of quasi-spherical particles, as shown in Figure

Table 3.2: Data for PMMA obtained by polymerizing MMA in $scCO_2$

Clays	Yield (%)	M_w (10^3g/mol)	Sample morphologies
Na-MMT	19	472	flake
10F-clay	85	449	fine powder
12C-clay	12	364	Flake/transparent paste
2C18-clay	38	392	aggregated powder/flake

3.3(a). The powder color was a little yellow to off white, since the fluorocarbon surfactant is yellow in color. The reaction exhibited a reasonably high yield (85%) with PMMA molar mass 449 KDa; this high conversion of polymer indicates a successful dispersion polymerization in CO_2. In contrast, polymerization suspensions with the two hydrocarbon surfactant-modified clays and unmodified Na-MMT were found to settle in the cell and the solution remained cloudy during the first two hours. This probably results from coalescing of clay platelets covered with PMMA oligomer. As a result, polymerizations using unmodified Na-MMT and 12C-clay resulted in either flake-like morphology (Figure 3.3(c)) or transparent paste (Figure 3.3(d)) with undesirably low yields (Table 3.2). While polymerization with 2C18-clay (Figure 3.3(b)) can produce a somewhat powdery PMMA, again the low yield (38%) may indicate poor stabilizing ability of the hydrocarbon surfactant-modified clay in CO_2 relative to the fluorinated surfactant-modified clay.

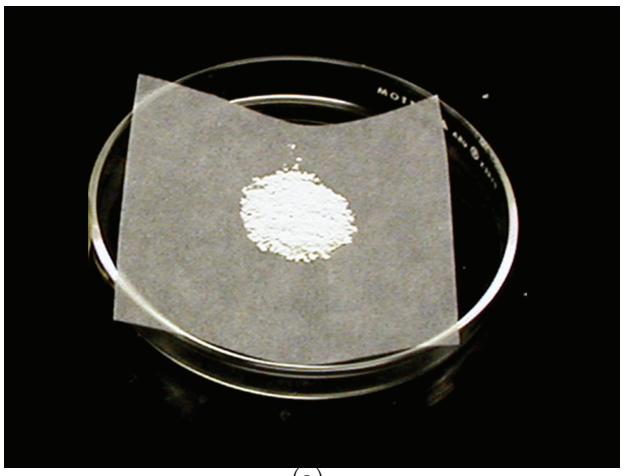

(a)

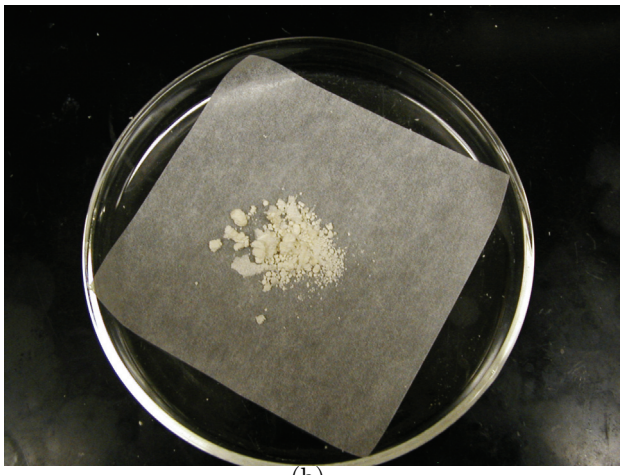

(b)

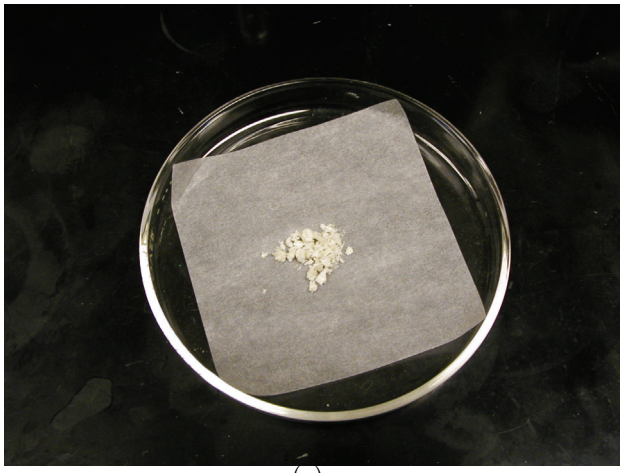

(c)

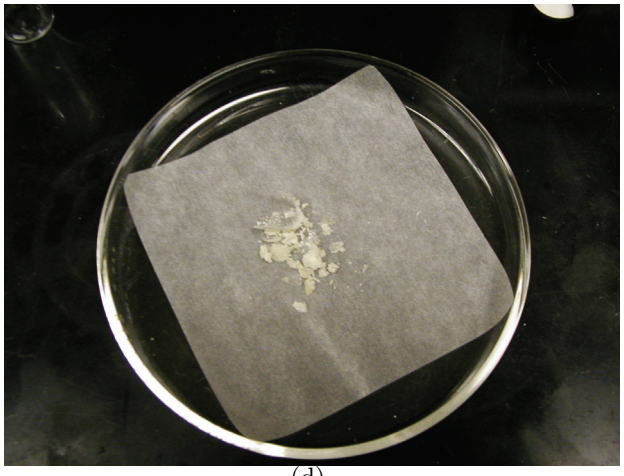

(d)

Figure 3.3: Pictures of PMMA nancomposites recovered from polymerization with (a) 10F-clay; (b) 2C18-clay; (c) Na-MMT; (d) 12C-clay.

Another interesting observation here is that the M_w of PMMA in all the nanocomposites, regardless of the yield, were higher than that reported for most PMMA synthesized in previous dispersion polymerizations [139, 148, 121]. GPC analysis (Figure 3.4) of the PMMA extracted from clay showed a bimodal distribution with a low molecular weight shoulder for all of the nanocomposites. This phenomenon is actually not uncommon. Meneghetti et al. has explained the bimodal distribution by a glass effect, i.e., low molecular weight PMMA becomes trapped between the clay galleries, while the higher molecular weight of PMMA corresponds to the amorphous matrix [172]. The higher molecular weight we observed may be attributed to the presence of clay, which can trap/scavenge free radicals and leads to an increase of molecular weight [173].

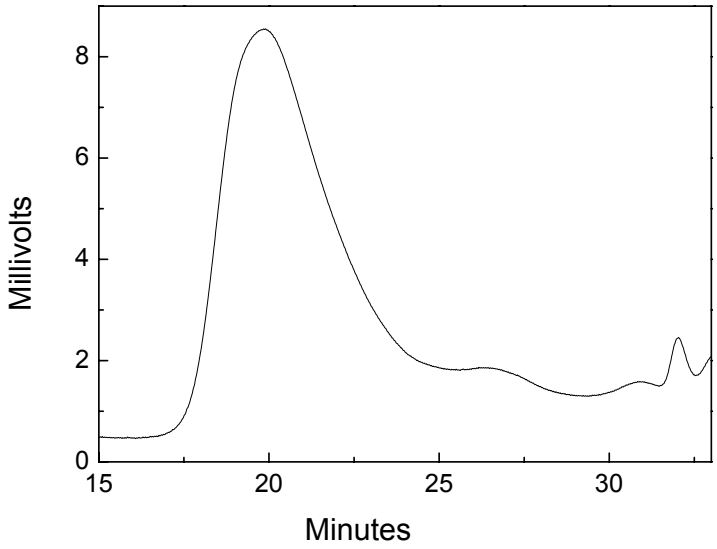
Millivolts
0
2
4
6
8
15
20
25
30
Minutes

(a)

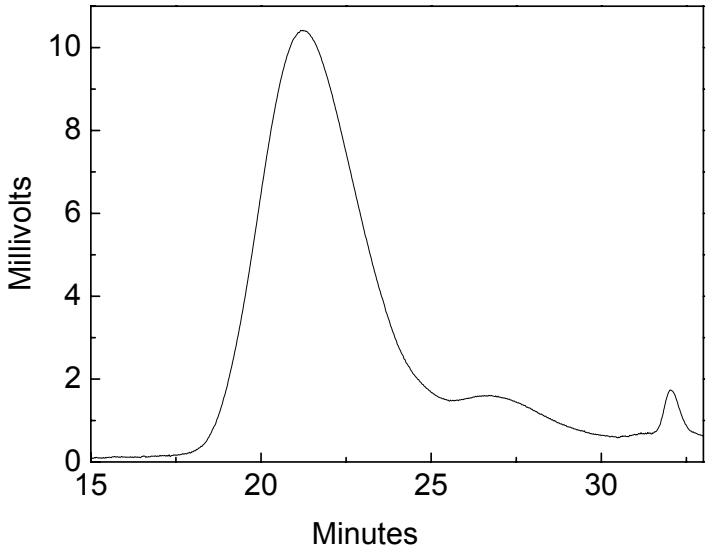
Millivolts
0
2
4
6
8
10
15
20
25
30
Minutes

(b)

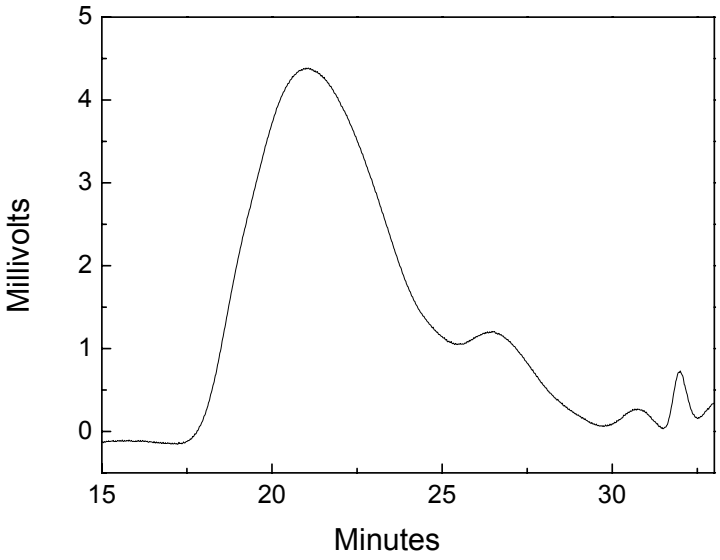

(c)

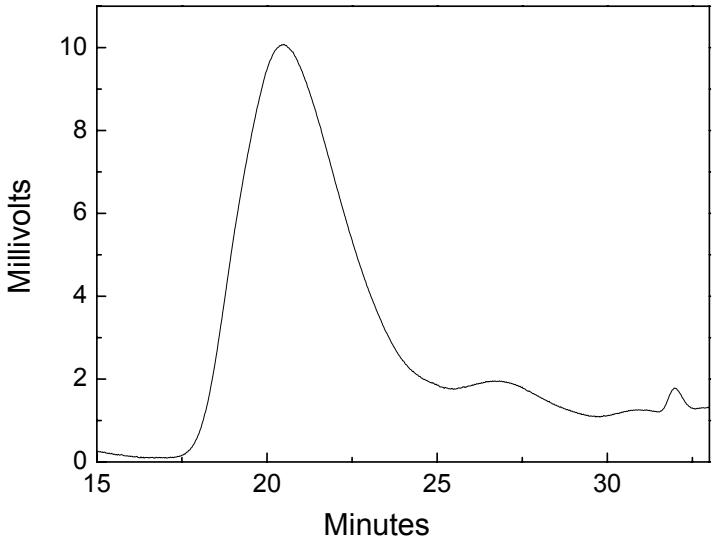

(d)

Figure 3.4: GPC traces of extracted PMMA from PMMA/clay nanocomposites containing (a) Na-MMT; (b) 10F-clay; (c) 12C-clay; (d) 2C18-clay.

3.3.2 Morphology

3.3.2.1 SEM Analysis

Analysis by SEM showed that the PMMA/10F-clay nanocomposites for the most part consisted of quasi-spherical PMMA particles (Figure 3.5 (a)) with clay platelets seen adsorbed on the particle surface. The average particle diameter is about 10 μm, which is significantly larger than the typical values (a few microns) for PMMA prepared previously in dispersion polymerizations in $scCO_2$. The greater particle size may be indicative of a greater amount of agglomeration occurring during polymerization. This is probably due to the short chain length of the fluorinated surfactant and less effective steric stabilization compared with most polymeric surfactants used in conventional dispersion polymerizations [115, 138, 118]. Different electron densities suggest that both intercalated clay tactoids (Figure 3.5(b)) and individual exfoliated clay platelets (Figure 3.5(c)) are present on the surfaces of PMMA particles. As for the PMMA/2C18-clay nanocomposites, Figure 3.5(d) showed similar particles but the boundaries were ill-defined. The close-up image (Figure 3.5(e)) showed there were many more clay aggregates on the PMMA particle surfaces compared with comparable images of PMMA/10F-clay nanocomposites. This further corroborates the less effective stabilizing ability of 2C18-surfactant in CO_2 compared to the fluorinated surfactant. Therefore, the growing PMMA particles need more 2C18 surfactant on the surface to provide steric stabilization in CO_2.

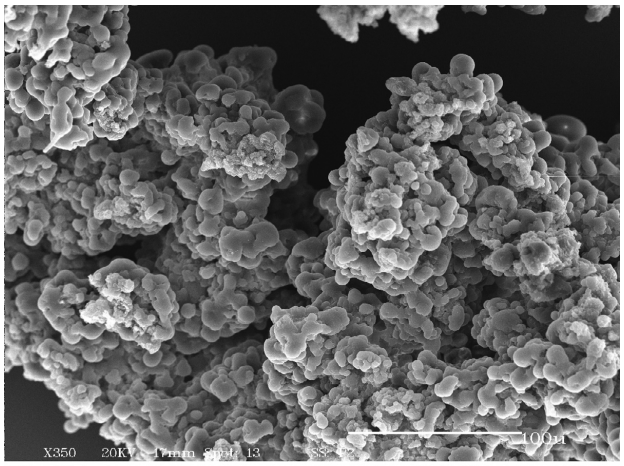

Title: 10f–6 –1
Comment:

Date: 06–09–2004 Time: 14:56
Filename: TEMP.TIF

(a)

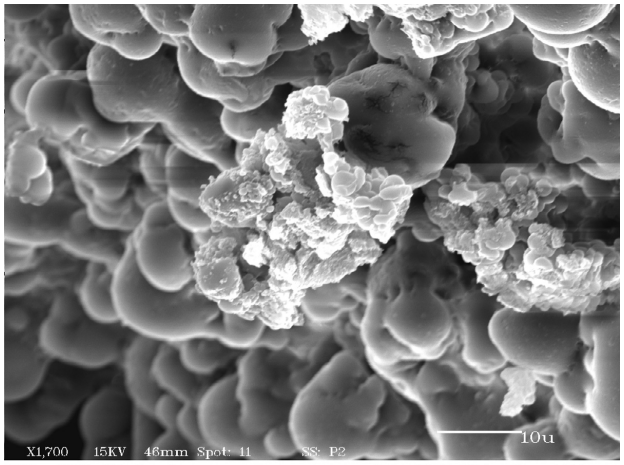

Title: PMMA–10F–clay–4
Comment:

Date: 03–12–2004 Time: 15:54
Filename: TEMP.TIF

(b)

Title: PMMA–10F–clay–3
Comment:

Date: 03–12–2004 Time: 15:49
Filename: TEMP.TIF

(c)

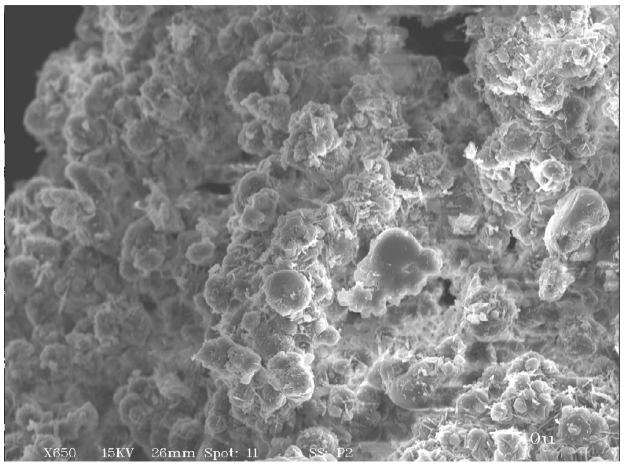

(d)

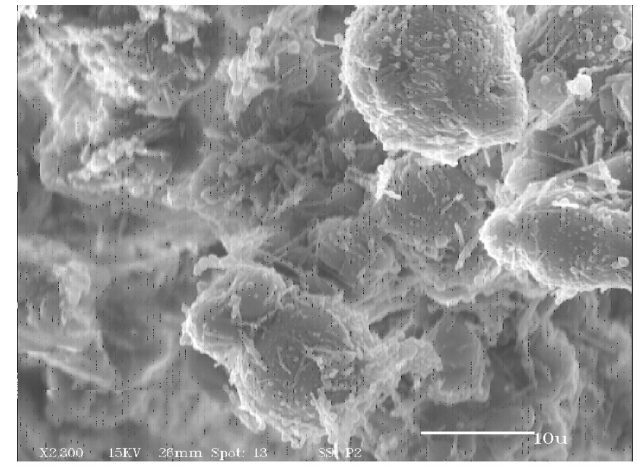

(e)

Figure 3.5: SEM images of PMMA/10F-clay nanocomposites:(a),(b),(c); SEM images of PMMA/2C18-clay nanocomposites: (d), (e).

3.3.2.2 XRD Analysis

Figure 3.6 shows the XRD patterns of PMMA nanocomposites with 10F-clay and 2C18-clay. For the PMMA/10F-clay nanocomposite, the (001) peak has shifted from 1.4 nm in the 10F-clay (see Table 3.1) to 3.1 nm in the composite, which indicates that PMMA

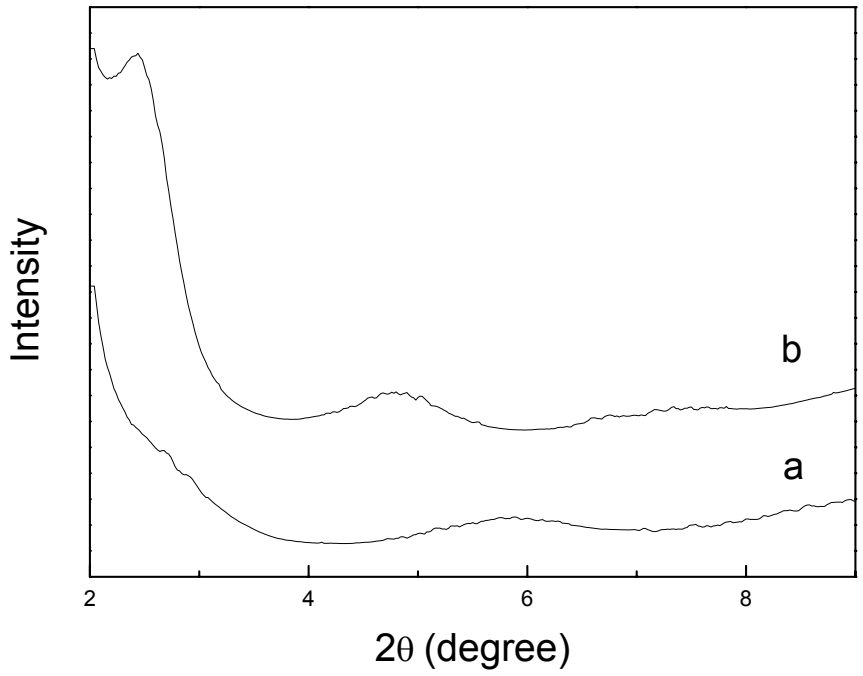

Figure 3.6: XRD patterns of (a) PMMA/10F-clay nanocomposites; (b) PMMA/2C18-clay nanocomposites.

has intercalated into the gallery of 10F-clay. Furthermore, the intensity of the diffraction peak at d=3.1 nm is noticeably weaker than the strong diffraction peak (d=3.9 nm) of the intercalated PMMA/2C18-clay nanocomposite. This suggests that most of the clay layers in the 10F-clay nanocomposites have exfoliated from their ordered intercalated structures, and the mixture has both intercalated and exfoliated structures.

3.3.2.3 TEM Analysis

More information about the morphology of PMMA/10F-clay nanocomposites was obtained by TEM observation. Figure 3.7(a) and (b) show the TEM images of PMMA/10F-

clay nanocomposites sectioned directly from powdery samples. In the lower magnification image Figure 3.7(a), it can be seen that the silicate layers of clay were exfoliated into secondary particles which are uniformly dispersed in the polymer matrix in the micron-size scale. Whereas a few individual silicate layers can also be seen, most secondary particles consist of several stacked, coplanar silicate sheets and thus appear to be denser tactoids as shown in the higher magnification image Figure 3.7(b). For comparison, we also melted pressed the powdery sample into a plastic film and imaged the dispersion of clay in the compression molded sample. As shown in Figure 3.7(c), both exfoliated individual sheets and intercalated tactoids are present and randomly distributed in the polymer matrix. A higher magnification image showing clay tactoids which contain the intercalated structure is shown in Figure 3.7(d). These TEM observations further supports the SEM and XRD analysis which suggests that partially exfoliate and partially intercalated nanocomposites were formed.

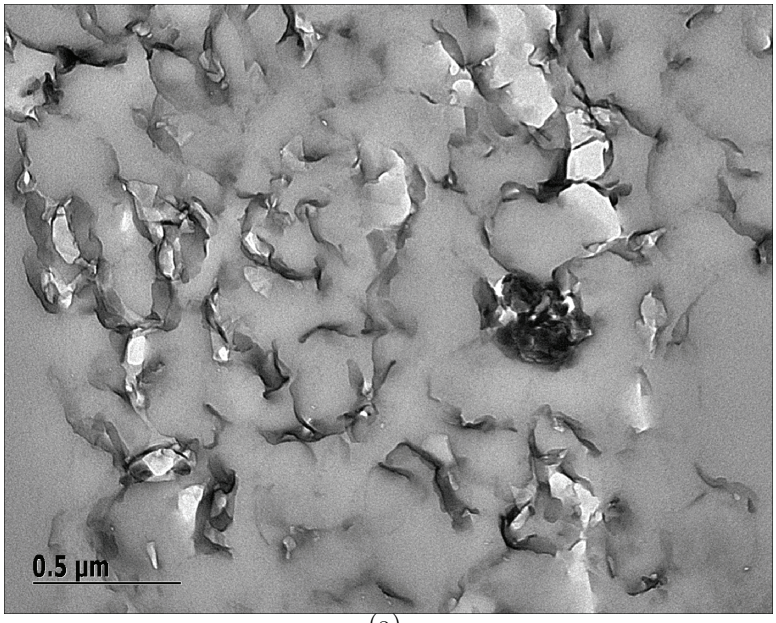

(a)

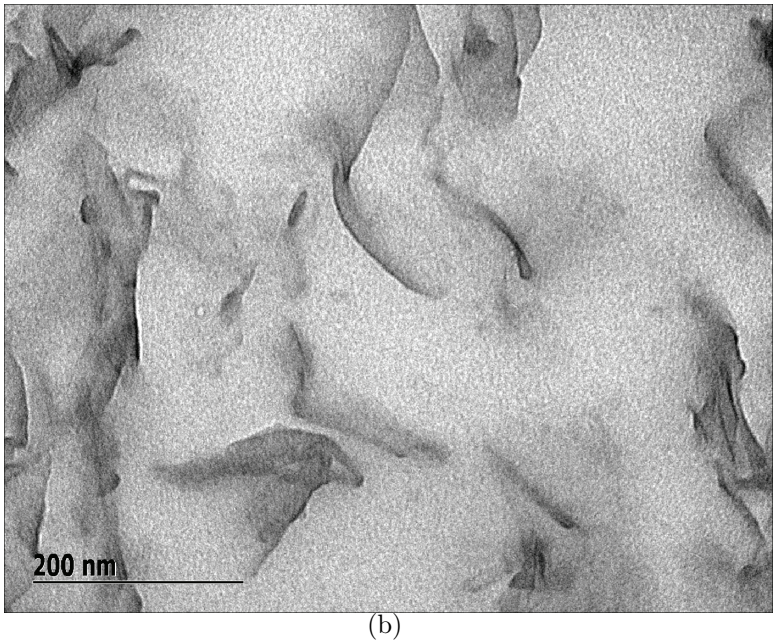

(b)

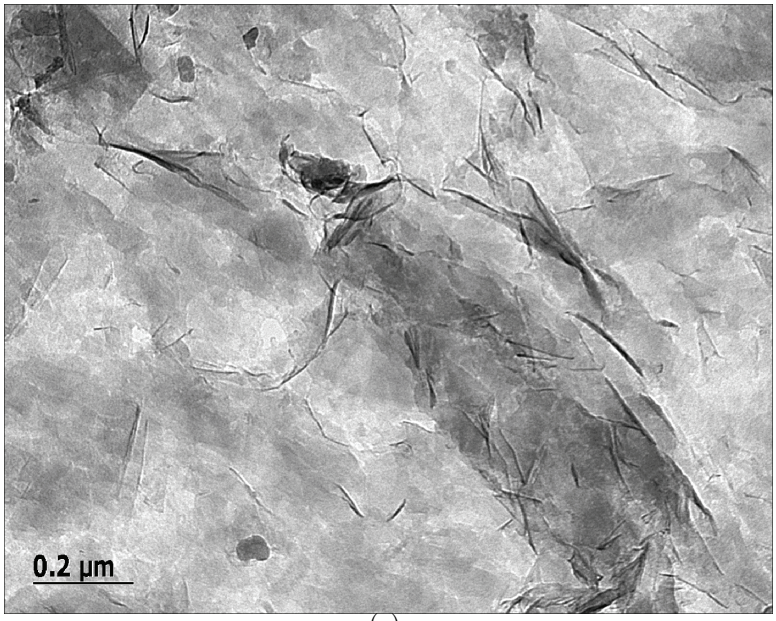

(c)

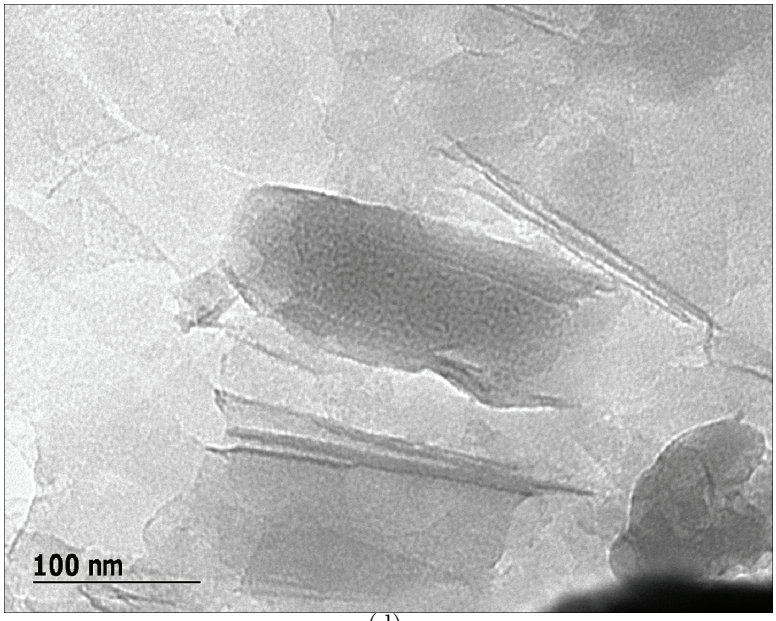

(d)

Figure 3.7: TEM images of (a), (b): powdery PMMA/10F-clay nanocomposite; (c), (d): compression molded PMMA/10F-clay nanocomposite.

3.3.3 Stabilization Mechanism

It is clear that the 10F-clay is not only acting as an inorganic filler, but also as a stabilizer for PMMA growth in CO_2. From SEM observations, we propose that it is the individual clay platelets which absorb on the surface of the PMMA particles that provide the stabilization mechanism in CO_2 (Figure 3.8). Evidence for the anchoring mechanism is provided by FT-IR spectroscopy. As is shown in Figure 3.9a and b, pure MMA has the carbonyl stretching mode at 1725 cm^{-1}, while 10F-clay is silent in this region except for a H-O-H deformation band around 1635 cm^{-1}. However, when MMA is mixed with 10F-clay, the carbonyl stretching band is apparently broadened (Figure 3.9c). The broadened band can be deconvoluted into two bands: One band (unreacted carbonyl stretch) remains about the same position while the other shifts to lower frequency by 20 cm^{-1}. Such a shift is indicative of a hydrogen bond interaction, which is a typical phenomenon when carbonyl containing compounds are adsorbed onto swelling clay minerals. It has been proposed that the C=O group is either bound to the exchangeable cation through a water molecule bridge (i.e., a hydrogen bond), or it is directly linked to the metallic cation [174]. Here, since most of the metallic cations in our clay have been exchanged with fluorinated surfactant, the interaction is most likely the first one, hydrogen bonding between the C=O group and the interlayer water of the partially hydrated clay.

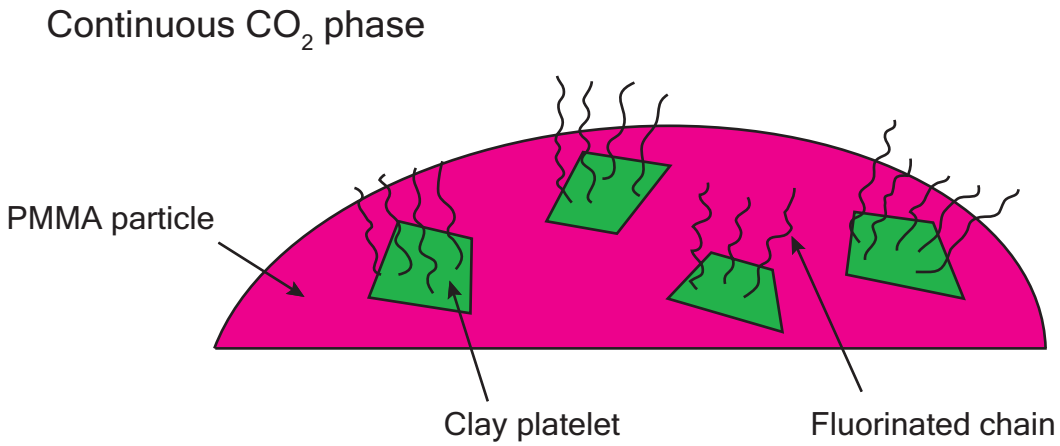

Figure 3.8: Schematic illustration of a growing PMMA particle (shown in red) stabilized by 10F-clay in which the clay platelet (shown in green) acts as an anchor.

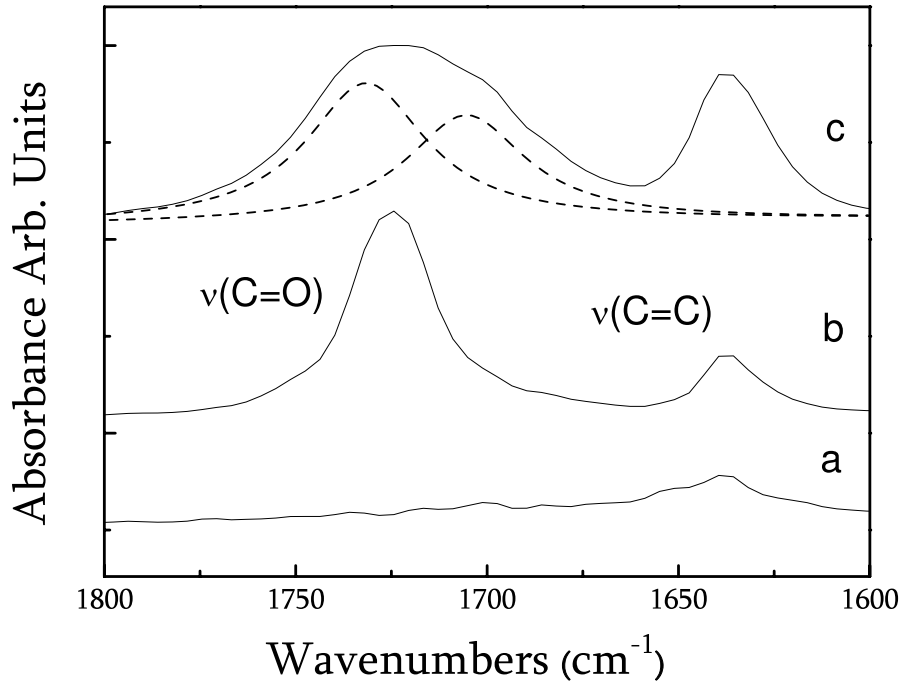

Figure 3.9: FT-IR spectra of (a) 10F-clay; (b) MMA; (c) mixture of 10F-clay and MMA.

3.3.4 Thermal Properties

Figure 3.10 shows the TGA curves of pure PMMA, PMMA/10F-clay nanocomposites and PMMA/2C18-clay nanocomposites. As is shown in curves b and c, the small weight loss between 100 °C and 150 °C can be attributed to evaporation of residual MMA monomers from the in-situ polymerized nanocomposites. Apparently, the onset of decomposition temperature of PMMA/10F-clay has increased from that of both pure PMMA and PMMA/2C18-clay; this is probably due to the barrier properties of the partially exfoliated 10F-clay in the polymer matrix, retarding the escape of decomposition products. As the temperature further increases above 350 °C, MMA/2C18-clay nanocomposites tend to have a slightly higher ending decomposition temperature than that of PMMA/10F-clay. A possible reason is that the weight percentage of 2C18-clay in the nanocompoistes is higher than that of 10F-clay due to the lower yield of polymer. That is, the higher concentration of inorganic filler may play a role in enhancing the thermal stability of the polymer.

3.3.5 Mechanical Properties

Dynamic mechanical analysis was used to measure the viscoelastic properties of the polymer nanocomposites. Figure 3.11 shows the temperature dependence of storage modulus and tanδ of PMMA and PMMA/10F-clay nanocomposites. As expected, the storage modulus increases with the addition of clay: at 26 °C, the modulus increases from 1.28 GPa for PMMA to 1.88 GPa for the nanocomposite. An enhanced glass transition temperature (T_g = 132 °C for the nanocomposites versus T_g = 124 °C for PMMA)

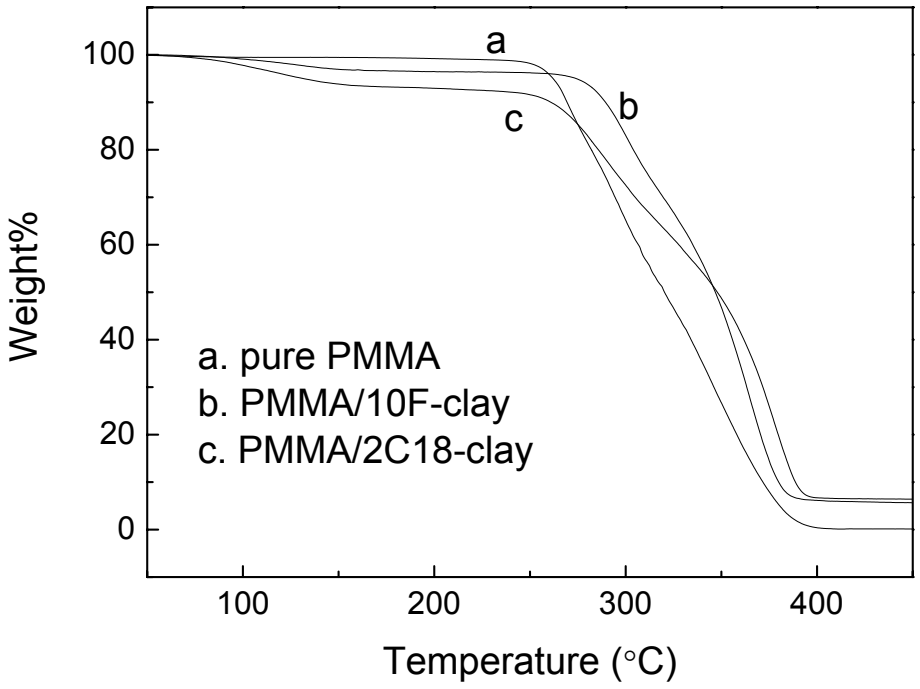

Figure 3.10: TGA curves of (a) pure PMMA; (b) PMMA/10F-clay nanocomposite; (c) PMMA/2C18-clay nanocomposite.

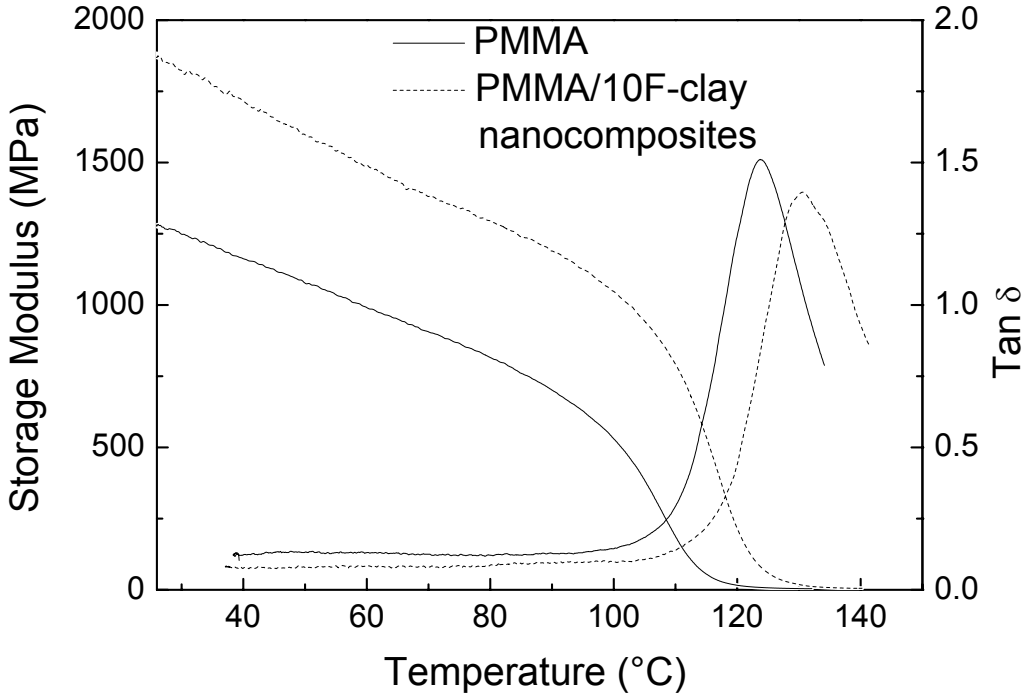

Figure 3.11: Storage modulus and loss tangent (tanδ) spectra of PMMA and PMMA/10F-clay nanocomposites.

corresponding to the peak of the loss tangent is also observed for the PMMA/10F-clay nanocomposites. It has been suggested [175, 176] that the enhancements of the storage modulus and glass transition temperature result from the strong interfacial interactions between the polymer and clay, the restricted segmental motions of polymer chains at the organic-inorganic interface, and the inherent high modulus of the clays.

3.4 Conclusions

PMMA/clay nanocomposites have been synthesized via a novel pseudo-dispersion polymerization technique in $scCO_2$. It has been found that the fluorinated surfactant-

modified clay (10F-clay), although not soluble in CO_2, can indeed serve as an effective stabilizer for PMMA polymerization in CO_2 and help improve polymer yields compared with conventional hydrocarbon surfactant-modified clay. The mechanism is most likely that the fluorinated surfactant provides steric stabilization in the CO_2 phase while the clay itself interacts with the carbonyl group of the methacrylate moiety via hydrogen bonding. The nanocomposites were characterized by SEM, TEM, XRD, TGA, and DMA, and showed partially exfoliated/intercalated structures as well as enhanced thermal stabilities, glass transition temperatures, and mechanical properties. This pseudo-dispersion polymerization route allows for clean synthesis of nanocomposites with high yields in scCO_2, without the need for adding extra surfactant to stabilize the polymerization system.

CHAPTER 4

PREPARATION OF PMMA AND PS/CLAY NANOCOMPOSITES WITH A PDMS-MODIFIED CLAY IN SUPERCRITICAL CO_2

4.1 Introduction

As described in chapter 3, we reported a route to produce partially exfoliated PMMA/clay nanocomposites via in-situ polymerization in $scCO_2$, in which we found that the fluorinated surfactant-modified clay can itself serve as a stabilizer and help produce PMMA in high yields in $scCO_2$. Although the clay is not soluble in CO_2, the stabilization mechanism is similar to that in a conventional dispersion polymerization; FT-IR results indicated hydrogen bond formation between the carbonyl group of the MMA

monomer and hydroxyl groups and/or interlayer water of the clay. We referred to this technique as a pseudo-dispersion polymerization.

In this chapter, we report the use of a different system, a commercially-available surfactant aminopropyl-terminated poly(dimethylsiloxane) (AP-PDMS) modified clay as the stabilizer for the pseudo-dispersion polymerization of methyl methacrylate and styrene in $scCO_2$. This PDMS-based surfactant is known to be CO_2-philic and its longer siloxane chain is expected to provide better steric stabilization compared to the shorter fluorinated chain used previously. Furthermore, we extend our system to polystyrene (PS), which does not have a hydrogen bonding site as PMMA does. Having different interaction mechanisms with clay, PMMA and PS are two model systems that allow us to study the effects of a clay-based stabilizer on both hydrogen-bonding polymers (e.g. PMMA) and non-hydrogen-bonding polymers (e.g. PS). In this chapter, the effects of PDMS-clay on the morphologies and properties of PMMA and PS nanocomposites are compared. Two stabilization mechanisms are proposed to account for the different microstructures and mechanical properties between PMMA and PS nanocomposites.

4.2 Experimental

4.2.1 Materials

Sodium Montmorrillonite (Na-MMT) was obtained from Gelest, Inc and used as received. Dimethyldistearylammonium bromide were supplied by TCI America and used as received. Aminopropyl-terminated poly(dimethylsiloxane) (AP-PDMS, M_w=3500,

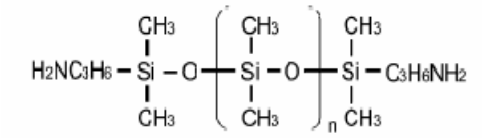

Figure 4.1: Aminopropyl-terminated PDMS (AP-PDMS, n ∼44)

structure shown in Figure 4.1) was obtained from United Chemical Technologies, Inc. Methyl methacrylate and styrene were purchased from Aldrich Chemical Company and purified by distillation before use. The free radical initiator, 2,2-azobis(isobutyronitrile) (AIBN) was supplied by Polysciences, Inc. PMMA (M_w=350 KDa) and PS (M_w=150 KDa), used as controls, were obtained from Aldrich Chemical Company.

4.2.2 Modification of Clay

2 g Na-MMT (1.19 meq/g) was placed in a 500 ml beaker and dispersed vigorously into 150 ml deionized water at 60 °C. In a separate vessel, 8 g AP-PDMS (2.3 mmol) was acidified with 0.24 g hydrochloric acid (37% in water, acidification ratio of H^+/NH_2=1/2) in 150 ml tetrahydrofuran. The solution was then poured into the beaker containing the swelled Na-MMT slurry. The mixture was stirred vigorously at 60 °C for 3 hours and then allowed to cool to room temperature. The resulting precipitate was collected and washed thoroughly with hot water followed by drying in a vacuum oven at 70 °C overnight. The resultant organo-clay was obtained as a yellowish sticky solid, and was denoted PDMS-clay. The schematic structure of PDMS-clay is shown in Figure 4.2. For comparison, we also modified the clay with a hydrocarbon surfactant dimethyldistearylammonium bromide using the method described in section 3.2.3. The modified clay

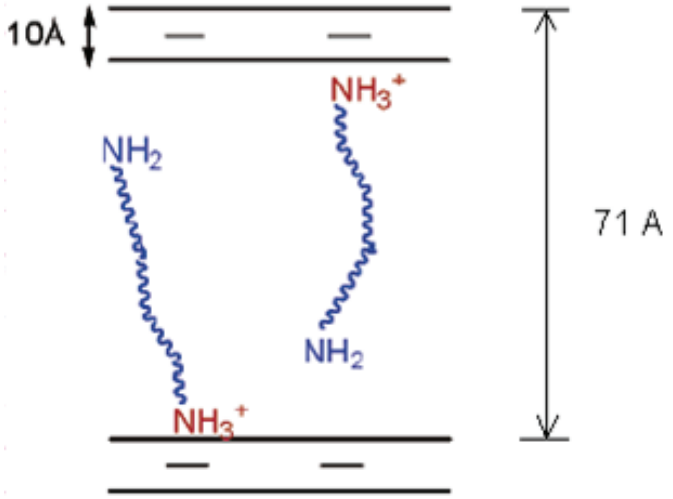

Figure 4.2: Schematic structure of PDMS-clay.

is comparable to a commercially-used clay (Cloisite 20A from Southern Clay) and was denoted 2C18-clay. The organic content in PDMS-clay and 2C18-clay was determined to be 65% and 40% respectively, according to thermogravimetric analysis.

4.2.3 Polymerization

Polymerizations were conducted in a 2.5 ml, high-pressure cell equipped with sapphire windows that allow visual observation of the mixture. In a typical polymerization, the initiator AIBN and PDMS-clay were weighed into the cell containing a magnetic stir bar. The cell was purged with CO_2 via an Isco automatic syringe pump (Model 260D) for a few minutes; then the monomer was injected into the cell. The cell was then filled with CO_2 to 70 bar, and heated to 65 °C. After the desired temperature was reached, the desired pressure was achieved by the addition of more CO_2. The reaction was allowed to proceed with stirring for a specific time, and then the cell was cooled

and the CO_2 was slowly vented. Unless specified, the final product was taken out and dried at 50 °C. in a vacuum oven overnight, and the resultant materials stored in a desiccator for characterization. Yields of the polymer were determined gravimetrically. For dynamical mechanical analysis, the composite was heated in a vacuum oven at 150 °C overnight to remove residual CO_2 trapped within the polymer. The sample was then pulverized and compression molded (180 °C, 54 MPa) into a thin plaque.

4.2.4 Characterization

Powder X-ray diffraction (XRD) data (2θ = 2° and 2θ =10°) were collected on a Rigaku multiflex diffractometer using Cu Kα radiation (40 kV, 40 mA) at a scan rate of 0.5°/min. Scanning electron microscopy (Hitachi S-4700 FE-SEM) and transmission electron microscopy (TEM) (Phillips CM12) were used to investigate the morphologies and microstructures of the nanocomposites. Samples for SEM were mounted on aluminum stubs using an adhesive carbon tab, then gold coated. Samples for TEM were either directly from the powdery sample or cut from the compression molded sample. The samples were embedded and cured in epoxy resin and thin-sectioned using a ultramicrotome (Reichert Supernova) equipped with a diamond knife. Thermogravimetric analysis (TGA) was performed using a Perkin-Elmer Pyris 1 TGA system in an argon atmosphere at a heating rate of 10 °C/min. The storage modulus and glass transition temperature of the PMMA nanocomposites were measured by a dynamic mechanical analyzer (Perkin Elmer DMA 7e) using a extension measuring system operating at a frequency of 1 Hz; measurements were conducted in the air from room temperature to

140 °C at a scan rate of 5 °C/min. Molecular weights of filtered polymers (through 0.2 micron syringe filter) were obtained by gel permeation chromatography (GPC) using Waters microstyragel columns (pore size 10^5, 10^4, and 10^3 Å) and differential refractometry (Waters model 410) detector. Polystyrene standards were used for calibration.

4.3 Results and Discussion

4.3.1 Synthesis

The pseudo-dispersion polymerizations of MMA were conducted with 0.5 ml MMA monomer at concentrations of 6 wt% PDMS-clay (with respect to monomer) and 0.6 wt% AIBN (with respect to monomer) at 65 °C, 241 bar for 4 hours in a 2.5 ml CO_2 cell. The pseudo-dispersion polymerizations of styrene were conducted with 0.5 ml styrene monomer at concentrations of 7 wt % PDMS-clay (with respect to monomer) and 1 wt% AIBN (with respect to monomer) at 65 °C, 344 bar for 48 hours in a 2.5ml CO_2 cell. Unlike typical dispersion polymerizations in which reactions start out homogeneously with a stabilizer soluble in the CO_2 phase, the pseudo-dispersion polymerizations were heterogeneous throughout the reaction. Although clay is not soluble in CO_2, the PDMS-modified clay formed a milk-like suspension under magnetic stirring (Figure 4.3). As the reaction proceeded, the suspension appeared to thicken, and precipitated powder accumulated on the windows. Upon venting CO_2 at the end of the reaction, a white dry powder was recovered in the form of fine particles (Figure 4.4). The yield of PMMA was 88% with M_w 450 KDa (entry 2 in Table 4.1); the yield of PS was 93% with M_w

Figure 4.3: Milk-like suspension in the pseudo-dispersion polymerization of MMA in $scCO_2$.

126 KDa (entry 8 in Table 4.1). These high conversions and high molecular weights of polymers indicate successful dispersion polymerizations in CO_2.

4.3.2 Effect of PDMS-clay Concentration on Polymerization of MMA

Analysis by SEM shows that the precipitated PMMA/PDMS-clay nanocomposites primarily consist of spherical PMMA particles (Figure 4.5(a)) with an average particle diameter about 10 um. These particles show a relatively broad size distribution, presumably due to the ill-defined interaction mechanism between the monomers and insoluble clay platelets as compared to the typical, molecular interactions between monomers and soluble (polymeric) surfactants. Nevertheless, as the concentrations of PDMS-clay increase from 6% to 10% and 17%, the average diameter of the PMMA particles de-

(a)

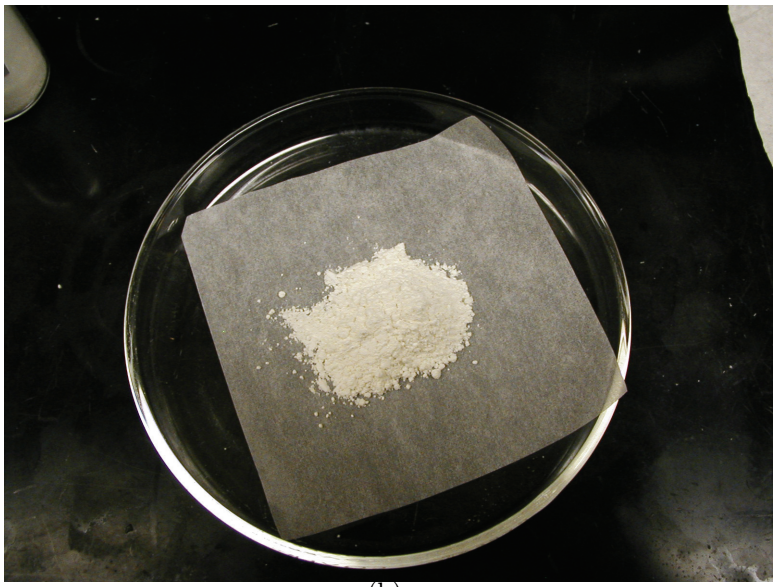

(b)

Figure 4.4: Picture of PMMA nanocompoistes recoved from CO_2 cell: (a) PMMA/PDMS-clay nanocomposite; (b) PS/PDMS-clay nanocomposite.

Table 4.1: Pseudo-Dispersion Polymerizations of MMA and Styrene in $scCO_2$

	Entry	PDMS-clay (%)	2C18-clay (%)	yield (%)	M_w (KDa)	Sample description
PMMA	1	4		57	381	aggregated powder
	2	6		88	450	fine powder
	3	8		85	524	fine powder
	4	10		87	590	fine powder
	5	17		96	367	fine powder
	6		6	38	392	aggregated powder/flake
PS	7	5		75	114	viscous block
	8	7		93	126	fine powder
	9	12		95	109	fine powder
	10	19		88	79	fine powder
	11		6	77	138	aggregated powder/block

creases and becomes more uniformly distributed, as shown in Figure 4.5(a), (b) and (c). This is consistent with a typical dispersion polymerization in $scCO_2$ and indicative of a more efficient stabilization of smaller particles with increasing stabilizer concentration. In addition, the molecular weights of PMMA increased with increased PDMS-clay concentration until the PDMS-clay concentration reaches 10% (table 4.1). For comparison, an identical polymerization of MMA was conducted with the 2C18-clay as the stabilizer. As shown in entry 6 in table 4.1, the relatively low yield (38%) and irregular morphologies of the resulting PMMA indicate the poor stabilizing ability of the hydrocarbon surfactant-modified clay in CO_2 relative to the PDMS-clay; the hydrocarbon surfactant is not CO_2-philic and cannot provide good steric stabilization for the monomer/polymer particles in $scCO_2$.

An interesting observation for PMMA with 6% PDMS-clay is that there are many small particles on the surface of primary PMMA particles (Figure 4.5(d), (e)). Clay platelets are irregular in shape however these small particles seem to be round and smooth, so we can exclude the possibility that these coordinated small particles are clay platelets. Instead, we believe that these small particles are secondary PMMA particles, and the formation of this interesting morphology can be attributed to the difunctional aminopropyl groups in the AP-PDMS surfactant. As is depicted in Figure 4.6, we have proposed previously that the stabilization mechanism is most likely steric stabilization in the CO_2 phase with the clay itself interacting with the carbonyl group of the methacrylate moiety via H-bonding. In our current system, although one end of aminopropyl group has been quaternized and attached to the cation exchange site of

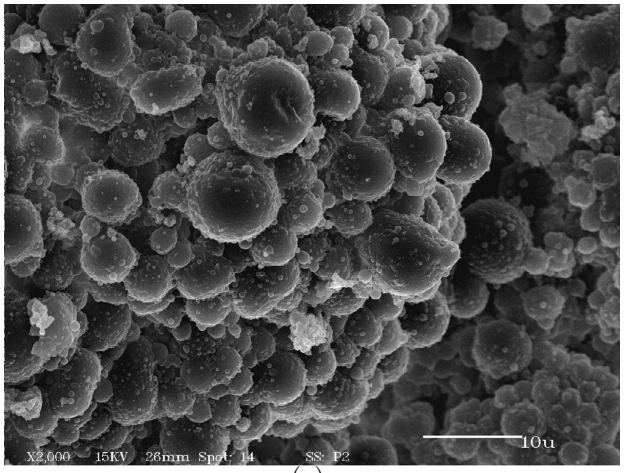
X2,000 15KV 26mm Spot: 14 SS: P2
10u

(a)

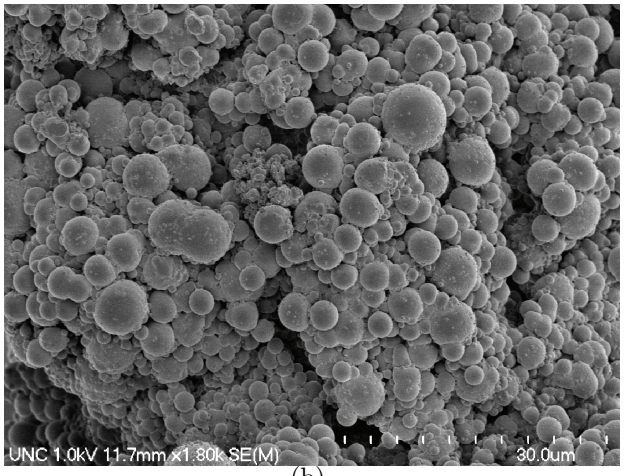
UNC 1.0kV 11.7mm x1.80k SE(M)
30.0um

(b)

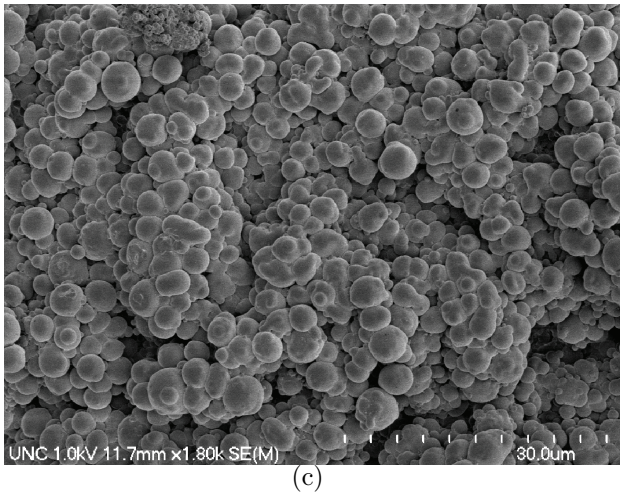
UNC 1.0kV 11.7mm x1.80k SE(M)
30.0um

(c)

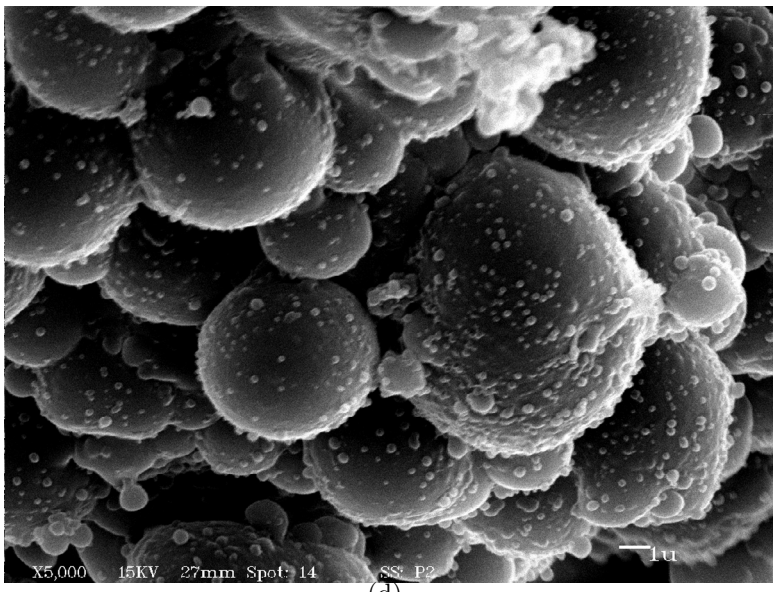

(d)

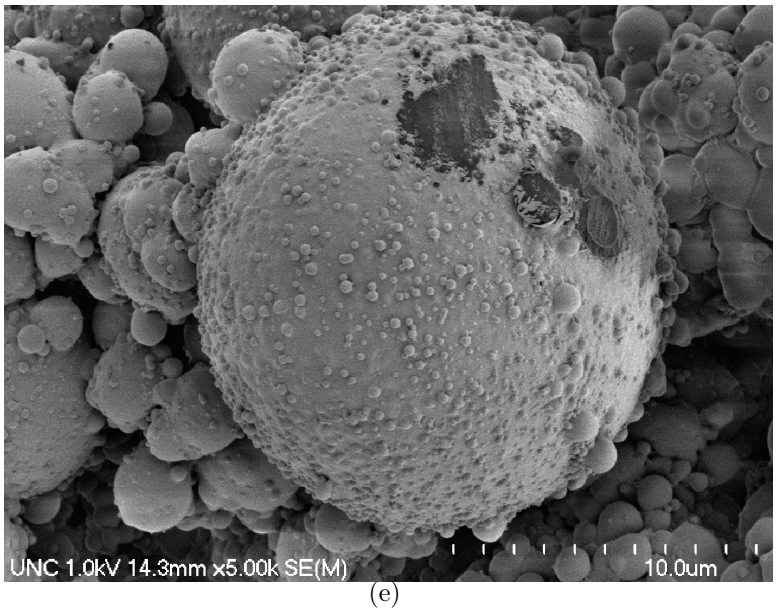

(e)

Figure 4.5: SEM images of PMMA/PDMS-clay nanocomposites with varying PDMS-clay concentrations: (a) 6%, (b) 10% and (c) 17%; (d), (e): Higher magnification SEM images of PMMA/PDMS-clay nanocomposites with 6 wt % PDMS-clay.

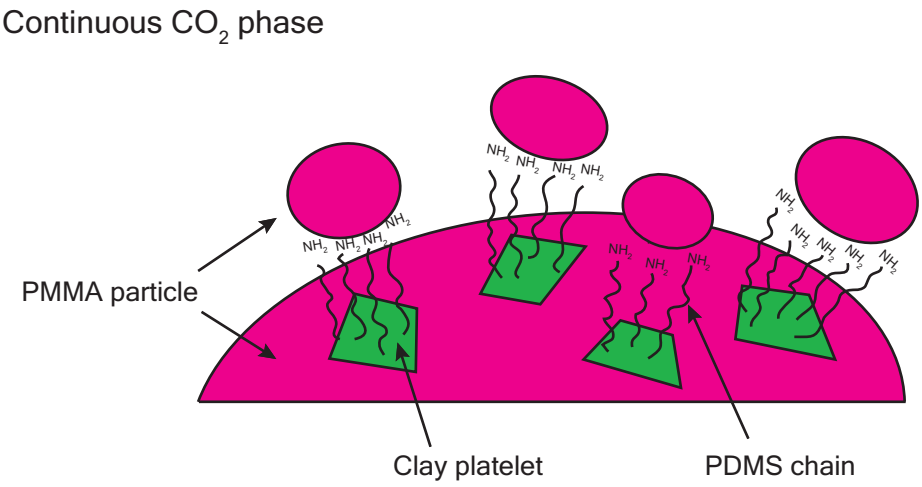

Figure 4.6: Schematic illustration of a primary PMMA particle (shown in red) stabilized by PDMS-clay in which the clay platelet (shown in green) acts as a primary anchor and the aminopropyl group on the free end of the PDMS chains serves as a secondary anchor for the small PMMA particles (shown in red).

clay, the other end may still interact with the carbonyl group of MMA monomer via a H-bond and serve as a secondary anchoring point for PMMA growth. Actually, it has been reported by Okubo and coworkers that AP-PDMS alone can stabilize dispersion polymerization of MMA in $scCO_2$ [177]. Since it is known that primary aliphatic amines react with CO_2 to form carbamic acid [39], they proposed that the interaction between AP-PDMS and MMA can be either hydrogen bonding between the carbamic acid group and the carbonyl group, or hydrogen bonding between the aminopropyl group and the carbonyl group (Figure 4.7)

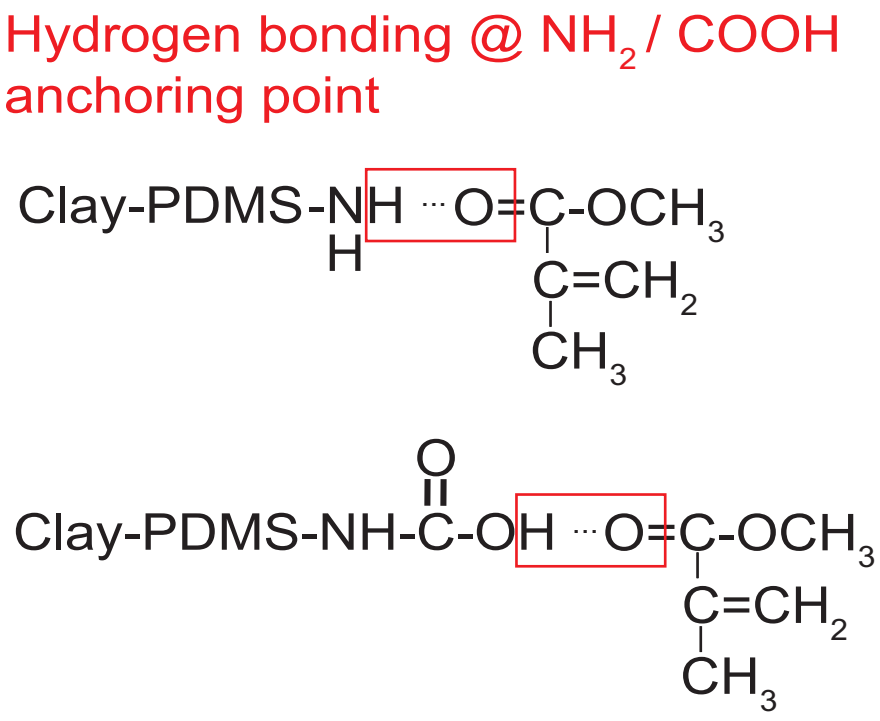

Figure 4.7: Schematic illustration of two types of hydrogen bonding between AP-PDMS and MMA.

4.3.3 Effect of PDMS-clay Concentration on Polymerization of Styrene

Again, in the case of PS/PDMS-clay nanocomposites, increasing the concentration of PDMS-clay also results in a decrease of composite particle diameter and a narrower size distribution (Figure 4.8(a), (b) and (c)). In contrast, the morphology of the PS/2C18-clay nanocomposite is ill-defined (Figure 4.8(d)) and the yield is low (entry 11 in table 4.1). Clearly the PDMS-clay is also acting as a stabilizer for styrene polymerization, although there is no hydrogen bond between styrene and clay as in the MMA-clay system. Styrene merely interacts with clay through a weak van der Waals interaction. This much weaker interaction is evidenced by a much longer polymerization time ($>$ 40 hours, Figure 4.9) to reach high polymer conversion than conventional dispersion polymerizations of styrene in $scCO_2$ (24$\sim$40 hours) [122, 125, 124]. In addition, the molecular weights of PS do not change much with increases in the PDMS-clay concentration (Table 4.1). However, the van der Waals interaction is clearly capable of bringing styrene into the clay gallery and providing sufficient anchoring to help produce PS in high yields in $scCO_2$. Additional proof that there must be an anchoring interaction between styrene and clay comes from a comparison with dispersion polymerization using the AP-PDMS surfactant alone. Although AP-PDMS has been shown to act as a stabilizer and help stabilize MMA polymerization in $scCO_2$, it was observed that in the case of styrene polymerization, no stabilized polymerization was obtained. With AP-PDMS alone, the polymerization of styrene resulted in a viscous liquid and an

undesirably-low yield, which is very similar to what is obtained in the complete absence of any stabilizer. This further confirms that there is no hydrogen bonding interaction between styrene and AP-PDMS and styrene must interact with clay to provide the necessary anchoring.

4.3.4 Comparison of XRD results of the PMMA and PS nanocomposites

X-ray diffraction (XRD) was used to characterize the layered structure of the polymer/clay nanocomposites. Figure 4.10 shows the XRD patterns of the organoclays and PMMA and PS nanocomposites with PDMS-clay and 2C18-clay. As is seen from curves a and b, the basal spacings of 2C18-clay and PDMS-clay are found to be 3.9 nm and 7.1 nm respectively, based on their diffraction peaks in the pattern (The (001) diffraction peak of PDMS-clay is not shown in the pattern, but can be calculated from the higher order diffraction peaks in the pattern). It is reasonable that PDMS-clay has a larger d-spacing than 2C18-clay, since the length of PDMS surfactant (n$\sim$44) is much longer than that of 2C18-surfactant. For PMMA and PS nanocomposites with 6 wt% 2C18-clay (curves c and d), the (001) peaks are almost unchanged from that of 2C18-clay, indicating that both nanocomposites are intercalated. These results are in agreement with what has been observed in previous studies [105, 178]. In PMMA and PS nanocomposites with PDMS-clay, the characteristic peak disappears in the pattern, as shown in curves e and f, suggesting that the d-spacings of clay in the nanocomposites are larger than 4 nm, the detection limit of the instrument used in this study. The


UNC 1.0kV 14.3mm x1.80k SE(M)
30.0um

(a)

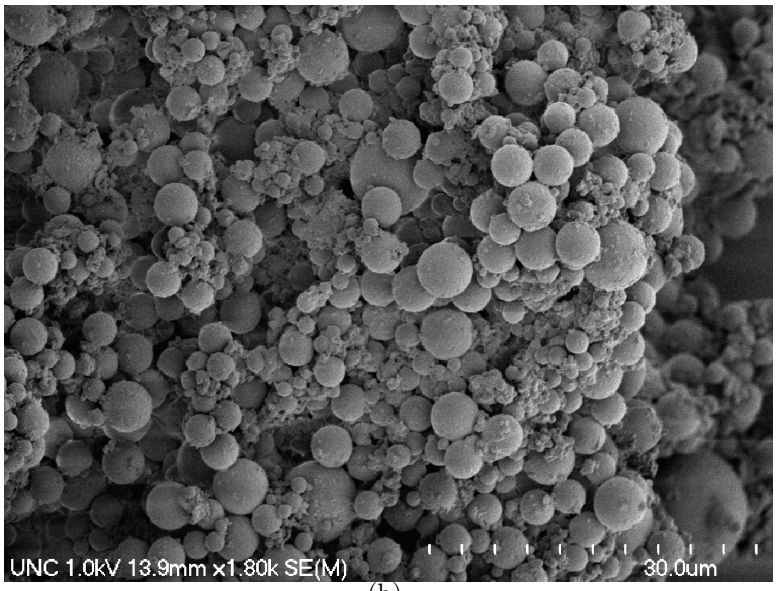
UNC 1.0kV 13.9mm x1.80k SE(M)
30.0um

(b)

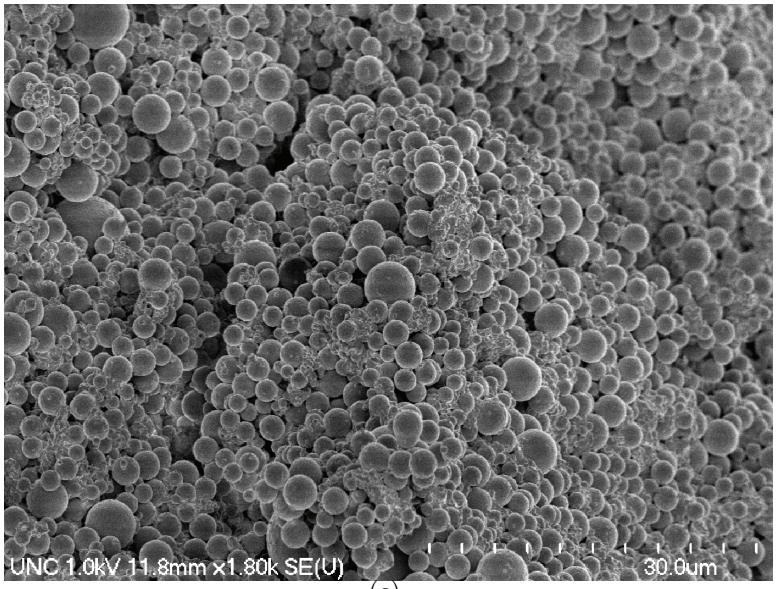

(c)

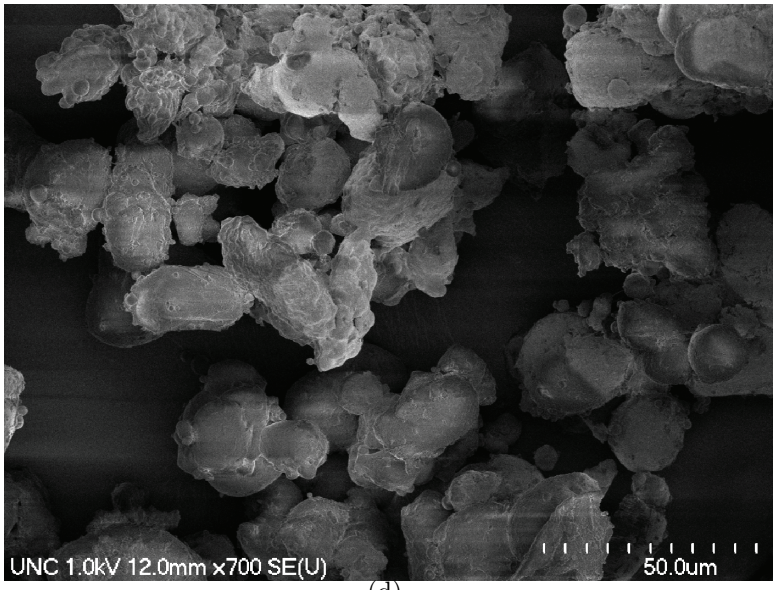

(d)

Figure 4.8: SEM images of PS/PDMS-clay nanocomposites with varying PDMS-clay concentration: (a) 7%, (b) 12% and (c) 19%. (d) SEM image of PS/2C18-clay nanocomposites with 6 wt % PDMS-clay.

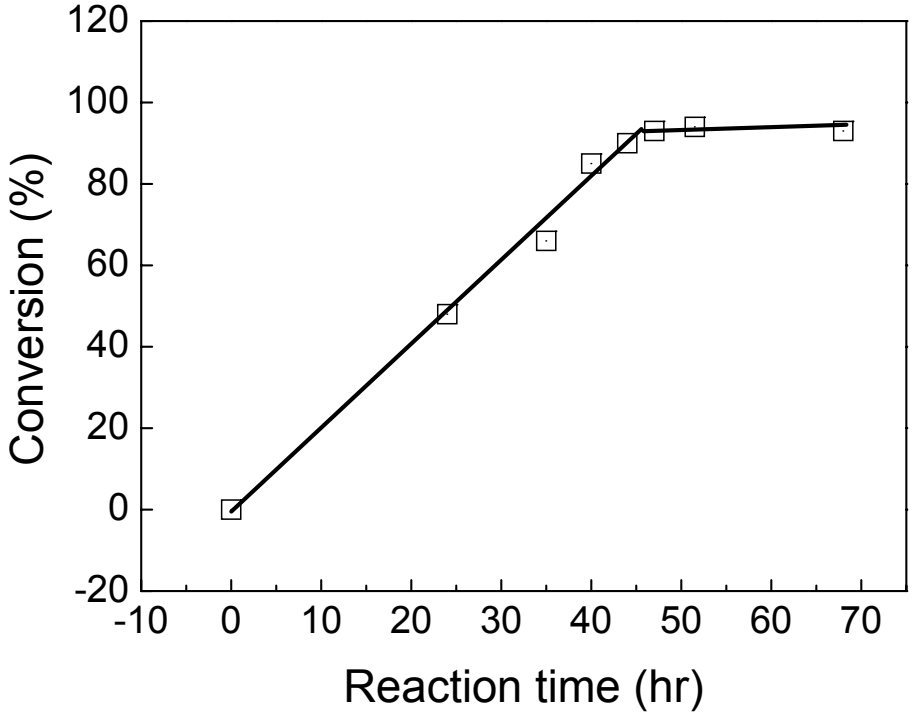

Figure 4.9: Conversion of polystyrene Vs. reaction time

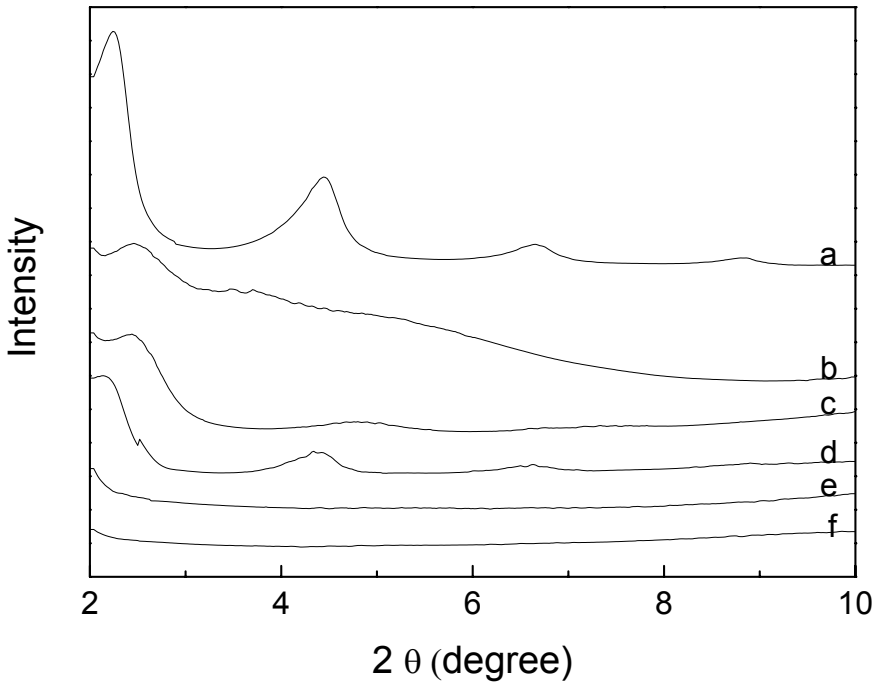

Figure 4.10: XRD patterns of (a) 2C18-clay; (b) PDMS-clay; (c) PMMA nanocomposite with 6 wt% 2C18-clay; (d) PS nanocomposite with 6 wt% 2C18-clay; (e) PMMA nanocomposite with 6 wt% PDMS-clay; (f) PS nanocomposite with 7 wt% PDMS-clay.

featureless patterns suggest that clay is nearly completely exfoliated in both polymers.

4.3.5 Comparison of TEM results of the PMMA and PS nanocomposites

More information about the microstructures of PMMA/PDMS-clay (6 wt% PDMS-clay) and PS/PDMS-clay (7 wt% PDMS-clay) nanocomposites was obtained by TEM observations. In the powdery PMMA/PDMS-clay nanocomposites shown in Figure 4.11(a) and (b), the dark line represents individual silicate layers, whereas the brighter

area represents the PMMA matrix. It can be seen that the silicate layers of clay have been completely exfoliated and uniformly dispersed in the PMMA matrix. This further supports the XRD analysis which suggests that exfoliated nanocomposites were formed. While for the powdery PS/PDMS-clay nanocomposites, as shown in Figure 4.11(c), many dark, distinct spherical particles are distributed in the micrograph. These dark particles are actually PS particles, the size and distribution of which agree well with the SEM observations in the previous study. The observation of these darker PS particles can be attributed to the stronger electron scattering of PS relative to the epoxy resin, which scatters electron much weaker therefore appears to be lighter in the TEM. Since the contrast between PMMA and epoxy is not as distinct as that between PS and epoxy, PMMA particles can not be readily distinguished in TEM. The brightest areas are voids, which are probably formed as PS particles are ripped off the epoxy resin during sample sectioning. Surprisingly, the silicate layers in the PS nanocomposites are not distributed randomly and uniformly throughout the PS particle matrix as in the PMMA matrix. Instead, it can be seen that the darkest silicate layers are for the most part located on the exterior surfaces of the PS particles, manifested by the contrasting electron densities in Figure 4.11(d). Clearly, the silicate layers are exfoliated into individual layers, or they consist of at most a few silicate sheets, as suggested by both TEM and XRD. However, when the powdery sample is compression molded into a continuous film, TEM reveals that these exfoliated silicate layers have re-aggregated together and formed stacks, as shown in Figure 4.11(e). This phenomenon of re-aggregation is not unexpected, since the concentration of silicate layers on the

exterior surfaces of neighboring PS particles makes possible a large number of contacts between silicate exterior layers on different PS particles. There is a kind of nanophase separation into silicate rich boundaries wherein the clay is no longer exfoliated in the compression molded PS/PDMS-clay nanocomposite.

4.3.6 Comparison of thermal properties of the PMMA and PS nanocomposites

The thermal stabilities of both nanocomposites and polymers were studied by TGA analysis. Figure 4.12(a) and (b) show the TGA curves (the residual weight percentage versus temperature) and DTG curves (derivative of the residual weight percentage versus temperature) for PMMA/PDMS-clay nanocomposites and pure PMMA. Evidently, the decomposition onsets of PMMA/PDMS-clay nanocomposites shift to higher temperatures compared to that of pure PMMA. As shown in Figure 4.12(b), pure PMMA appears to have two degradation steps at 288 °C and 333 °C, which were generally attributed to scissions at the chain-end initiation from vinylidene ends and random internal scission of the polymer chain, respectively [179]. While for PMMA/PDMS-clay nanocomposites, it can be seen that the first degradation step (288 °C) is largely depressed whereas the second degradation temperature is delayed by about 19 °C from that of pure PMMA. Therefore, it is apparent that the presence of clay stabilizes both steps of degradation, though further increase of clay concentration from 6% to 10% does not seem to affect decomposition temperature much. TGA and DTG curves for PS/PDMS-clay nanocomposites and pure PS are shown in Figure 4.12(c) and (d). As

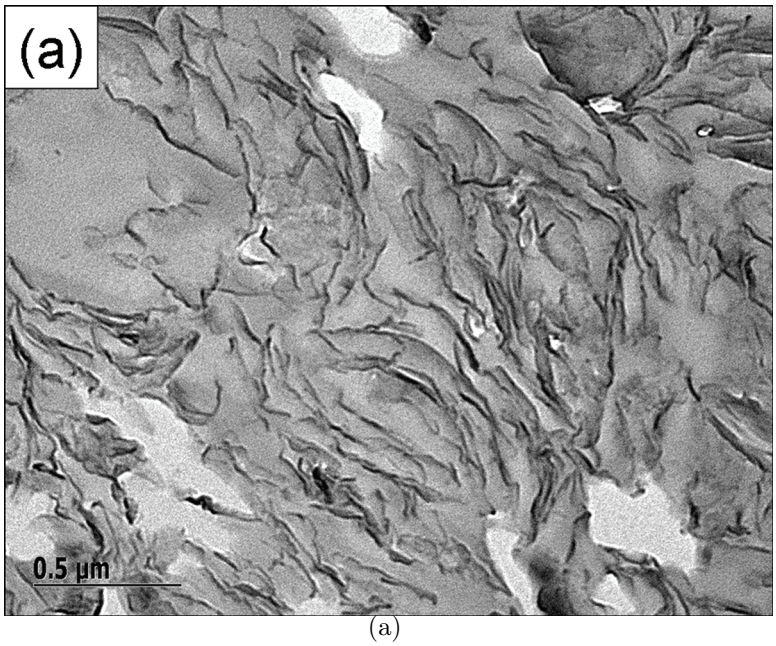

(a)

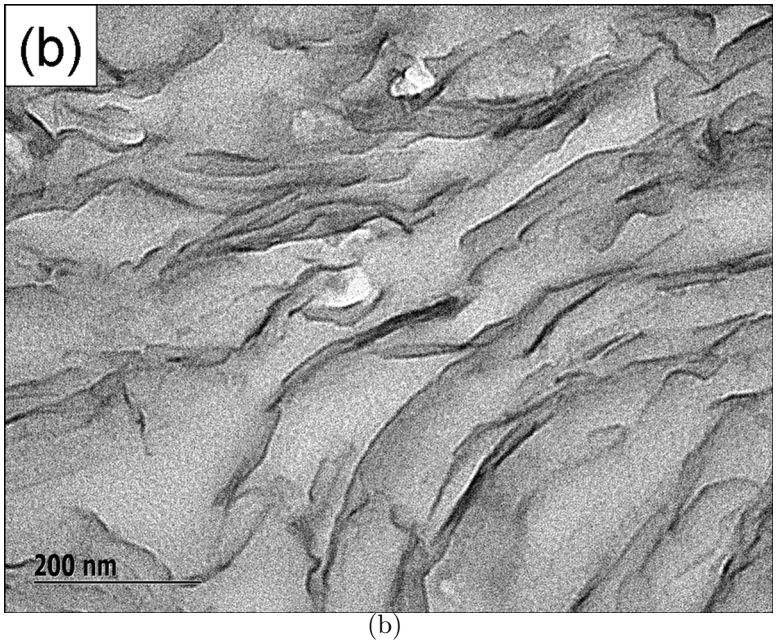

(b)

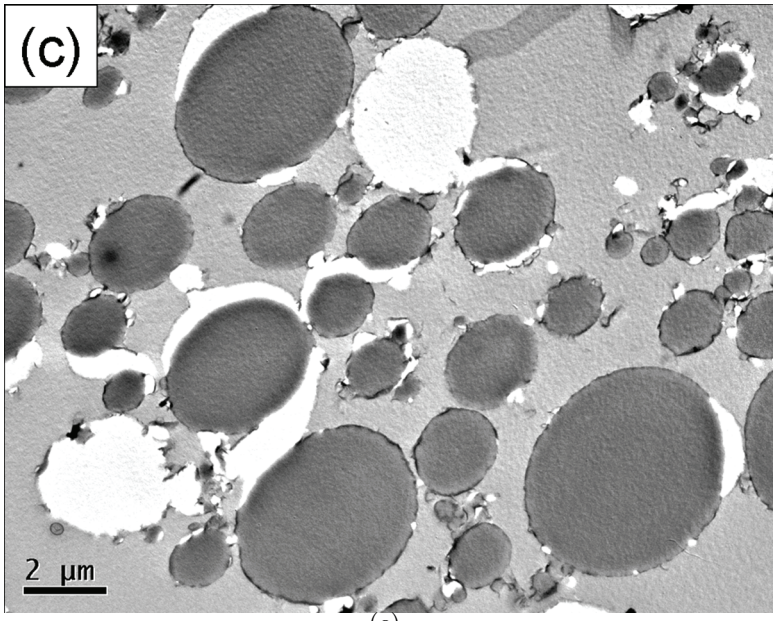

(c)

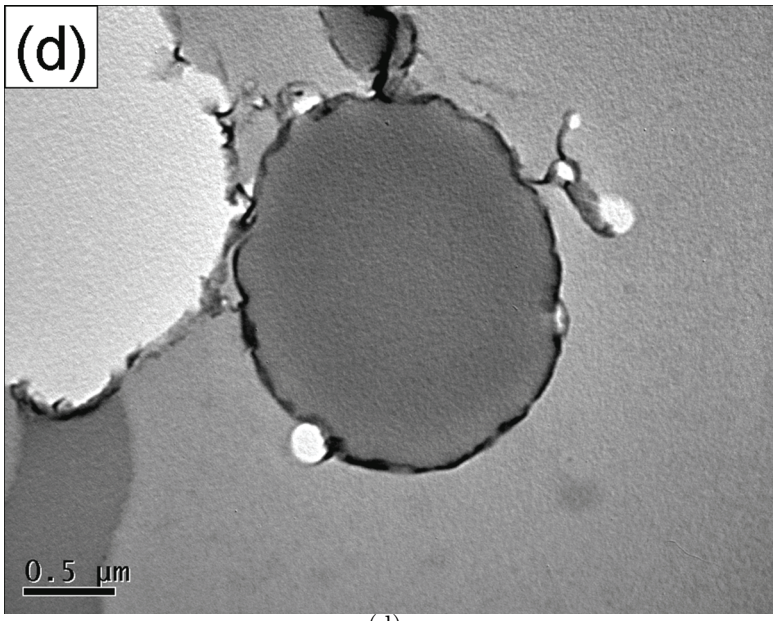

(d)

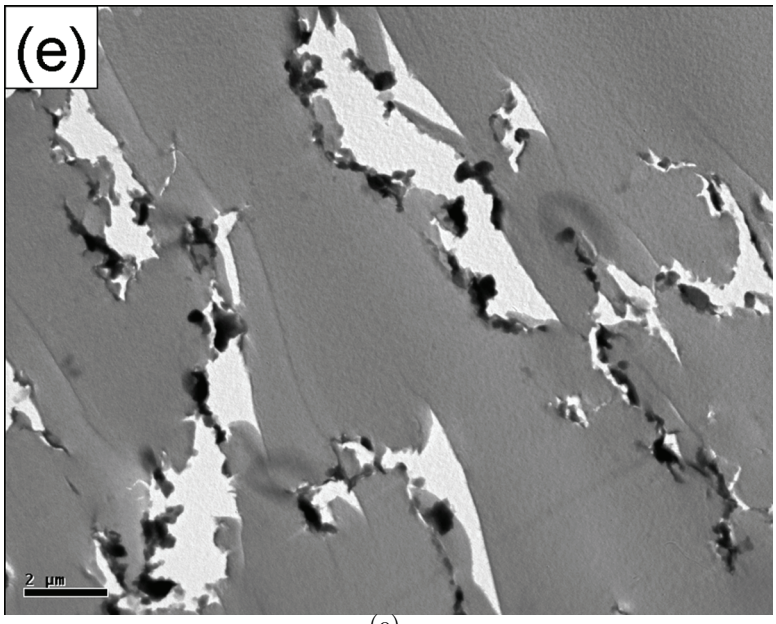

(e)

Figure 4.11: TEM images of (a) powdery PMMA/PDMS-clay nanocomposite at low magnification image; (b) powdery PMMA/PDMS-clay nanocomposite at high magnification; (c) powdery PS/PDMS-clay nanocomposite at low magnification; (d) powdery PS/PDMS-clay nanocomposite at high magnification; (e) compression molded PS/PDMS-clay nanocomposite.

seen in Figure 4.12(d), the temperature at maximum degradation rate increases largely from 369 °C for pure PS to 398 °C for PS nanocomposites with 7 wt% clay and to 419 °C for PS nanocomposites with 12 wt% clay. Although clay is known to be concentrated on the exterior surfaces of PS particles, it seems that the presence of clay still plays an important role in enhancing the thermal stabilities of PS, by hindering the out-diffusion of the volatile decomposition products.

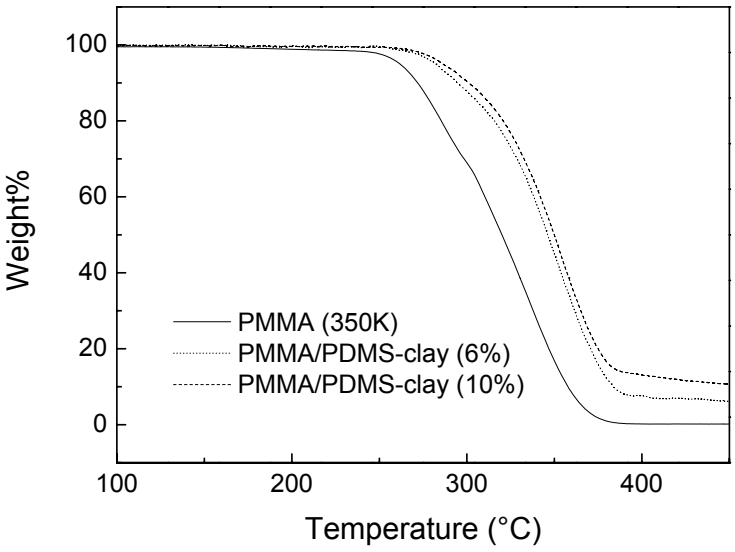
Weight%
Temperature (°C)
PMMA (350K)
PMMA/PDMS-clay (6%)
PMMA/PDMS-clay (10%)
100
80
60
40
20
0
100
200
300
400

(a)

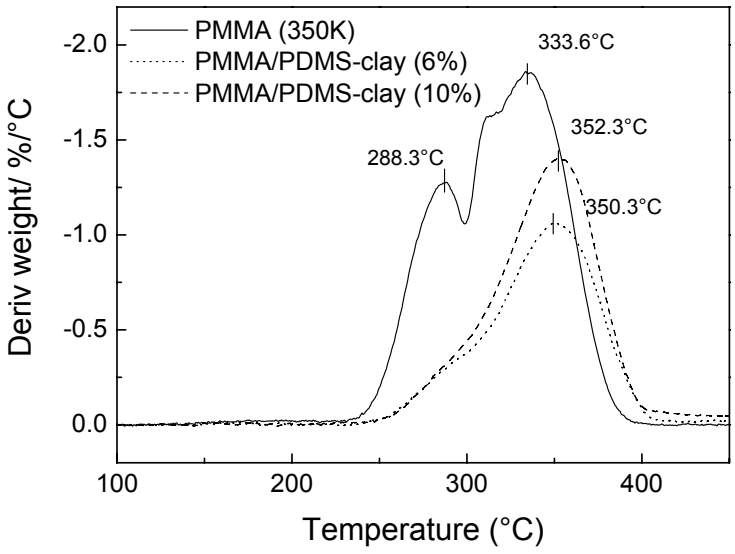
Deriv weight/ %/°C
Temperature (°C)
PMMA (350K)
PMMA/PDMS-clay (6%)
PMMA/PDMS-clay (10%)
333.6°C
352.3°C
288.3°C
350.3°C
-2.0
-1.5
-1.0
-0.5
0.0
100
200
300
400

(b)

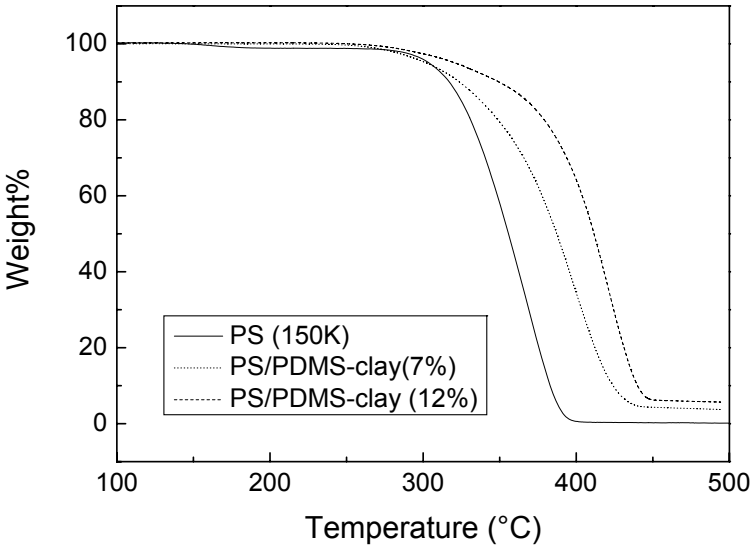

(c)

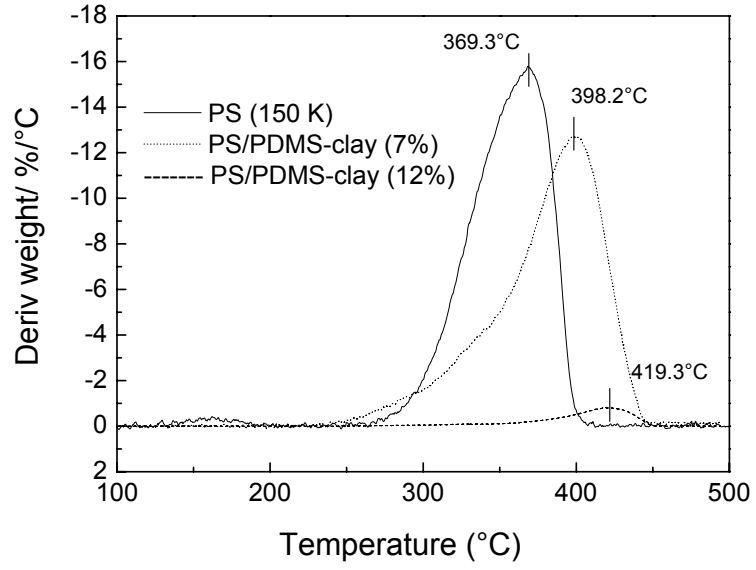

(d)

Figure 4.12: (a) TGA curves of PMMA and PMMA/PDMS-clay nanocomposites; (b) DTG curves of PMMA and PMMA/PDMS-clay nanocomposites; (c) TGA curves of PS and PS/PDMS-clay nanocomposites; (d) DTG curves of PS and PS/PDMS-clay nanocomposites.

4.3.7 Comparison of mechanical properties of the PMMA and PS nanocomposites

Dynamic mechanical analysis (DMA) was used to measure the viscoelastic properties of the polymer nanocomposites. Figure 4.13 shows the temperature dependence of storage modulus and tanδ of PMMA and PMMA/PDMS-clay nanocomposites with 6 wt% PDMS-clay. As expected, the storage modulus of the PMMA nanocomposites increases compared to that of pure PMMA. A slightly enhanced glass transition temperature (T_g = 125 °C for the nanocomposites versus T_g = 122 °C for pure PMMA) corresponding to the peak of the loss tangent is also observed for the PMMA/PDMS-clay nanocomposites. It has been suggested that the enhancements of the storage modulus and glass transition temperature result from the strong interfacial interactions between the polymer and clay, the restricted segmental motions of polymer chains at the organic-inorganic interface, and the inherent high modulus of the clays [175, 176]. In Chapter 3, we synthesized PMMA nanocomposites with a fluorinated surfactant-modified clay (10F-clay), and also observed a increase of glass transition temperature over pure PMMA by 8 °C. Here, it should be noted that the increase of T_g for PMMA/PDMS-clay nanocomposites is only 3 °C. This is probably due to the dual role organoclay plays in the nanocomposites: on one hand, it serves as an nano-filler leading to the increase of T_g and storage modulus; on the other hand, it is a plasticizer leading to the decrease of T_g and modulus [180]. Here, the longer PDMS chain may have a larger plasticizing effect than the fluorinated surfactant, which may be the reason why the

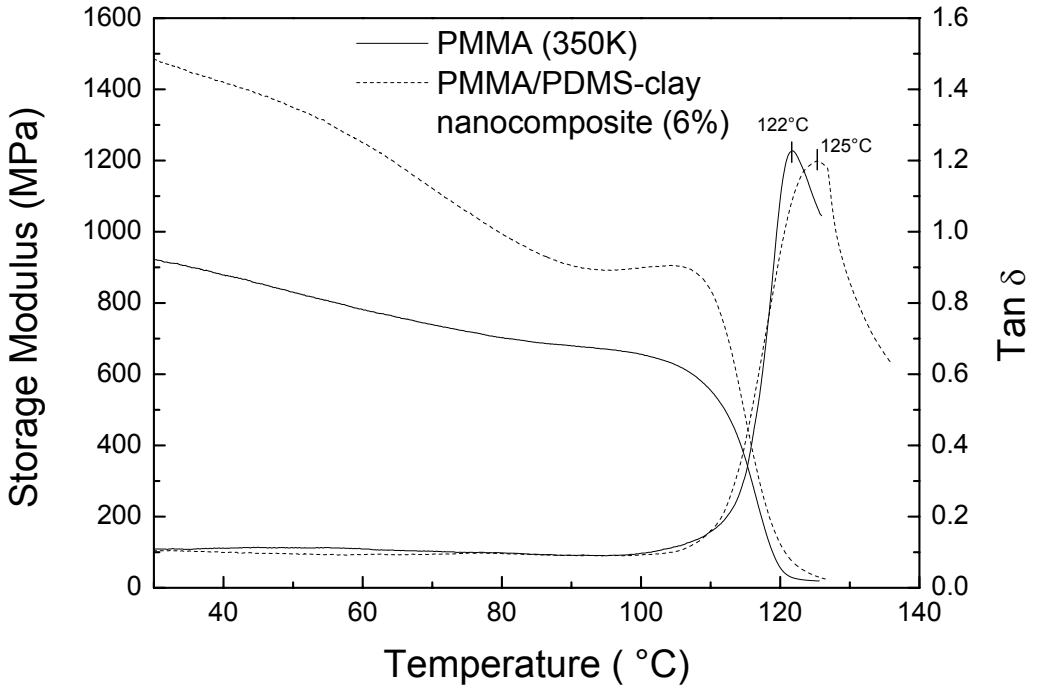

Figure 4.13: Storage modulus and loss tangent spectra of PMMA and PMMA/PDMS-clay nanocomposites.

PMMA/PDMS-clay nanocomposites have a slightly smaller increase of T_g compared to PMMA/10F-clay nanocomposites. As for PS/PDMS-clay nanocomposites, we have been unable to perform dynamic mechanical analysis because the samples are too brittle. In conjunction with TEM observations, it is possible that the re-aggregation of clay in the compression molded sample contributes to brittle nanophase-separated inorganic grain boundaries in the PS nanocomposites. However, further study is needed to confirm this hypothesis.

4.4 Conclusions

PMMA/PDMS-clay and PS/PDMS-clay nanocomposites have been synthesized with high yields via a pseudo-dispersion polymerization technique in $scCO_2$. It has been found that insoluble PDMS-clay dispersions are an effective stabilizer for polymerizations of methyl methacrylate and styrene in $scCO_2$. The morphologies of PMMA and PS depend strongly on the concentration of PDMS-clay, as anticipated for a conventional stabilizer. Whereas XRD results show featureless patterns for both PMMA and PS nanocomposites, TEM studies suggest that the distribution of clay are quite different in the two nanocomposites. In the case of the PMMA/PDMS-clay nanocomposites where the interaction between PMMA with clay is via hydrogen bonding, the silicate layers are completely exfoliated and uniformly dispersed in the PMMA matrix. While for PS/PDMS-clay nanocomposites where PS interacts with clay via a weaker van der Waals interaction, the silicate layers are exfoliated but concentrated mostly on the exterior surfaces of PS particles. As a result, the silicate layers of clay re-aggregate in the PS matrix after compression molding. Both PMMA and PS nanocomposites show enhanced thermal stabilities compared to the pure polymers, whereas the different distributions of clay seem to play an important role in mechanical properties of the nanocomposites.

4.5 Future Directions

With this project, it is encouraging to see that the PDMS-clay works as an effective stabilizer for both PMMA and PS polymerizations and helps produce them in high yields in $scCO_2$. It leads one to believe that the pseudo-dispersion polymerization would work for many other vinyl polymers previously demonstrated by conventional dispersion polymerization in $scCO_2$, irrespective of the hydrogen-bonding capabilities of the polymers. Interesting polymer systems to explore in this context include poly(vinylidene fluoride) (PVDF), poly(vinyl acetate) (PVAc), polyacrylonitrile (PAN), etc.

In addition, we have proposed in section 4.3.7 that the T_g of PMMA obtained from DMA experiment is a compromised value resulting from both raising T_g by the role of PDMS-clay as the nanofiller and decreasing T_g by the role of PDMS-clay as the plasticizer. We assumed that the longer the PDMS chain, the larger the plasticization effect this surfactant has on nanocomposites. In order to test this hypothesis, proposed future studies would include modifying clay with AP-PDMS of different moleculer weights. (The AP-PDMS used in this study has a M_w of 3500. AP-PDMS with M_w of 1000 and 25000 are also commercially available from Scientific Polymer, Inc.) In addition to the plasticization effect of the surfactant chain lengh on T_g and the storage modulus of the polymer, the effect of the PDMS chain length on polymer morphologies is also an area of interest worthy of further study.

Another promising extension of this project could be fluoropolymer/clay nanocomposites. Fluoropolymers are industrially important polymers that are noted for their excellent resistance against chemicals, weathering and high temperature. However, there

have been very few investigations of fluoropolymer/clay nanocomposites, presumably due to the their ultralow surface tension and the difficulty of overcoming the thermodynamic barrier associated with dispersing clay in polymers. In general, dispersion of clay in a polymer requires a sufficiently favorable enthalpic contribution to overcome any entropic penalties. A favorable enthalpy of mixing for the polymer/organoclay is achieved when the polymer-clay interactions are more favorable than the surfactant-clay interactions [32, 164, 181]. Therefore, one way to overcome this challenge is to decrease the enthalpic interaction between the surfactant and the clay, which can be realized by using fluorinated surfactants to modify clay [182]. Herein, our fluorinated or PDMS surfactant has a much lower surface energy than conventional hydrocarbon surfactants, thus are able to lower the enthalpic interaction between the surfactant and the clay. In addition, CO_2 has been shown to be an excellent solvent medium for the synthesis and processing of many fluoropolymers. Therefore, we have reasons to believe that our system in $scCO_2$ is a great starting point for making better dispersed fluoropolymer/clay nanocomposites.

Proposed future work could start with making PVDF nanocomposites with fluorinated surfactant-modified clay. Previous work on melt intercalation of PVDF/clay nanocomposites has been described by Priya [183] and Kim [184]. In their work, they used conventional hydrocarbon surfactants to modify clay. As a result, only intercalated nanocomposites were obtained. In contrast, our work would focus on examing the effect of fluorinated surfactants on dispersion of clay in PVDF matrix. Studies should be done comparing the difference between a fluorinated surfactant and a hydrocarbon

surfactant in clay dispersions as well as in thermal/mechanical properties. Additionally, CO_2 could be another variable to study in terms of controlling PVDF cystalline structures. Some preliminary work in our laboratory by Jinrong Liu suggests that this would be a viable dissertation topic.

BIBLIOGRAPHY

[1] Mark, J. E. *Polym. Eng. Sci.* **1996,** *36,* 2905.

[2] Reynaud, E.; Gauthier, C.; Perez, J. *Rev. Metall./Cah. Inf. Tech.* **1999,** *96,* 169.

[3] von Werne, T.; Patten, T. E. *J. Am. Chem. Soc.* **1999,** *121,* 7409.

[4] Herron, N.; Thorn, D. L. *Adv. Mater.* **1998,** *10,* 1173.

[5] Shioyama, H. *Carbon* **1997,** *35,* 1664.

[6] Harris, D. J.; Bonagamba, T. J.; Schmidt-Rohr, K. *Macromolecules* **1999,** *32,* 6718.

[7] Matsuo, Y.; Tahara, K.; Sugie, Y. *Carbon* **1996,** *34,* 672.

[8] Matsuo, Y.; Tahara, K.; Sugie, Y. *Carbon* **1997,** *35,* 113.

[9] Ding, Y.; Jones, D. J.; Maireles-Torres, P. *Chem. Mater.* **1995,** *7,* 562.

[10] Wilson Jr., O. C.; Olorunyolemi, T.; Jaworski, A.; Borum, L.; Young, D.; Siriwat, A.; Dickens, E.; Oriakhi, C.; Lerner, M. *Appl. Clay Sci.* **1999,** *15,* 265.

[11] Oriakhi, C. O.; Farr, I. V.; Lerner, M. M. *Clays and Clay Minerals* **1997,** *45,* 194.

[12] Theng, B. K. G. *The Chemistry of Clay-Organic Reactions;* Wiley, New York, NY: 1974.

[13] Kojima, Y.; Usuki, A.; Kawasumi, M.; Okada, A.; Kurauchi, T.; Kamigaito, O. *J. Polym. Sci., Part A: Polym. Chem.* **1993,** *31,* 983.

[14] Burnside, S. D.; Giannelis, E. P. *Chem. Mater.* **1995,** *7,* 1597.

[15] Giannelis, E. P.; Krishnamoorti, R.; Manias, E. *Adv. Polym. Sci.* **1999,** *138,* 107.

[16] Vaia, R. A.; Vasudevan, S.; Krawiec, W.; Scanlon, L. G.; Giannelis, E. P. *Adv. Mater.* **1995,** *7,* 154.

[17] Vaia, R. A.; Ishii, H.; Giannelis, E. P. *Chem. Mater.* **1993,** *5,* 1694.

[18] Ogata, N.; Kawakage, S.; Ogihara, T. *J. Appl. Polym. Sci.* **1997,** *66,* 573.

[19] Lemmon, J. P.; Lerner, M. M. *Chem. Mater.* **1994,** *6,* 207.

[20] Greenland, D. J. *J. Colloid Sci.* **1963,** *18,* 647.

[21] Levy, R.; Francis, C. W. *J. Colloid Interface Sci.* **1975,** *50,* 442.

[22] Billingham, J.; Breen, C.; Yarwood, J. *J. Vibr. Spectrosc.* **1997,** *14,* 19.

[23] Jeon, H. G.; Jung, H. T.; Hudson, S. D. *Polym. Bull.* **1998,** *42,* 107.

[24] Ogata, N.; Jimenez, G.; Kawai, H.; Ogihara, T. *J. Polym. Sci. Part B: Polym. Phys.* **1997,** *35,* 389.

[25] Chen, X.; Gonsalves, K. E. *J. Mater. Res.* **1997,** *12,* 274.

[26] Usuki, A.; Kojima, Y.; Kawasumi, M.; Okada, A.; Fukushima, Y.; Kurauchi, T.; Kamigaito, O. *J. Mater. Res.* **1993,** *8,* 1179.

[27] Akelah, A.; Moet, A. *J. Mater. Sci.* **1996,** *31,* 3589.

[28] Tudor, J.; Willington, L.; O'Hare, D.; Royan, B. *Chem. Commun.* **1996,** 2031.

[29] Messersmith, P. B.; Giannelis, E. P. *Chem. Mater.* **1994,** *6,* 1719.

[30] Kornmann, X.; Berglund, L. A.; Sterte, J. *Polym. Eng. Sci.* **1998,** *38,* 1351.

[31] Wang, Z.; Pinnavaia, T. J. *Chem. Mater.* **1998,** *10,* 3769.

[32] Vaia, R. A.; Giannelis, E. P. *Macromolecules* **1997,** *30,* 7990.

[33] Vaia, R. A.; Jandt, K. D.; Kramer, E. J.; Giannelis, E. P. *Macromolecules* **1995,** *28,* 8080.

[34] Lee, D. C.; Jang, L. W. *J. Appl. Polym. Sci.* **1996,** *61,* 1117.

[35] Noh, M. W.; Lee, D. C. *Polym. Bull.* **1999,** *42,* 619.

[36] Lee, J.; Takekoshi, T.; Giannelis, E. *Mater. Res. Soc. Symp. Proc.* **1997,** *457,* 513.

[37] Shaffer, K. A.; DeSimone, J. M. *Trends Polym. Sci.* **1995,** *3,* 146.

[38] Quinn, E. L.; Jones, C. L. *Carbon Dioxide;* Reinhold: New York: 1936.

[39] McHugh, M. A.; Krukonis, V. J. *Supercritical Fluids Extraction: Principles and Practice, 2nd ed.;* Butterworth- Heinemann: Boston: 1994.

[40] Chiou, J. S.; Barlow, J. W.; Paul, D. R. *J. Appl. Polym. Sci.* **1985,** *30,* 2633.

[41] Kendall, J. L.; Canelas, D. A.; Young, J. L.; DeSimone, J. M. *Chem. Rev.* **1999,** *99,* 543.

[42] Lee, M.; Park, C. B.; Tzoganakis, C. *Polym. Sci. Eng.* **1999,** *39,* 99.

[43] Zhang, Y.; Gangwani, K. K.; Lemert, R. M. *J. Supercrit. Fluids* **1997,** *11,* 115.

[44] Wissinger, R. G.; Paulaitis, M. E. *Ind. Eng. Chem. Res.* **1991,** *30,* 842.

[45] Wissinger, R. G.; Paulaitis, M. E. *J. Polym. Sci. Part B: Polym. Phys.* **1987,** *25,* 2497.

[46] Wang, W. C. V.; Kramer, E. J.; Sachse, W. H. *J. Polym. Sci., Polym. Phys. Ed.* **1982,** *20,* 1371.

[47] Shieh, Y.-T.; Su, J.-H.; Manivannan, G.; Lee, P. H. C.; Sawan, S. P.; Spall, W. D. *J. Appl. Polym. Sci.* **1996,** *59,* 695.

[48] Hirose, T.; Mizoguchi, K.; Kamiya, Y. *J. Polym. Sci. Part B: Polym. Phys.* **1986,** *24,* 2107.

[49] Shieh, Y.-T.; Su, J.-H.; Manivannan, G.; Lee, P. H. C.; Sawan, S. P.; Spall, W. D. *J. Appl. Polym. Sci.* **1996,** *59,* 707.

[50] Edwards, R. R.; Tao, Y. M.; Xu, S. H.; Wells, P. S.; Yun, K. S.; Parcher, J. F. *J. Polym. Sci. Part B: Polym. Phys.* **1998,** *36,* 2537.

[51] Kamiya, Y.; Mizoguchi, K.; Terada, K.; Fujiwara, Y.; Wang, J.-S. *Macromolecules* **1998,** *31,* 472.

[52] Condo, P. D.; Johnston, K. P. *J. Polym. Sci. Part B: Polym. Phys.* **1994,** *32,* 523.

[53] Condo, P. D.; Paul, D. R.; Johnston, K. P. *Macromolecules* **1994,** *27,* 365.

[54] Wissinger, R. G.; Paulaitis, M. E. *J. Polym. Sci. Part B: Polym. Phys.* **1991,** *29,* 631.

[55] Kamiya, Y.; Mizoguchi, K.; Naito, Y. *J. Polym. Sci. Part B: Polym. Phys.* **1990,** *28,* 1955.

[56] Smith, P. B.; Moll, D. J. *Macromolecules* **1990,** *23,* 3250.

[57] Kamiya, Y.; Mizoguchi, K.; Hirose, T.; Naito, Y. *J. Polym. Sci. Part B: Polym. Phys.* **1989,** *27,* 879.

[58] Banerjee, T.; Lipscomb, G. G. *J. Appl. Polym. Sci.* **1998,** *68,* 1441.

[59] Briscoe, B. J.; Kelly, C. T. *Polymer* **1995,** *36,* 3099.

[60] Goel, S. K.; Beckman, E. J. *Polymer* **1992,** *33,* 5032.

[61] Goel, S. K.; Beckman, E. J. *Polymer* **1993,** *34,* 1410.

[62] Lee, M.; Tzoganakis, C.; Park, C. B. *Polym. Eng. Sci.* **1998,** *38,* 1112.

[63] Kato, S.; Tsujita, T.; Yoshimizu, H.; Kinoshita, T.; Higgins, J. S. *Polymer* **1997,** *38,* 2807.

[64] Mokdad, A.; Dubault, A.; Monnerie, L. *J. Polym. Sci. Part B: Polym. Phys.* **1996,** *34,* 2723.

[65] Handa, Y. P.; Zhang, Z. *Macromolecules* **1997,** *30,* 8505.

[66] Beckman, E. J.; Porter, R. S. *J. Polym. Sci. Part B: Polym. Phys.* **1987,** *25,* 1511.

[67] Hobbs, T.; Lesser, A. J. **1999,** *37,* 1881.

[68] Hobbs, T.; Lesser, A. J. **2000,** *41,* 6223.

[69] Schultze, J. D.; Bohning, M. *J. Macromol. Chem.* **1993,** *194,* 431.

[70] Schultze, J. D.; Bohning, M. *J. Macromol. Chem.* **1993,** *194,* 339.

[71] Gross, S. M.; Roberts, G. W.; Kiserov, D. J.; DeSimone, J. M. *Macromolecules* **2000,** *33,* 40.

[72] Handa, Y. P.; Capowski, S.; O'Neil, M. *Thermochim. Acta* **1993,** *226,* 177.

[73] Kazarian, S. G.; Briscoe, B. J.; Lawrence, C. J. *Polymer Process Engineering'99* **1999,** 28.

[74] Handa, Y. P.; Zhang, Z. Y.; Wong, B. *Macromolecules* **1997,** *30,* 8499.

[75] Briscoe, B. J.; Lorge, O.; Wajs, A.; Dang, P. *J. Polym. Sci. Part B: Polym. Phys.* **1998,** *36,* 2435.

[76] Kumar, V.; Weller, J. E. *ANTEC'91* **1991,** 1401.

[77] Kumar, V.; Gebizlioglu, O. S. *ANTEC'91* **1991,** 1297.

[78] Arora, K. A.; Lesser, A. J.; McCarthy, T. J. *Polym. Eng. Sic.* **1998,** *38,* 2055.

[79] Park, C. B.; Cheung, L. K. *Polym. Eng. Sci.* **1997,** *37,* 1.

[80] Colton, J. S. *Plastics Eng.* **1998,** 53.

[81] Handa, Y. P.; Zhang, Z. *J. Polym. Sci., Part B: Polym. Phys.* **2000,** *38,* 716.

[82] Sparacio, D.; Beckman, E. J. *Polym. Prepr.* **1997,** *38,* 422.

[83] Park, C. B.; Suh, N. P. *Polym. Eng. Sci.* **1996,** *36,* 34.

[84] Park, C. B.; Suh, N. P. *J. Manuf. Sci. Eng.* **1996,** *118,* 639.

[85] Zeng, C.; Han, X.; Lee, L. J.; Koelling,; W., K.; Tomasko, D. L. *Adv. Mater.* **2003,** *15,* 1743.

[86] Garcia-Leiner, M.; Lesser, A. J. *Polym. Mater. Sci. Eng.* **2003,** *88,* 92.

[87] Gerhardt, L. J.; Manke, C. W.; Gulari, E. *J. Polym. Sci., Part B: Polym. Phys.* **1997,** *35,* 523.

[88] Weidner, E.; Wiesmet, V.; Knez, Z.; Skerget, M. *J. Supercrit. Fluids* **1997,** *10,* 139.

[89] Lopes, J. A.; Gourgouillon, D.; Pereira, P. J.; Ramos, A. M.; Nunes da Ponte, M. *J. Supercrit. Fluids.* **2000,** *16,* 261.

[90] Gourgouillon, D.; Nunes da Ponte, M. *Phys. Chem. Chem. Phys.* **1999,** *1,* 5369.

[91] Gourgouillon, D.; Avelino, H. M. N. T.; Fareleira, J. M. N. A.; Nunes da Ponte, M. *J. Supercrit. Fluids.* **1998,** *13,* 177.

[92] Daneshvar, M.; Kim, S.; Gulari, E. *J. Phys. Chem.* **1990,** *94,* 2124.

[93] Kwag, C.; Manke, C. W.; Gulari, E. *J. Polym. Sci., Part B: Polym. Phys.* **1999,** *37,* 2771.

[94] Gendron, R.; Daigneault, L. E. *ANTEC'97* **1997,** 1096.

[95] Lee, M.; Park, C. B.; Tzoganakis, C. *ANTEC'98* **1998,** 1902.

[96] Elkovitch, M. D.; Lee, L. J.; Tomasko, D. J. *ANTEC'98* **1998,** 2538.

[97] Elkovitch, M. D.; Tomasko, D. L.; Lee, L. J. *Polym. Eng. Sci.* **1999,** *39,* 2075.

[98] Watkins, J. J.; McCarthy, T. J. *Macromolecules* **1994,** *27,* 4845.

[99] Watkins, J. J.; McCarthy, T. J. *Macromolecules* **1995,** *28,* 4067.

[100] Watkins, J. J.; McCarthy, T. J. *Polym. Mater. Sci. Eng.* **1996,** *74,* 402.

[101] Kung, E.; Lesser, A. J.; McCarthy, T. J. *Macromolecules* **1998,** *31,* 4160.

[102] Muth, O.; Hirth, T.; Vogel, H. *Proc. 6th Meeting on Supercritical Fluids, Chemistry and Materials, Nottingham* **1999,** 127.

[103] Arora, K. A.; Lesser, A. J.; McCarthy, T. J. *Macromolecules* **1999,** *32,* 2562.

[104] Muth, O.; Hirth, T.; Vogel, H. *J. Supercrit. Fluids* **2000,** *17,* 65.

[105] Zerda, A.; Caskey, T.; Lesser, A. *Macromolecules* **2003,** *36,* 1603.

[106] Ober, C. K.; Lok, K. P.; Hair, M. L. *J. Polym. Sci.: Polym. Letter. Ed.* **1985,** *23,* 103.

[107] Dawkins, J. V.; Taylor, G. *Polymer* **1979,** *20,* 599.

[108] Dawkins, J. V.; Taylor, G.; Baker, S. P.; Collett, R. W. R.; Higgins, J. S. *ACS Symp. Ser.* **1981,** *165,* 189.

[109] Dawkins, J. V.; Taylor, G.; Ghaem-Maghami, G.; Higgins, J. S. *ACS Symp. Ser.* **1984,** *240,* 267.

[110] Dawkins, J. V.; Shakir, S. A.; Croucher, T. G. *Eur. Polym. J.* **1987,** *23,* 173.

[111] Arshady, R. *Colloid Polym. Sci.* **1992,** *270,* 717.

[112] Fitch, R. M. *Polymer Colloids: A Comprehensive Introduction;* Academic Press: New York: 1997.

[113] Gilbert, R. G. *Emulsion Polymerization: A Mechanistic Approach;* Academic Press: New York: 1995.

[114] Odian, G. *Principles of Polymerization;* John Wiley & Sons, Inc.: New York: 1991.

[115] DeSimone, J. M.; Maury, E.; Menceloglu, Y.; Mcclain, J.; Romack, T.; Combes, J. *Science* **1994,** *265,* 356.

[116] Hsiao, Y. L.; Maury, E. E.; DeSimone, J. M.; Mawson, S.; Johnston, K. P. *Macromolecules* **1995,** *28,* 8159.

[117] Hsiao, Y. L.; DeSimone, J. M. *J. Polym. Sci. Part A: Polym. Chem.* **1997,** *35,* 2009.

[118] Lepilleur, C.; Beckman, E. J. *Macromolecules* **1997,** *30,* 745.

[119] O'Neill, M. L.; Yate, M. Z.; Johnston, K. P.; Smith, C. D.; Wilkinson, S. P. *Macromolecules* **1998,** *31,* 2838, 2848.

[120] Shaffer, K. A.; Jones, T. A.; Canelas, D. A.; DeSimone, J. M.; Wilkinson, S. P. *Macromolecules* **1996,** *29,* 2704.

[121] Yong, T. M.; Hems, W. P.; van Nunen, J. L. M.; Holmes, A. B.; Steinke, J. H. G.; Taylor, P. L. e. a. *Chem. Commun.* **1997,** *18,* 1811.

[122] Canelas, D. A.; DeSimone, J. M. *Macromolecules* **1997,** *30,* 5673.

[123] Canelas, D. A.; Betts, D. E.; DeSimone, J. M. *Macromolecules* **1996,** *29,* 2818.

[124] Shiho, H.; DeSimone, J. M. *J. Polym. Sci. Part A: Polym. Chem.* **1999,** *37,* 2429.

[125] Shiho, H.; DeSimone, J. M. *J. Polym. Sci. Part A: Polym. Chem.* **2000,** *38,* 1146.

[126] Shiho, H.; DeSimone, J. M. *J. Polym. Sci. Part A: Polym. Chem.* **2000,** *38,* 3783.

[127] Canelas, D. A.; Betts, D. E.; DeSimone, J. M.; Yates, M. Z.; Johnston, K. P. *Macromolecules* **1998,** *31,* 6794.

[128] Shiho, H.; DeSimone, J. M. *Macromolecules* **2000,** *33,* 1565.

[129] Berger, T.; McGhee, B.; Scherf, U.; Steffen, W. *Macromolecules* **2000,** *33,* 3505.

[130] Carson, T.; Lizotte, J.; DeSimone, J. M. *Macromolecules* **2000,** *33,* 1917.

[131] Shiho, H.; DeSimone, J. M. *Macromolecules* **2001,** *34,* 1198.

[132] Wang, W. X.; Griffiths, R. M. T.; Naylor, A.; Giles, M. R.; Irvine, D. J.; Howdle, S. M. *Polymer* **2002,** *43,* 6653.

[133] Giles, M. R.; Hay, J. N.; Howdle, S. M. *Macromol. Rapid Commun.* **2000,** *21,* 1019.

[134] Kappellen, K. K.; Mistele, C. D.; DeSimone, J. M. *Macromolecules* **1996,** *29,* 495.

[135] Clark, M. R.; Kendall, J. L.; DeSimone, J. M. *Macromolecules* **1997,** *30,* 6011.

[136] Cooper, A. I.; Hems, W. P.; Holmes, A. B. *Macromol. Rapid Commun.* **1998,** *19,* 353.

[137] Cooper, A. I.; Hems, W. P.; Holmes, A. B. *Macromolecules* **1999,** *32,* 2156.

[138] Hems, W. P.; Yong, T. M.; van Nunen, J. L. M.; Cooper, A. I.; Holmes, A. B.; Griffin, D. A. *J. Mater. Chem.* **1999,** *9,* 1403.

[139] Yates, M.; Li, G.; Shim, J.; Maniar, S.; Johnston, K.; Lim, K.; Webber, S. *Macromolecules* **1999,** *32,* 1018.

[140] Rindfleisch, F.; Becker, R.; Hergeth, W. D. *Polym. Prepr.* **1999,** *80,* 518.

[141] Giles, M. R.; Griffiths, R. M. T.; Aguiar-Ricardo, A.; Silva, M. M. C. G.; Howdle, S. M. *Macromolecules* **2001,** *34,* 20.

[142] Ye, W. J.; DeSimone, J. M. *Ind. Eng. Chem. Res.* **2000,** *39,* 4564.

[143] Ding, L.; Olesik, S. V. *Macromolecules* **2003,** *36,* 4779.

[144] Cooper, A. I. *J. Mater. Chem.* **2000,** *10,* 207.

[145] Giles, M. R.; Hay, J. N.; Howdle, S. M.; Winder, R. J. *Polymer* **2000,** *41,* 6715.

[146] Galia, A.; Muratore, A.; Filardo, G. *Ind. Eng. Chem. Res.* **2003,** *42,* 448.

[147] Giles, M. R.; Griffiths, R. M. T.; Irvine, D. J.; Howdle, S. M. *Eur. Polym. J.* **2003,** *39,* 1785.

[148] Christian, P.; Giles, M. R.; Griffiths, R. M. T.; Irvine, D. J.; Major, R. C.; Howdle, S. M. *Macromolecules* **2000,** *33,* 9222.

[149] Christian, P.; Howdle, S. M.; Irvine, D. J. *Macromolecules* **2000,** *33,* 237.

[150] Wang, W.; Naylor, A.; Howdle, S. M. *Macromolecules* **2003,** *36,* 5424.

[151] Theng, B. K. G. *Formation and Properties of Clay-Polymer Complexes;* Elsevier Scientific Pub. Co., New York: 1979.

[152] Wu, J. H.; Lerner, M. M. *Chem. Mater.* **1993,** *5,* 835.

[153] Canelas, D. A.; DeSimone, J. M. *Adv. Polym. Sci.* **1997,** *133,* 103.

[154] Liu, Z. M.; Wang, J. Q.; Dai, X. H.; Han, B. X.; Dong, Z. X.; Yang, G. Y.; Zhang, X. L.; Xu, J. *J. Mater. Chem.* **2002,** *12,* 2688.

[155] Hayes, H. J.; McCarthy, T. J. *Macromolecules* **1998,** *31,* 4813.

[156] Shi, T. P.; Yao, K.; Nishimura, S.; Imai, Y.; Yamada, N.; Abe, E. *Chem. Lett.* **2002,** 440.

[157] Yoda, S.; Sakurai, Y.; Endo, A.; Miyata, T.; Otake, K.; Yanagishita, H.; Tsuchiya, T. *Chem. Commun.* **2002,** 1526.

[158] Ishii, R.; Wada, H.; Ooi, K. *Chem. Commun.* **1998,** 1705.

[159] Ishii, R.; Wada, H.; Ooi, K. *J. Colloid Interface Sci.* **2002,** *254,* 250.

[160] Shen, Z. Q.; Simon, G. P.; Cheng, Y. B. *Polymer* **2002,** *43,* 4251.

[161] Shen, Z. Q.; Simon, G. P.; Cheng, Y. B. *Polym. Eng. Sci.* **2002,** *42,* 2369.

[162] Zhang, Z. Y.; Handa, Y. P. *Macromolecules* **1997,** *30,* 8505.

[163] Heldebrant, D. J.; Jessop, P. G. *J. Am. Chem. Soc.* **2003,** *125,* 5600.

[164] Vaia, R. A.; Giannelis, E. P. *Macromolecules* **1997,** *30,* 8000.

[165] Manias, E.; Chen, H.; Krishnamoorti, R.; Genzer, J.; Kramer, E. J.; Giannelis, E. P. *Macromolecules* **2000,** *33,* 7955.

[166] Vaia, R. A.; Sauer, B. B.; Tse, O. K.; Giannelis, E. P. *J. Polym. Sci., Part B: Polym. Phys.* **1997,** *35,* 59.

[167] Kuppa, V.; Menakanit, S.; Krishnamoorti, R.; Manias, E. *J. Polym. Sci., Part B: Polym. Phys.* **2003,** *41,* 3285.

[168] Wong, S.; Vaia, R. A.; Giannelis, E. P.; Zax, D. B. *Solid State Ionics* **1996,** *86-88,* 547.

[169] Hou, S. S.; Beyer, F. L.; Schmidt-Rohr, K. *Solid State Nucl. Magn. Reson.* **2002,** *22,* 110.

[170] Manias, E. *MRS Bulletin* **2001,** *26,* 862.

[171] Asakawa, T.; Hisamatsu, H.; Miyagishi, S. *Langmuir* **1995,** *11,* 478.

[172] Meneghetti, P.; Qutubuddin, S. *Macromolecules* **2004,** *20,* 3424.

[173] Solomon, D. H.; Swift, J. D. *J. Appl. Pol. Sci.* **1967,** *11,* 2567.

[174] Yariv, S.; Cross, H. *Organo-Clay Complexes and Interactions.;* Marcel Dekker, Inc: New York: 2002.

[175] Okamoto, M.; Morita, S.; Taguchi, H.; Kim, Y.; Kotaka, T.; Tateyama, H. *Polymer* **2000,** *41,* 3887.

[176] Mcnally, T.; Murphy, W. R.; Lew, C.; Turner, R.; Brennan, G. *Polymer* **2003,** *44,* 2761.

[177] Okubo, M.; Fujii, S.; Minami, H. *Progr. Colloid Polym. Sci.* **2004,** *124,* 121.

[178] Dong, Z.; Liu, Z.; Zhang, J.; Han, B.; Sun, D.; Wang, Y.; Huang, Y. *J. Appl. Polym. Sci.* **2004,** *94,* 1194.

[179] Kashiwagi, T.; Inaba, A.; Brown, J. E.; Hatada, K.; Kitayama, T.; Masuda, E. *Macromolecules* **1986,** *19,* 2160.

[180] Xie, W.; Hwu, J. M.; Jiang, G. J.; Buthelezi, T. M.; Pan, W.-P. *Polym. Eng. Sci.* **2003,** *43,* 214.

[181] Balazs, A. C.; Singh, C.; Zhulina, E. *Macromolecules* **1998,** *31,* 8370.

[182] Manias, E.; Touny, A.; Wu, L.; Strawhecker, K.; Lu, B.; Chung, T. C. *Chem. Mater.* **2001,** *13,* 3516.

[183] Priya, L.; Jog, J. P. *J. Polym. Sci., Part B: Polym. Phys.* **2002,** *40,* 1682.

[184] Kim, Y. H.; White, J. L. *J. Appl. Polym. Sci.* **2004,** *92,* 1061.